

https://dspace.org/

Investigation of load behaviour of an industrial grinding mill

Couvas, Constantinos

2009-03-24T07:22:06Z
http://hdl.handle.net/10539/6778

Downloaded from a DSpace repository. https://dspace.org/

INVESTIGATION OF LOAD BEHAVIOUR OF AN INDUSTRIAL GRINDING MILL

Constantinos Couvas
B.Sc (Mech), G.D.E. (Ind)

A Dissertation submitted to the Faculty of Engineering, University of the Witwatersrand, Johannesburg, in fulfilment of the requirements for the degree of Master of Science in Engineering.

Johannesburg, October 2008

DECLARATION

I declare that the work presented in this dissertation is to the best of my knowledge and belief, original, except as acknowledged in the text, and that the material has not been submitted, either in whole or in part, for a degree at this or any other University.

This material is submitted for a Masters Degree to the University of the Witwatersrand, Johannesburg.

_____

Constantinos Couvas

_____ day of _____ 200_

ABSTRACT

The dynamic behaviour of the ball load (specifically toe and shoulder positions) within a dry Φ4.74m by 7.4m long, 2.15MW powered, ball mill was investigated as a function of worn and new liners. The mill operating conditions and charge composition where kept constant. Three types of experimental probes were designed, manufactured and mounted strategically on the mill to determine the orientation of the load inside the mill. These included a combination of electrical conductivity, movement and photo-detector probes. Data recorded from each probe was processed, analysed and compared with each other and to Millsoft's 2D theoretical numerical simulation model. Achieving good electrical contact proved to be a very difficult task, hence conductivity did not compare well to Millsoft simulations. It was deduced that the conductivity probe design and electronics data capturing system limited accurate recording of the ball trajectory positions and tended to represent more of the load 'locked-in-state' region (or the period where maximum pressure is applied to the mill walls) instead of the extreme load toe and shoulder positions. The movement probe data compared best with Millsoft predicted load toe and shoulder results at 133 and 282 degrees, respectively. The probe design was however susceptible to forces from different directions thus decreasing its accuracy. Only two tests from only one photo detector probe (measuring ball reflection) were successfully recorded. The one test showed high variances while the other was affected by an inaccurate datum signal; the low number of effective detector data resulted in defining the detector data as unreliable. Measured experimental power was compared to three published power prediction models and Millsoft. The relative error percentages concluded that only Millsoft best predicted mill input power for both the worn and new liners, at 1871kW and 1887kW, respectively. These results have provided valuable information on probe design for dry industrial type mills and mill internal load dynamics.

ACKNOWLEDGEMENTS

I would like to acknowledge and thank the following people for their contributions to the preparation of this report:

- Professor Michael H. Moys, my academic project supervisor, for all the time and energy he has committed to assisting me through this journey. His guidance and knowledge have been an invaluable contribution to the realisation of this report.

- Staff and students of the Mineral Processing Research team and Process and Materials Engineering workshop at Wits University, in particular: Johnny Kalala, for his encouragement and assistance with all the experimental work conducted at Matimba Power Station; Godfrey Monama, for his assistance in conducting milling simulations; Anna van Nierop, for her assistance in compiling the Visual Basic data processing program; Aristidis Michalopoulos, for his assistance in the design and assembly of the electronics circuit and Theo Prassinos and his team for the construction of the experimental probes.

- The project sponsors (Eskom Pty Ltd) and Matimba Power Station personnel, in particular Hennie Pretorius and Bob Swaton. Anton Jansen van Vuuren (Alstom Engineering, Matimba) for his assistance with the experimental work conducted at the Power Station.

A very special acknowledgement to my wife Eleni for always believing in me, for her incredible endurance and continual encouragement and assistance throughout the progression of this dissertation.

Lastly but most importantly, I would like to thank our Lord, God and Savior Jesus Christ for the opportunity to study further and for helping and guiding me to complete this project.

This work is dedicated to my brother and grandmother:
Ioannis and Georgette,
may their memory be eternal.

TABLE OF CONTENTS

TITLE PAGE ..... **I**
Declaration ..... **II**
Abstract ..... **III**
Acknowledgements ..... **IV**
Table of Contents ..... **VI**
List of Figures ..... **X**
List of Tables ..... **XIII**

CHAPTER 1 INTRODUCTORY SECTIONS **1**
1.1 Importance of efficient milling 2
1.2 Load behaviour, milling efficiency and power 2
1.3 Benefits of better understanding internal dynamics of mills 3
1.4 Objectives of research 3
1.5 Report structure 4

CHAPTER 2 LITERATURE REVIEW **5**
2.1 Load motion and factors affecting its behaviour 6
2.1.1 Dynamic behaviour of load in cylindrical grinding mills 6
2.1.2 Effect of liners on load behaviour 8
2.2 Coal grinding process and load behaviour 9
2.3 Mill power and load behaviour 12
2.3.1 Introduction 12
2.3.2 Mill power models 13
2.3.3 Discrete Element Method (DEM) 15
2.3.4 Sensor types available for recording mill load behaviour 16
2.4 Conclusion 16

CHAPTER 3 EXPERIMENTAL APPARATUS, FACILITIES AND PROGRAMS **17**
3.1 Introduction 18
3.2 Mill 2C, Matimba Power Station (Eskom Pty Ltd) 18
3.2.1 Matimba Power Station 18
3.2.2 Process specifications 18
3.2.3 Mill 2C technical specifications 19
3.3 Types of measurements and selection of experimental probes: Mechanical design 21
3.3.1 Electrical conductivity probes 22

3.3.2 Movement probes 23
3.3.3 Photo-detector and laser signal probes 23
3.3.4 CCD and Video camera probe 25
3.4 Data capturing apparatus: Sensor design 25
3.5 Experimental Programs 27
3.6 First experimental program 27
3.6.1 Probe positions 28
3.6.2 Electronics circuit 30
3.6.3 Installation of experimental equipment 30
3.6.4 Experimental procedure 32
3.6.5 Observations 33
3.6.6 Problems 36
3.6.7 Conclusions 36
3.7 Second experimental program 37
3.7.1 Probe positions 37
3.7.2 Electronics circuit 39
3.7.3 Installation of experimental equipment 40
3.7.4 Observations 41
3.7.5 Problems 42
3.7.6 Conclusions 44

CHAPTER 4 CONDUCTIVITY, MOVEMENT AND PHOTO DETECTOR DATA 45
4.1 Introduction 46
4.2 Data processing methodology 46
4.3 Conductivity probe data analysis 48
4.3.1 Data analysis per cycle 48
4.3.2 Selection of load toe and shoulder positions 50
4.4 Conductivity probe results and discussion: First program 52
4.4.1 Analysis of experimental data and results 54
4.4.2 Discussion of first experimental program results 60
4.4.3 First experimental program conductivity data conclusions 62
4.5 Conductivity probe results and discussion: Second program 62
4.5.1 Analysis of experimental data and results 64
4.5.2 Discussion of second experimental program results 66
4.5.3 Second experimental program conductivity data conclusions 68
4.6 Conductivity probe data conclusions 68
4.7 Movement probe data analysis, results and discussion 69
4.7.1 Data analysis per cycle 69
4.7.2 Selection of toe and shoulder positions 70

4.7.3 Analysis of experimental data and results 72
4.7.4 Discussion of experimental results 74
4.7.5 Movement probe data conclusions 77
4.8 Photo detector probe data analysis, results and discussion 77
4.8.1 Data analysis per cycle and selection methodology 77
4.8.2 Analysis of experimental data and results 79
4.8.3 Discussion of experimental results 80
4.8.4 Photo detector probe data conclusions 83
4.9 Worn and new liner simulation results 84
4.9.1 Millsoft simulation setup 84
4.9.2 Simulation analysis and selection of toe and shoulder positions 85
4.9.3 Discussion of simulation results 86
4.9.4 Millsoft simulation conclusions 88
4.10 Comparison of experimental data with Millsoft results 88
4.10.1 Millsoft comparison to movement and conductivity results 88
4.10.2 Conclusions of Millsoft comparison 90

CHAPTER 5 MILL POWER 92
5.1 Introduction 93
5.2 Experimental measurement of power: Mill 2C 93
5.3. Power model definitions 94
5.3.1 Bond 94
5.3.2 Harris, Schnock and Arbiter 95
5.3.3 Morrell 95
5.3.4 The Discrete Element Method (DEM) 97
5.4 Power comparisons and discussion 98
5.5 Conclusion 100

CHAPTER 6 CONCLUSION AND RECOMMENDATIONS 101
6.1 Summary of experimental test work 102
6.2 Summary of probe effectiveness, load behaviour results & simulation comparativeness 102
6.3 Summary of Mill-2C's measured versus calculated mill input power results 103
6.4 Recommendations 104
6.4.1 General project recommendations 103
6.4.2 Recommendations specific to sensor selection 104

REFERENCES **105**
APPENDIX 1 Ball mill apparatus and technical specifications **108**
APPENDIX 2 Probe mechanical design drawings **131**
APPENDIX 3 First & second program probe installation pictures **144**
APPENDIX 4 First and second program project schedules **149**
APPENDIX 5 Experimental test results **155**

LIST OF FIGURES

CHAPTER 2

Figure 2.1: Load orientation in a grinding mill 6
Figure 2.2: Cross-sectional view of typical Stein Industrie type tube mill (Spiral direction to be reversed) 9
Figure 2.3: Load orientation of coal grinding mill (Steyn et al, 2002) 10
Figure 2.4: Illustration of coal flow process through a typical Stein Industrie BBD type tube mill 11

CHAPTER 3

Figure 3.1: Flow diagram indicating Mill 2C's direct firing cycle 19
Figure 3.2: Schematic profile of shell liner illustrating typical wear pattern 20
Figure 3.3: Cross-sectional view of conductivity and movement probes used to extract data from inside the mill shell 22
Figure 3.4: Cross-sectional view displaying typical positioning of the of emitter and receiver probes as installed at the mil ends to extract data from inside the mill shell. 24
Figure 3.5: Variation of key conductivity signals during a rotation in the mill 26
Figure 3.6: Diagram representing experimental apparatus positioning on mill 2C for the first experimental program 28
Figure 3.7: Experimental apparatus positioning on mill 2C for the first experimental program, indicating conductivity and photo-detector probe locations 29
Figure 3.8: Picture of screw conveyor taken from inside the mill shell (mill rotates in an anti-clockwise direction). Picture indicates the approximately 15mm thick layer of coal dust present inside the mill 34
Figure 3.9: Ball load distribution at the surface; 800mm from mill feed drive end in a hole 100mm deep after barring 35
Figure 3.10: Ball load distribution at the surface; 800mm from mill feed drive end in a hole 170mm deep after barring 35
Figure 3.11: Experimental apparatus positioning on mill 2C for the second experimental program 37

Figure 3.12: Experimental apparatus positioning on mill 2C for the second experimental program, indicating additional conductivity, photo-detector and movement probe locations 38
Figure 3.13: Graphical illustration indicating how a typical raw signal is transformed using raw-hold and OR-Gate signals 40
Figure 3.14: Steel particles collecting around conductivity probe (CM1) 43

CHAPTER 4

Figure 4.1: ARM graphical display of recorded data from first experimental visit (Nov02, Test 3 (Raw-hold 5minDelay) Cycles (1-42)) 47
Figure 4.2: An example of typical conductivity probe data profiles from second experimental program (probe CM1, Test 3 (OR-Gate data), Cycles (26-30)). Profile indicates load toe (T) and shoulder (S) positions as well as other load shape characteristics 49
Figure 4.3: Detailed analysis of cycle 26 extracted from second experimental program (probe CM1, Test 3 (OR-Gatedata)). Profile indicates moving average analysis used in the selection of toe and shoulder positions 50
Figure 4.4: Conductivity probe data profiles from first experimental program (probe CM6 and datum signal, Test 3 (Raw-hold5minDelay), Cycles (11-15)). Profile indicates datum signals; voltage spikes; and probe CM6 conductivity signals per cycle 57
Figure 4.5: Conductivity probe data profile from first experimental program (probe CF4: Test 2 (Raw-holdNoDelay), Cycle (4) and Test 4 (RawNoDelay), Cycle (25)). Figure compares the raw-hold to raw signal electrical conductivity signal and affect these signals have on the moving average trend line and hence data selection process 59
Figure 4.6: Typical movement probe profile, indicating toe and shoulder region characteristics (second experimental program, Test 3 (OR-Gatedata), Cycle 14) 70
Figure 4.7: Processed movement probe data profile (M1), using moving variance analysis. Second experimental program, Test 3 (OR-Gatedata), cycle (14). Moving variance graph is truncated for clarity purposes 71
Figure 4.8: Diagram illustrating movement probe installation and effect of normal and tangential forces on strain gauge and in turn movement probe results. Force A tends to bend the probe downwards, while force B bends the probe upwards 74
Figure 4.9: Movement probe (second experimental program) toe and shoulder position plots (cycles 7-42) for: Test 3 (ORGateNODelay) and Test 7 (DatumTestNoDelay) 76

Figure 4.10: Typical (PDCR) photo-detector probe profile, including moving average analysis, indicating positions A and B (second experimental program, Test 3 (OR-Gatedata), cycles (31-35) 78

Figure 4.11: ARM graphical display of conductivity probe CM6 and datum signal data from second experimental program. X and Y scales represent time and voltage, respectively. Test 4 (ORGate2minDelay) Cycles (5-15) 82

Figure 4.12: Photo-detector (PDCR) plot comparing test 3 (ORGateNoDelay) and test 4 (ORGate2minDelay) 75 per cent degree values for positions A and B, between cycles 7 – 42 83

Figure 4.13: Ball density plot representing worn liner load behaviour for a Φ4.74m ball mill (effective diameter Φ4.656m); 19.4% load volume; 50mm balls. Display indicates turbulent toe region thought to have been caused by the cascading ball action rushing towards the toe. 86

Figure 4.14: Ball density plot representing new liner load behaviour for a Φ4.74m ball mill (effective diameter Φ4.642m); 19.4% load volume; 50mm balls. Display a substantially expanded cataracting region resulting in a similar toe value to that of Figure 4:13. Shoulder position is slightly lower than that of the worn liners (this unexpected behaviour is thought to have occurred due to the more aggressive new liner profile). 86

Figure 4.15: Millsoft plot comparing simulation results selected from worn and new liners simulations (revolution 11, 121 frames (frame no. 600 -720). Plot indicates similarity in toe positions and a higher shoulder position for worn liners, implying more cataracting ball action 87

Figure 4.16: First experimental program (worn liner) load arithmetic mean toe and shoulder results indicated along the mill shell 90

Figure 4.17: Second experimental program (new liner) load arithmetic mean toe and shoulder results indicated along the mill shell 90

LIST OF TABLES

CHAPTER 3

Table 3.1: Details of experimental programs 27

CHAPTER 4

Table 4.1: Toe and shoulder results produced from the data processing program using moving average analysis. Data used for the analysis was extracted from the second experimental program, probe CM1 (Test 3 (OR-Gatedata), Cycles (26-30)) 51
Table 4.2: First experimental program (worn liner) test schedule, indicating: conductivity probe and signal type used per test; quality of recorded data; and test details 53
Table 4.3: First experimental program conductivity toe and shoulder position statistical results. Raw-hold signal (Tests 1 and 2) 55
Table 4.4: First experimental program conductivity toe and shoulder position statistical results. Raw-hold signal (Test 3) 56
Table 4.5: First experimental program conductivity toe and shoulder position statistical results. Raw signal (Tests 4 and 5) 58
Table 4.6: Second experimental program (new liner) test schedule, indicating: conductivity probe and signal type used per test; quality of recorded data; and test details 63
Table 4.7: Second experimental program conductivity toe and shoulder position statistical results. OR-Gate signals (Tests 3 and 4) 65
Table 4.8: Second experimental program conductivity toe and shoulder position statistical results. Raw-hold signals (Test 8) 67
Table 4.9: Second experimental program (new liner) test schedule, indicating movement probe (M1) experimental test details 72
Table 4.10: Second experimental program movement probe toe and shoulder position statistical results for: Test 3 (ORGateNODelay) and Test 7 (DatumTestNoDelay) 75
Table 4.11: Second experimental program (new liner) test schedule, indicating three types of photo-detector probes and experimental test details per probe 80

Table 4.12: Photo-detector probe results (PDCR): Test 3 (ORGateNoDelay) and Test 4 (ORGate2minDelay), calculated by calculating the average values from the 25, 50 and 75 per cent data generated from the moving average curves 81
Table 4.13: Millsoft contact parameters used for both worn and new liner simulations 85
Table 4.14: Millsoft simulation toe and shoulder statistical analysis results for worn and new liners (revolution 11) 87
Table 4.15: Millsoft worn and new liner load toe and shoulder results compared to conductivity and movement probe experimental program results 89

CHAPTER 5

Table 5.1: First and second experimental program calculation of average mill powers 94
Table 5.2: Input values used for both worn and new liner power calculations 99

CHAPTER 1

INTRODUCTORY SECTIONS

1.1 Importance of efficient milling

Cylindrical grinding mills play a vital role in particle comminution[1] as their performance directly affects mineral beneficiation[2] and hence productivity. In the coal fuelled power generation industry, grinding efficiency is a key contributing factor in achieving superior pulverised fuel quality (hence cleaner and more efficient combustion within the boiler), resulting in an increase in overall process efficiency. Milling however is highly inefficient process as only a small fraction (ranging between 1- 5 per cent) is used in actually breaking of the particles (Cleary, 2000); the remainder is dissipated in the form of heat, noise and other losses such as: over-grinding; wear of media and liners; or in impacts which do not result in particle breakage.

Eskom supplies approximately 88 per cent of South Africa's electricity from 10 coal fired power stations; approximately 64 per cent of this power is generated from stations using cylindrical grinding mills (this accumulates to a total of 180 grinding mills). Thus by increasing the milling efficiency, substantial savings can be made from the comminution process, resulting in greater power being generated at a lower cost.

1.2 Load behaviour, milling efficiency and power

Three proven key factors which are directly related to rotary grinding efficiency and consume approximately 80% of ball mill operating costs are: mill power, mill interior liners and ball loading. These factors are functions of the complex behaviour of the load inside a grinding mill, and thus are directly related to the initial mill design and current control variables. Mill design variables include mill geometry and internal liner design whereas mill control variables include the mill's operating conditions such as mill speed (in some cases), mill feed rate, ball feed size and rate, load volume etc. Both these types of variables influence the load behaviour properties i.e. cataracting and cascading; load mixing; angle of repose; percentage of voids filled; load volume etc.; hence developing a better understanding of these concepts can lead to improvements in both mill control and efficiency.

[1] Comminution is defined as the process that progressively reduces the size of the ore before the actual separation between the minerals and the ore is undertaken (Wills, 1992).
[2] Mineral beneficiation entails separation of valuable components of the ore from worthless parts (Napier-Nunn et al, 1996).

The importance of understanding the effects of load behaviour on milling efficiency and mill power has been clear from the early 1900's. Researches initially adopted a mechanistic approach to model the behaviour of the load, where the laws of mechanics were applied to flight paths of individual balls (Davis, 1919); these initial models were found to be very idealistic as they excluded the frictional forces between the particles themselves as well as that of the mill walls as well as the interaction effects between particle trajectories and interaction between different trajectories (Hogg et al, 1972). Tests conducted by Moys and Liddell (1988) comparing measured power draw with published empirical and semi-empirical power prediction models were found to overestimate mill power, making torque-arm dependant models inaccurate. These models generally did not account for the underlining mechanics of the motion of the ball charge and treated the dynamic load as a 'locked mass'.

Over the past decade, through the advent of high-speed computing and improved numerical simulation techniques, the dynamic load is modeled to much greater detail, incorporating a mechanistic approach which includes multibody collision calculations; hence, it is now possible to compute the trajectories of each ball of the charge resulting in the power draw computation and milling efficiency becoming a mere beneficial subsidiary of this analysis (Mishra et al, 1993).

1.3 Benefits of better understanding internal dynamics of mills

One can thus appreciate the importance of technological and hence resulting economic benefits for further advancement through improved understanding of the internal dynamics of grinding mills. Consequently more experimental work is required to be performed on industrial type mills to validate these models.

1.4 Objectives of research

The main objectives of the research are as follows:

a. Design, manufacture and assemble various types of probes (including electronics circuit) to be used in order to detect and record the ball orientation (more specifically load toe and shoulder positions) inside an operating industrial ball mill.

b. Compare, analyse and discuss experimental results recorded for worn and new liners with each other and with a theoretical numerical simulation model; experimental mill power to also be compared with simulation model power and published empirical and semi-empirical power prediction models based on the ‘torque-arm’ principle.

1.5 Report structure

Chapter 2 includes a literature review followed by chapter 3 which comprises of a detailed explanation of the experimental programs, processes and design of all equipment used to record the behaviour of the load in an industrial scale ball mill. This chapter also discusses details of the experimental planning, procedures and observations noted during the experiment.

The methodology adopted to process the signal data from all the probes, as well as the results processed from the two experimental programs are presented in chapter 4. An in-depth comparison of these results and discussion per test is also included. Chapter 5 compares the measured power for both tests to several power prediction models as well as a numerical simulation model.

Chapter 6 completes the report by summarizing the main conclusions and recommendations.

CHAPTER 2
LITERATURE REVIEW

2.1 Load motion and factors affecting its behaviour

2.1.1 Dynamic behaviour of load in cylindrical grinding mills

Since the early 1900's studies of load behaviour in a grinding mills have been performed via construction of transparent ended, laboratory type (roller, end or girth-pinion driven) grinding mills. Morrell (1993) used a glass fronted 0.3m diameter by 0.15m inner length roller driven laboratory mill to determine how the shape of the mill charge changed as both the volume of the charge and rotational speed were varied. Morrell also adopted a photographic technique to analyse the load motion inside the mill; generating particle streamlines and measuring the radial displacement with respect to the centre of rotation of the mill. Capturing high speed photographs of the load behaviour inside laboratory grinding mills is now done in many grinding research laboratories.

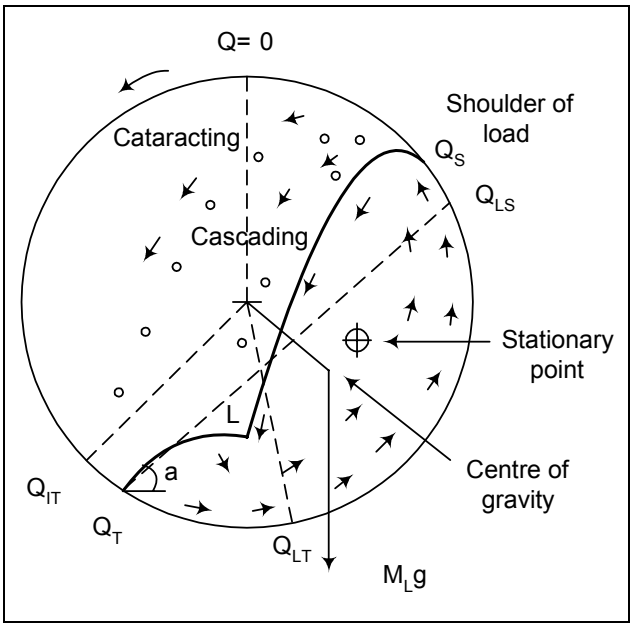


Figure 2.1: Load orientation in a grinding mill

The behaviour of the ball load in an anti-clockwise rotating mill including liners of a chosen profile and a ball charge of approximately 40 per cent is illustrated in Figure 2.1. The kidney-shaped profile of the load is achieved as soon as the mill has reached equilibrium (or steady-state) condition; this type of profile was initially observed by White (1904) from his work conducted in this field and is typical of ball mill behaviour, operating at common ball mill operating speeds (70 to 80 per cent of critical speed).

As illustrated the load profile is bound by the toe and shoulder positions, located at the bottom and top positions of the load, respectively. The directions of the arrows indicate the observed movement of the steel ball charge as the mill rotates (Moys et al, 1992). The 'stationary point' or "eye" refers to an area within the load that experiences no grinding as there is very little ball movement; this position is also referred to as the "centre of motion" of the load (not be confused with the centre of gravity of the load) (Moys et al, op.cit).

Angles, θ and α are defined as the angular displacement of a point in a mill and the dynamic angle of repose of the load, respectively.

The toe area is the most turbulent region in the mill and lies between angular positions θ_{IT} and θ_T. θ_{IT} denotes the start of the 'initial toe' region or the impact zone (Wills, 1992) and at high mill speeds primarily results from the cataracting action of the balls. Between angular positions θ_T and θ_{LT}, the balls are accelerated until they achieve the same angular velocity as the liner. The region located between θ_{LT} and θ_{LS} is defined as the load 'locked condition' i.e. balls within this region travel at the same angular velocity as the liner and do not experience slip with respect to the other balls (Austin et al, 1984), (if the liner profile is smooth, slip between balls and liner may indeed occur).

As the balls are lifted on the rising side of the mill and approach the region $\theta>\theta_{LS}$ the radial force component starts to decrease and the gravitational force increases resulting in slip between the liner and the load. At the point where the force due to gravity becomes greater than the radial force component of the balls (at θ_S), the balls are thrown from the shell liner and follow a path which is a function of their velocity at the time of ejection and is also influenced by the current position of the surrounding balls.

The mill's speed affects the balls' path i.e. if the mill is rotating at common ball mill operating speeds, once the balls loose contact with their neighbours (and are under the influence of gravity) the outer layers of falling balls have parabolic paths and impact onto the shell or into the toe region, whereas the remaining balls as observed by Moys (1992), make contact with the load at L.

At speeds exceeding about 85 per cent of critical, cataracting action starts becoming the predominant motion, resulting in the toe position rising up the down-coming side of the mill. This is because the bulk of these balls make contact with the outer regions of the toe area and the liners. This steel-to-liner-impact does not only add to grinding mill

inefficiency, but also decreases the life of liners. Furthermore, some of the kinetic energy of the balls (impacting at the toe region), is converted into a turning moment and thus contributes to the rotation of the mill. Both these factors tend to reduce the torque, and compensate for the increase in torque required to maintain the load in a more elevated position.

At higher mill speeds (close to, or greater than 100 per cent of critical), the balls start to centrifuge on the outer walls of the shell, thus reducing the mill effective diameter and hence mill internal active load. Both of these factors contribute substantially to loss of power (Moys, 1992).

2.1.2 Effect of liners on load behaviour

Mill liners consist of the inner working faces of the mill which are in constant contact with the tumbling load, thus their design influences load behaviour, mill performance and in turn grinding efficiency.

The purpose of the liners (or more specifically lifters) is to transmit energy as effectively as possible to the outer layer of the charge, so as to promote particle breakage i.e. for a mill operating at common ball mill speeds, high lifters promote a cataracting ball action (thus breakage occurs via impact), whereas low lifters promote more of a cascading type ball action.

Mills with smooth liners, excessively worn or lower lifters experience slippage, thus energy is consumed without substantial breakage resulting in a significant decrease in grinding efficiency. Furthermore, Djordjevic (2003) proved (via a series of simulations), that lifter conditions not only have a significant influence on the mode of energy consumption, but also on the mill power draw i.e. high lifters consume less power than low lifters, under otherwise identical conditions.

A great variety of mill liners exist, differing in geometric shape, profile and material. Due to their influence on the behaviour of the load and hence grinding efficiency, liners are specifically designed for a particular application.

2.2 Coal grinding process and load behaviour

Unlike wet grinding mills in the mineral processing industry, coal grinding mills are of the double ended type i.e. feeding and discharging occurs at both mill ends, thus better utilization of mill length is achieved. Three types of double-ended design mills are adopted by Eskom power stations, namely: Stein Industrie SA (Pty) [now Alsthom SA (Pty) Ltd], Kennedy van Saun (KVS) and Riley mills. For the purpose of this report, emphasis will be placed on the Stein Industrie type mills.

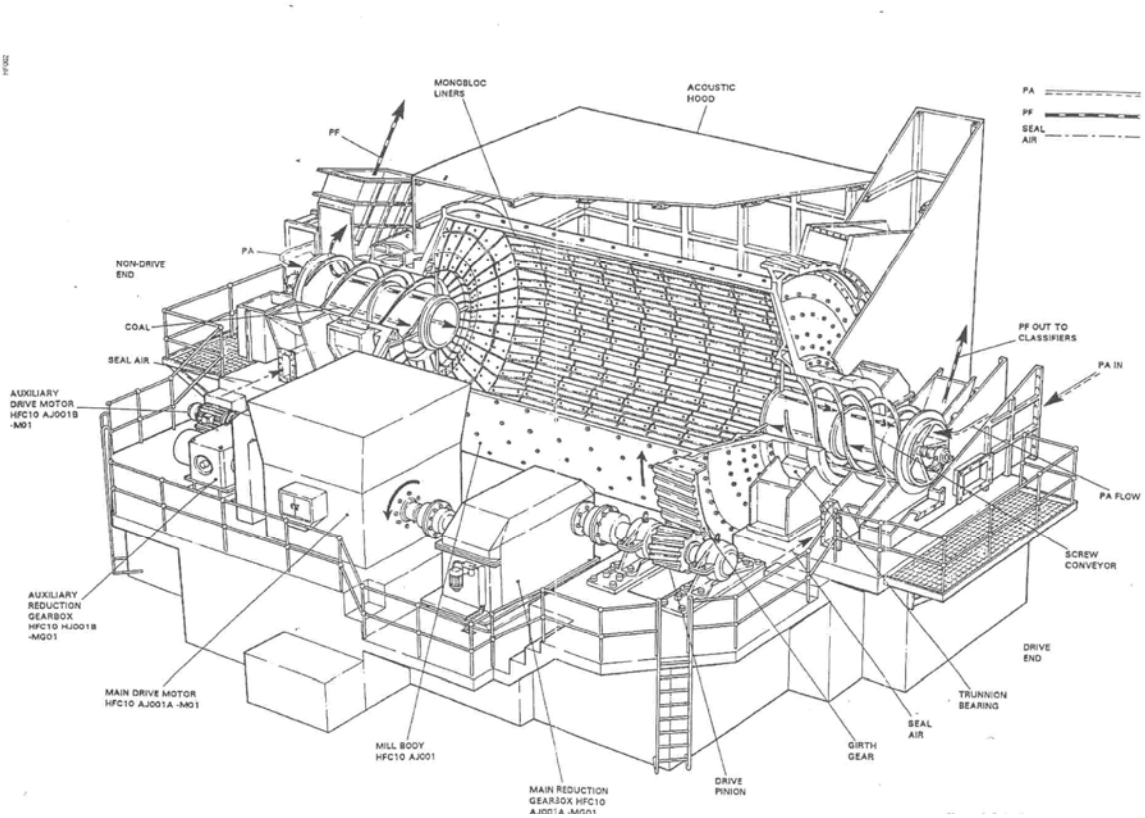


Figure 2.2: Cross-sectional view of typical Stein Industrie type tube mill (Spiral direction to be reversed)

Figure 2.2 illustrates a cross-sectional view of a typical Stein Industrie mill. The screw conveyor at each of mill ends consists of the following three main components: the hot air tube (used to convey the primary airflow (PA) into the mill); the screw flights (designed to transport the raw coal and classifier rejects from the area below the raw coal chute and classifier reject discharge device to the inside of the drum); and the outlet area located between the hot air tube and screw flights. This outlet area is used to transport the mixture

of pulverized fuel (PF) and primary air out of the mill towards the classifier. The screw conveyor hot air tube is attached to the mill drum via four drive rods, permanently secured inside the mill drum, thus, the screw conveyor rotates at the same rotational speed as the mill.

Stein Industrie mills are typically filled with a ball loading of approximately 20 per cent of total mill volume and accept a throughput of over 100t/h.

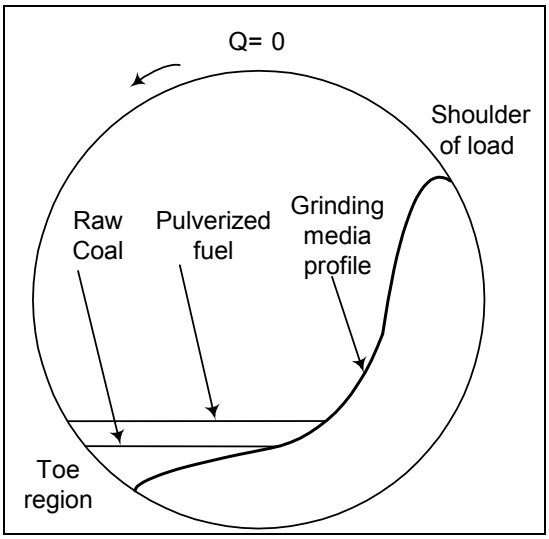


Figure 2.3: Load orientation of coal grinding mill (Steyn et al, 2002)

Figure 2.3 illustrates the load behaviour inside a coal grinding mill once it reaches steady-state conditions[1]. The nature of the load motion inside the mill results in a separation of the pool i.e. fine less dense particles (PF) tend to move upwards, whilst higher density particles (pyrites and quartz contaminants) together with raw coal move downwards (towards the bottom of the load), ready to be introduced into the grinding media charge. Primary classification occurs inside the mill prior to particles reaching the classifier. This process is illustrated in Figure 2.4 and is thought to occur in the following way: initially the high entry velocity of the PA collects both heavy particles (ejected from the load shoulder) and fine less dense particles (located at surface of the pool); thereafter as the airflow reaches the centre of the mill it expands over a wider area thus decreases in velocity, causing the heavier particles to be released back into the mill load, while the remaining particles are transferred to the classifier.

[1] This schematic defining the behaviour of the load inside the mill is a result of an audible level control device used to determine the amount of raw coal and PF inside the mill while in operation.

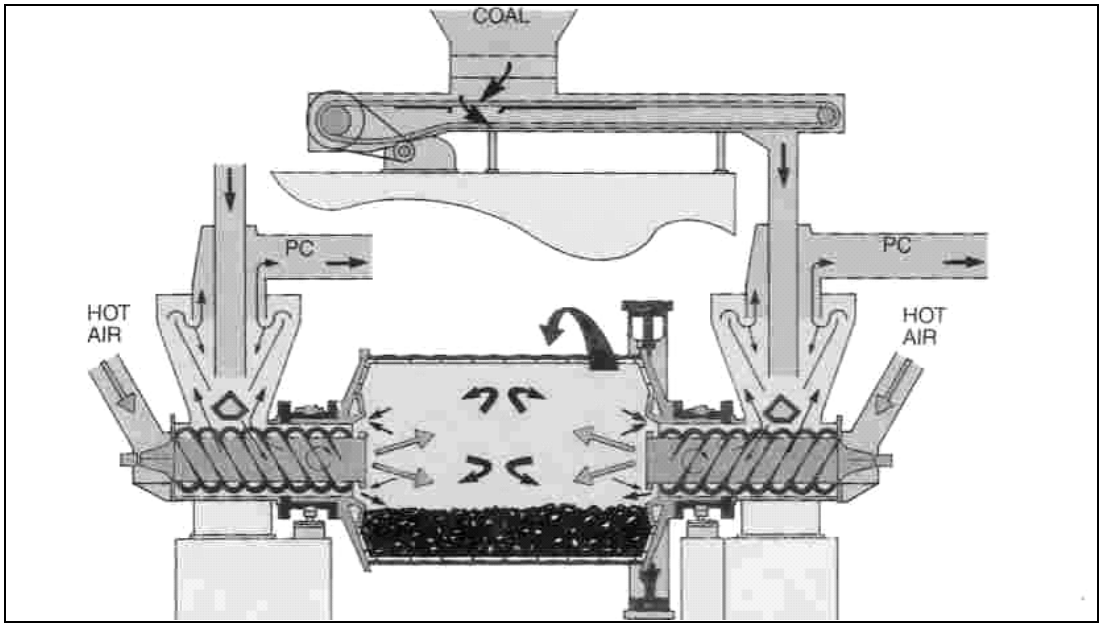


Figure 2.4: Illustration of coal flow process through a typical Stein Industrie BBD type tube mill

Secondary classification occurs in two different classifiers located at either end of the mill. On sorting, the fine less dense particles travel to the boiler; whereas the remainder is re-circulated back to the mill for further grinding. It's thought that particles will re-circulate because of: inefficient flow of primary air i.e. air velocity is too low; or particles are too heavy, or a combination of each of these factors. Heavy particles are either: too large; or are high in moisture content; or are high in density. High density particles (such as pyrites and quartz) more often end up staying inside the mill thus adding to the mills grinding load and giving rise to wasted energy and increased media and liner wear.

Poor air distribution in the mill can result in particles being picked up prematurely, or rejected unnecessarily (Steyn et al, 2002). Furthermore, low air velocity in the classifier results in fine grinded particles being returned back to the mill instead of passed through to the boiler, thus making the overall process less efficient. Re-circulation is directly related to milling efficiency, as the more efficient the milling process, the less re-circulating and hence, regrinding will take place.

2.3 Mill power and load behaviour

2.3.1 Introduction

In most comminution circuits, milling is the main power consumer and hence demands the highest capital and operating costs. Present grinding philosophy adopted by milling circuit experts is to opt for fewer, higher-powered mills, consisting of single lines of production. This preference at the very least is aimed at decreasing milling plant operating and capital costs, however this directly affects plant flexibility and plant start-up production timing (as the larger the mill, the longer it takes to manufacture). These stringent controls necessitate the plant comminution circuit (more importantly mill size and power) to be designed to the highest level of accuracy – thus it is vital that the predicted (or specified) power to run the mill corresponds to the specific grinding energy required per ton of product and hence product size distribution.

The importance of understanding the dynamic behaviour of the load and its relationship to mill power and efficiency was recognised almost one hundred years ago (White, 1904). Even though an understanding of the behaviour existed, lack of numerical analysis tools led researches to develop empirical (and/or semi-empirical) equations based on over-simplifications of the load behaviour i.e. load (or components of the load), were treated as a 'locked mass', resulting in most of mill power draft calculations making use of the 'torque-arm formula', or an improved variation of it.

The torque-arm formula (2.1) and hence power draft (2.2) for a mill operating at N (RPM), may be defined as the torque required in maintaining the load in a state of dynamic equilibrium about its centre. This relationship holds true for low mill speeds (N<50 per cent of critical) (Moys et al, 1992).

$$T = M_b r_g \sin\alpha \qquad (2.1)$$

where, T is the torque (Nm), M_b is the mass of the balls (kg), r_g defines the distance from the mill centre to the centre of gravity of the ball load (m) and α is the dynamic angle of repose of the load (degrees). Mill power is given by:

$$P = 2\pi NT / 60 \qquad (2.2)$$

Moys and Liddell (1988) proved that power prediction models based on the torque-arm principle tended to overestimate the mill power especially at speeds greater than 60 per cent of critical speed, resulting in torque-arm dependant models being inaccurate.

Over the past decade the increasing rate of development of information technology, coupled with better numerical analysis tools, has led to the introduction of computer simulations, predicting mill power by simulating the behaviour of the load in the mill. One such proven numerical technique which caused a paradigm shift in the way load behaviour is examined in grinding mills is the Discrete Element Method (DEM), developed by Mishra and Rajamani (1993). Several other numerical models have also been developed, with each attempting to improve and expand from the previous, proposing and defining enhanced methods for modelling mill power.

Due to the little practical information available describing the load behaviour of industrial type grinding mills and the influence of different variables such as liner characteristics, mill speed, mill filling etc. validation of these computational models has proved to be a difficult task. It is thus appropriate to investigate the load behaviour of grinding mills.

For the purpose of this research report, emphasis is placed on three mill power models that have showed significant development in the field of mill power prediction and hence better understanding of mill load behaviour. In addition, the DEM is used as both: mill behaviour analysis; and mill power prediction, tool.

2.3.2 Mill power models

2.3.2.1 Bond

Bond (1961/2) was one of the early pioneers in developing relationships for the power requirements of grinding mills. Using the ‘torque-arm formulae’ together with an extensive range of industrial-scale and laboratory experimental power measurements, Bond defined equations relating mill power consumption to: mill dimensions; mill rotational speed; and mill filling. Rowland (1972) defined Bond’s ‘mill input power’ to be the mill input power at the pinion shaft (as quoted by Morrell, 1993).

2.3.2.2 Harris, Schnock and Arbiter

Harris, Schnock and Arbiter (1985), having reviewed common power prediction models, presented a simple semi-empirical, correlating equation, derived from the torque-arm model, relating dimensions and operating mill variables (such as mill length; effect of mill loading on torque arm length; load weight etc.) with power. Their equation aimed to provide a basis for both correlation purposes and for comparing existing design methods.

It was deduced by Harris et al that errors arising in the calculation of mill power and data correlation do not only depend on the particular power prediction model used but also depend on the accuracy of mill dimension measurements and operating variables. Hence, Harris et al noted the importance and need for an accurate data-base of mill power related parameters documenting mill scale-up details, similar to that of Taggarts' attempt in 1947.

2.3.2.3 Morrell

To predict mill power Morrell (1993) developed three models, all largely based on experimental observations of the load behaviour inside a transparent roller driven laboratory mill. Morrell initially derived equations describing charge shape (using load toe and shoulder angles) as a function of both mill speed and filling; thereafter he related this to the movement of grinding media and hence derived a theoretical power equation 2.3:

$$P_{net} = 2\ \pi\ g\ \rho_C \int_{r_i}^{r_m} \int_{\theta_T}^{\theta_S} N_r\ r^2 \cos\theta\ d\theta\ dr \qquad (2.3)$$

where, the thickness of the cascading layer of balls spans a distance from charge centre (radius r_i) to mill wall (radius r_m) with the charge occupying vertically the space between toe-angle θ_T and shoulder θ_S. N_r is defined as the angular speed of the balls, L is the mill length and ρ is defined as ball bulk density. This equation was then adapted to suit grinding mill geometric shapes before validating the model with actual ball, semi-autogenous (SAG) and autogenous (AG) grinding mill operating data. The resulting power prediction equation is defined as Morrell's 'C-Model'. Even though this model is based on substantial approximation of load behaviour inside a laboratory grinding mill; it has shown to predict the power draw by a wide range of mills with exceptional accuracy (van Nierop et al, 2000).

On calibrating of the 'C-model', Morrell compared its results with that of other published power prediction equations and developed a relatively simple semi-empirical equation, E-model (based on the 'C-models' performance). D-model was also derived to account for the ball/rock effects inside grinding mills.

2.3.3 Discrete Element Method (DEM)

2.3.3.1 Introduction

Mishra and Rajamani (1993) pioneered the application of DEM to grinding mills and offered a numerical tool that is able to: describe the effects of liner profile, media size distribution, load volume, mill speed etc., as well as predict power draw of production mills with reasonable accuracy over a wide range of mill diameters (van Nierop et al, 2000). This technique (through its micro-scale simulations, impact energy distribution plots etc.) allows for a better understanding of the load internal dynamics; and for developing improvements in both the mill design and mill operation. These improvements can thus lead to more efficient scale-up and control techniques for grinding mill circuits; resulting in lower capital and operational costs.

DEM adopts the philosophy that the power draw is calculated from the total energy dissipated within the mill over a specific period. The model performs this by monitoring all friction and impacts per revolution and storing their corresponding energy loss for each specific time-step. On completion of the required revolutions, the computer program sums all the collision energies to calculate the total energy loss (and hence power draw) over a period of time.

2.3.3.2. Major Limitations to the DEM

The 2D DEM modeling has two major limitations: the computational intensive nature of the software, and the lack of an established methodology to determine the particle properties to best accurately model a given physical system.

The first limitation contributes to the large amount of computing time to keep the total simulation time to a tolerable level; in this case usually only a 2D slice of the mill load is simulated (having a width equal to that of the largest ball diameter) is used to perform the

simulation. Due to the poor methodology to determine particle properties, depending on mill operating parameters (such as mill speed, inner diameter, ball load etc.) the second limitation results in inaccurate mill power draw results.

2.3.4 Sensor types available for recording mill load behaviour

The harsh environment inside an industrial grinding mill limits the amount of types of measurements (and hence sensors) that one can employ to record mill load position, however keeping in mind that the duration of each test is relatively short and that the sensor(s) can be protected by a well designed housing, increases the types of sensors that may be selected.

At the time of the experiment unfortunately not much published material with regards to industrial type mill load behaviour measurements were available (Moys et al, 1996); however a considerable amount of published laboratory-type mill load measurement techniques were readily available (Moys et al, 1988). On reviewing the above mentioned available data, and after brainstorming what further types of measurements could be utilized, the following list was compiled:

1. sound measurements (acoustic devices),
2. light measurements (photo-detector signal probes),
3. direct contact measurements (force, movement, electrical conductivity, inductive or capacitive proximity probes etc.) and
4. video recordings.

A selection of the types of measurements (and their respective sensors) used to measure the mill load behaviour is discussed in Chapter 3.

2.4 Conclusion

Grinding mills are known to consume the highest capital and operating costs in most comminution circuits hence understanding their behaviour is imperative. The benefits of better understanding their behaviour can lead to more efficient, cost effective milling circuits with improved control.

This report is aimed at: better understanding of Eskom's Stein Industrie type, coal grinding mill load behaviour; and contributing to the validation of power prediction models.

CHAPTER 3

EXPERIMENTAL APPARATUS, FACILITIES AND PROGRAMS

3.1 Introduction

This chapter discusses details of the experimental process and equipment used to record the behaviour of the load in an industrial scale ball mill. The behaviour of the steel ball load was recorded using various specifically designed probes which were inserted into the mill via the mill's shell and end liner bolt holes.

Details of the two experimental programs conducted (including experimental planning, procedure and observations) on the industrial scale ball mill are also discussed.

3.2 Mill 2C, Matimba Power Station (Eskom Pty Ltd)

3.2.1 Matimba Power Station

Matimba Power Station (fully commissioned in 1989) is one of Eskom's ten currently operational coal fired power stations and is situated in the Northern Province of South Africa, next to the town of Ellisras. Matimba's operational characteristics are unique as due to the water shortage in that region, Matimba was designed to utilize as little water as possible, making it the largest direct dry cooling power station in the world.

Matimba's installed capacity is 3990MW, and average send-out power of approximately 24000GWh (or 2.739GW per year). Coal supply to the station is from Grootegeluk Colliery (situated 10km from Matimba) which has sufficient reserves to guarantee Matimba a minimum lifespan of 35 years at 3 800 tons of coal per hour. Matimba's current coal consumption per hour is approximately 2800 tons.

3.2.2 Process specifications

Measurements were conducted on Mill 2C at Matimba; an overview of its circuit is shown in Figure (3.1). Raw coal fed at approximately 100t/h, together with hot primary air is mixed in a mixing box, before being introduced into the mill from each end. The temperature of the primary air entering Mill 2C ranges between 160 to 230 degrees Celsius (depending on the coal surface moisture, coal volatility, coal feed capacity etc.), with a constant air pressure and flow rate of 5.6kPa and 20kg/sec, respectively. The average discharge pulverized fuel (PF) temperature and pressure is approximately 88 degrees Celsius and 4kPa. The PF is then transported via the primary air to the classifier

which returns any oversize particles back to the mill; and transfers the remaining fine coal directly to the burners. This method by which the coal flow is admitted directly to the burners and is adjusted in accordance with the boiler load by variation of the primary air flow is termed direct firing.

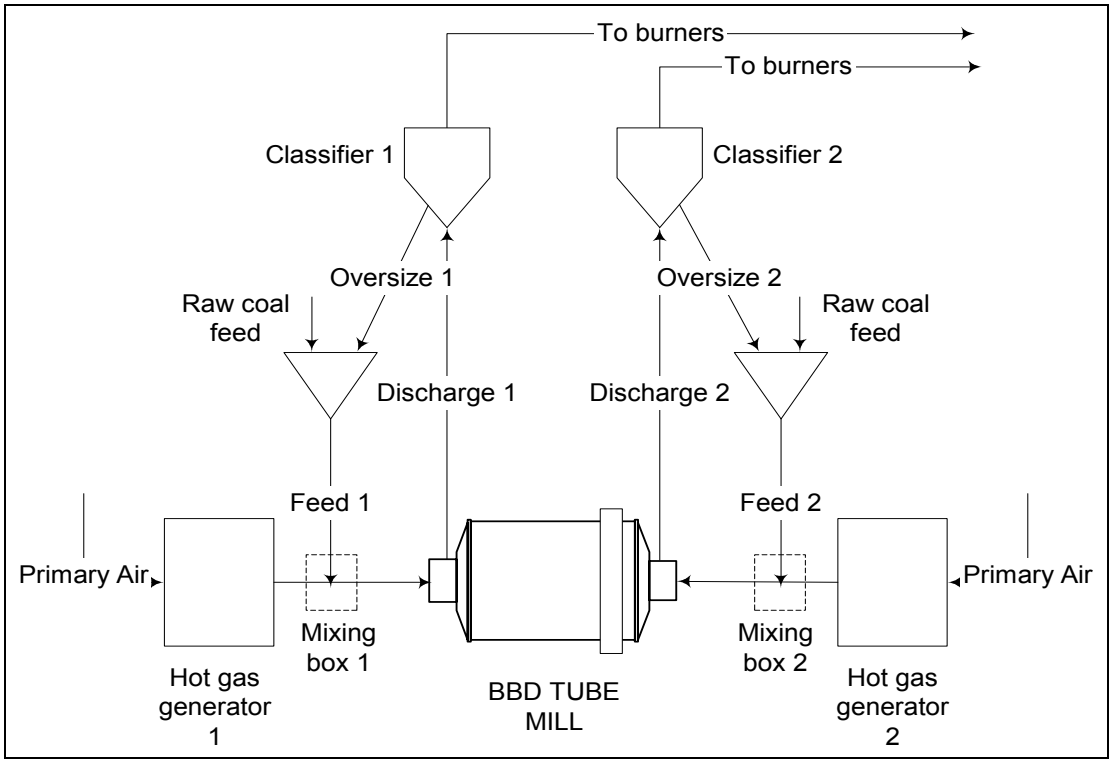


Figure 3.1: Flow diagram indicating Mill 2C's direct firing cycle.

All six boilers installed at Matimba were designed to achieve full load on only four out of the six mills installed per boiler; this operating philosophy was adopted to increase probability of full load. An advantage of selecting tube mills for a direct firing operation is the flexibility in production i.e. all thirty-six identical Stein Industrie type tube mills at Matimba can operate on minimum throughputs, thus meeting the requirements of boilers operating at low loads.

3.2.3 Mill 2C technical specifications

Mill 2C is supported via two 20 degree conical ends (shell integral end plate assembly); with an inner shell diameter measuring 4.74m and shell length of 7.4m. The mill's main power train consists of: a Brown Boveri (slipring type) 2.15MW (993RPM) motor; one

David Brown double-reduction gearbox; and a single helical girth/pinion type arrangement. Mill 2C operates in a dry environment with a measured ball load of approximately 19.4 per cent of mill volume (or 112.7t) at a mill speed of 15.32 RPM (equivalent to 77.6 per cent of critical). Refer to Appendix 1 to review additional mill specifications.

Shell liners are steel (27 per cent hi-chrome) and are rectangular in shape. Mill shell and outer row of conical end liners are changed every 8 years (equivalent to 60 000 – 65 000 hours of operation). Liners are made to operate on one working face for the first four years, thereafter they are rotated to operate on the opposite face for the remaining time. Figure 3.2 displays schematic of a new shell liner. The dotted line illustrates the typical wear profile of rectangular liners[1]; refer to the Appendix 2 to view detailed drawing of new shell liner.

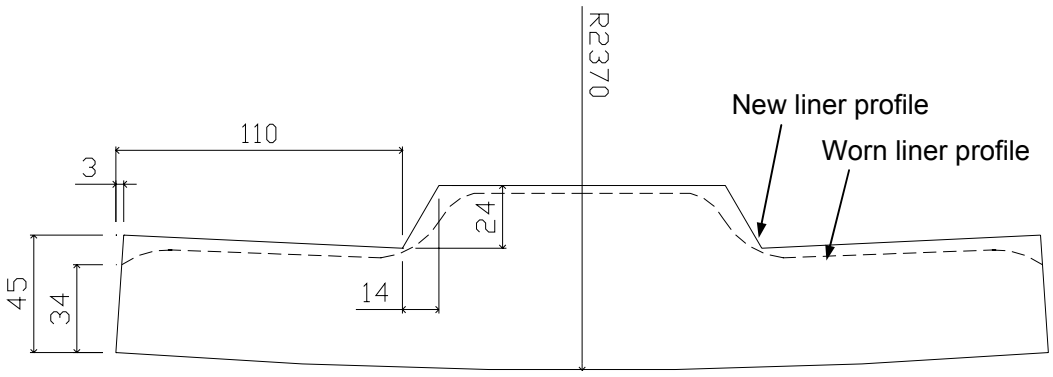


Figure 3.2: Schematic profile of shell liner illustrating typical wear pattern.

Twelve liners fit across the length of the mill. The first and last i.e. numbers 1 and 12, include a diagonal lifter arrangement, whereas the ten liners in between (numbers 2 to 11) are the rectangular type, as shown in Figure 3.2. The mill consists of 40 rows of shell liners, thus totaling 400 of the rectangular type and 80 of the diagonal type shell liners.

The outer conical end liners are secured on the mill ends via two bolts, one situated closer to the mill shell, while the other is closer to the mill centre. The total number of end liners amounts to 40 liners per mill end.

[1] Wear pattern is based on comparisons conducted between Mill 2C's new and worn rectangular shell liners.

3.3 Types of measurements and selection of experimental probes: Mechanical design

During the selection of the type of measurements that were to be conducted, the following constraints were taken into account:

1. Mill environment: Due to the highly corrosive, unstable and dusty environment inside the mill, the sensors selected would have to be robust and dust resistant.
2. Sensor location: The mill load makes direct contact with the liner shell and bolts. The shell liners of the selected mill were all wedged in place, thus making it difficult and time consuming to remove, install the sensors, and place back into the mill. The existing shell liner bolts however could be easily removed, thus allowing for specifically modified liner bolts to be fitted, on which the sensors would be firmly attached.
3. Sensor size: The size of sensors could not exceed the diameter (or the total length) of the liner bolt. It was also important that the liner bolt would maintain its core function i.e. since the liner bolts would be drilled through to fit the probes, a calculated minimum liner bolt wall thickness was to be maintained so that the bolt would hold the liner in position.
4. Reliability and availability of the sensors themselves.

As a result of the above constraints the following three different types of probes were used to detect the ball position from inside the mill, namely: electrical conductivity, movement and photo-detector signal probes. All three types were constructed by modifying original mill shell and end liner bolts i.e. modification of bolt was based on nature of specific measurement. These bolts were later inserted in the mill via the liners in such way as to extract data from inside the rotating mill. Schematic of conductivity and movement probes is shown in Figure 3.3.

In addition to the experimental probes, two cameras were also installed in the mill recording the load behaviour at two different instances. Both were mounted on a steel support structure, which was installed inside the mill's screw conveyor. Appendix 2 includes a copy of all the engineering design drawings used in the modification of the existing liner bolts as well as additional apparatus used.

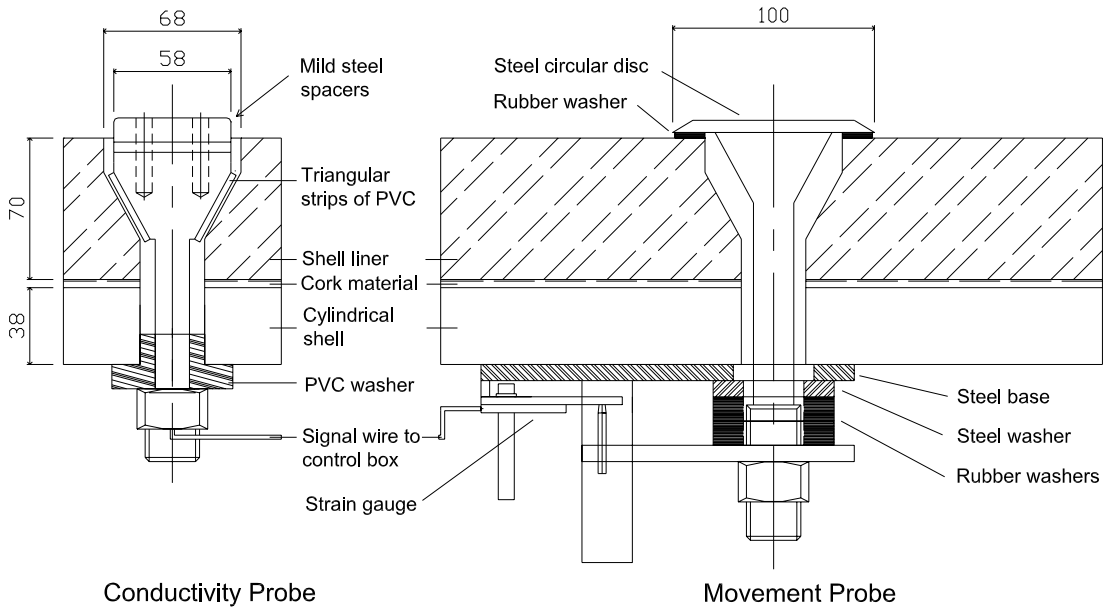


Figure 3.3: Cross-sectional view of conductivity and movement probes used to extract data from inside the mill shell.

3.3.1 Electrical conductivity probes

By electrically isolating the liner bolt from the mill shell and steel liner, electrical conductivity between a steel ball and modified shell liner bolt could be achieved. Electrical isolation of liner bolts was performed by machining the bolt down by approximately 10mm, gluing triangular strips of PVC on strategic areas of the bolt head and body, and securing it in position for the duration of the tests by isolating it with quick setting polyurethane casting resin or pieces of Pratley epoxy putty (Figure 3.3).

To achieve good electrical contact between the steel balls and bolt head it necessitated the probe to protrude slightly above the shell liner, just high enough to achieve good electrical conductivity and low enough so as to not interfere with the behaviour of the load. The ‘variable’ height was achieved by adding mild steel spacers of various thicknesses above the original bolt head. To ensure that the bolt and spacer assembly was rigid, two 8mm diameter threaded holes were drilled at the top of the bolt head, lying 28mm apart and approximately 8mm deep. Spaces designed to suit these dimensions were fabricated and secured to the bolt via two 8mm countersunk bolts.

3.3.2 Movement probes

The movement probe consisted of a modified 205mm long end liner bolt, one 100mm diameter by 10mm thick steel disc, two 8mm thick rectangular steel plates, several 8mm thick rubber washers cut to suit the plate dimensions and a set of strain gauges mounted on a PVC bridge.

The bolt was machined down by 10mm and 7mm, at the bolt head and stem, respectively, to ensure that it would remain completely independent of the liner and shell. One steel disc was welded to the bolt head. The purpose of the disc was to heighten the sensitivity of the probe as the greater the disc diameter, the more responsive it would be to the impacting balls. A rubber washer was glued to the bottom of the steel disc, to enhance bolt movement due to forces exerted on the bolt head by the load. The PVC bridge was positioned in such a way so that any bolt movement relative to the mill shell would bend the PVC bridge, and hence activate the strain gauge arrangement.

3.3.3 Photo-detector and laser signal probes

The photo-detector signal probe consists of a laser emitter and receiver (or photo-detector). This set is positioned directly opposite each other so that the laser signal focuses directly on the photo-detector unit.

A total of two emitters and three receivers were used. Two of these laser and photo-detector probes were each housed inside four modified end liner bolts, positioned directly opposite each other at either conical end of the mill. The purpose of these probes was to record the mills load profile a certain distance away from the mill shell i.e. unlike the conductivity and movement probes that recorded load behaviour signals at the mill shell; the photo-detector probes were designed to capture traces of the load behaviour relative to their distance from the mill shell. The additional receiver was positioned next to one of the emitters (Figure 3.4). Refer to Appendix 1 to review technical specifications of the emitters and receivers used.

Mill conical end liner bolts were used to house the laser probes (Figure 3.5). Lengths of these bolts range between 205mm up to 310mm. Because the mill ends are conical and have a 20 degree slope, to achieve a horizontal signal between the transmitter and

detector, the end liner bolts were drilled at 20 degree angle to their vertical axis at the head of the bolt. Holes of 18mm and 10.5mm diameter were drilled through the bolts to cater for the transmitter and detector probes, respectively.

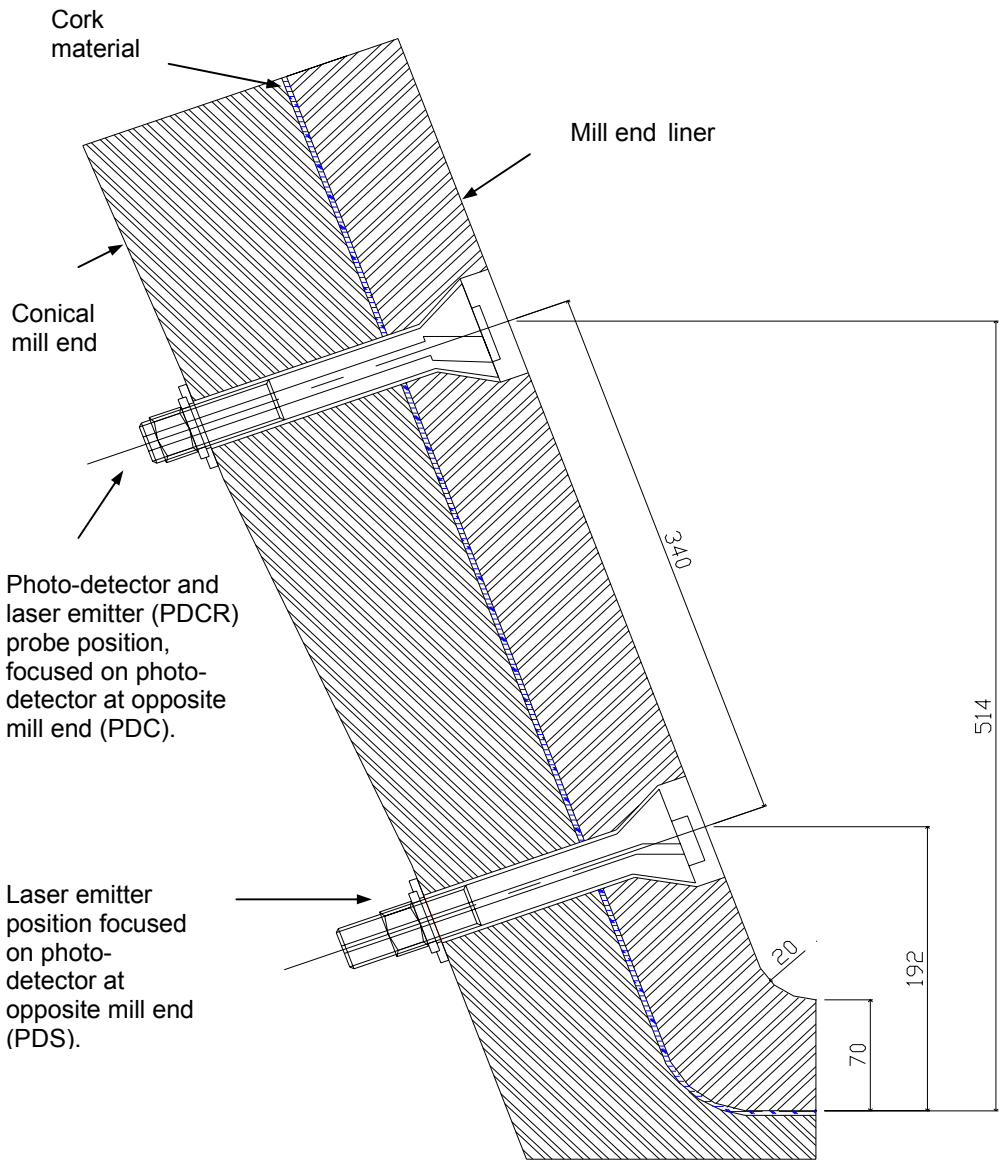


Figure 3.4: Cross-sectional view displaying typical positioning of the of emitter and receiver probes as installed at the mil ends to extract data from inside the mill shell.

3.3.4 CCD and Video camera probe

Two methods were adopted to record the behaviour of the rotating mill: one method incorporated the use of a high-resolution 8.5mm colour CCD camera connected to a Hi8 Sony video camera to record its signal; the other involved only the video camera. Refer to Appendix 1 to view technical specifications of each apparatus.

A power pack needed to be constructed for the CCD camera to ensure a regulated 12V DC voltage supply. The CCD camera was placed inside a cylindrical PVC frame, specifically designed to protect it from the hazardous grinding environment.

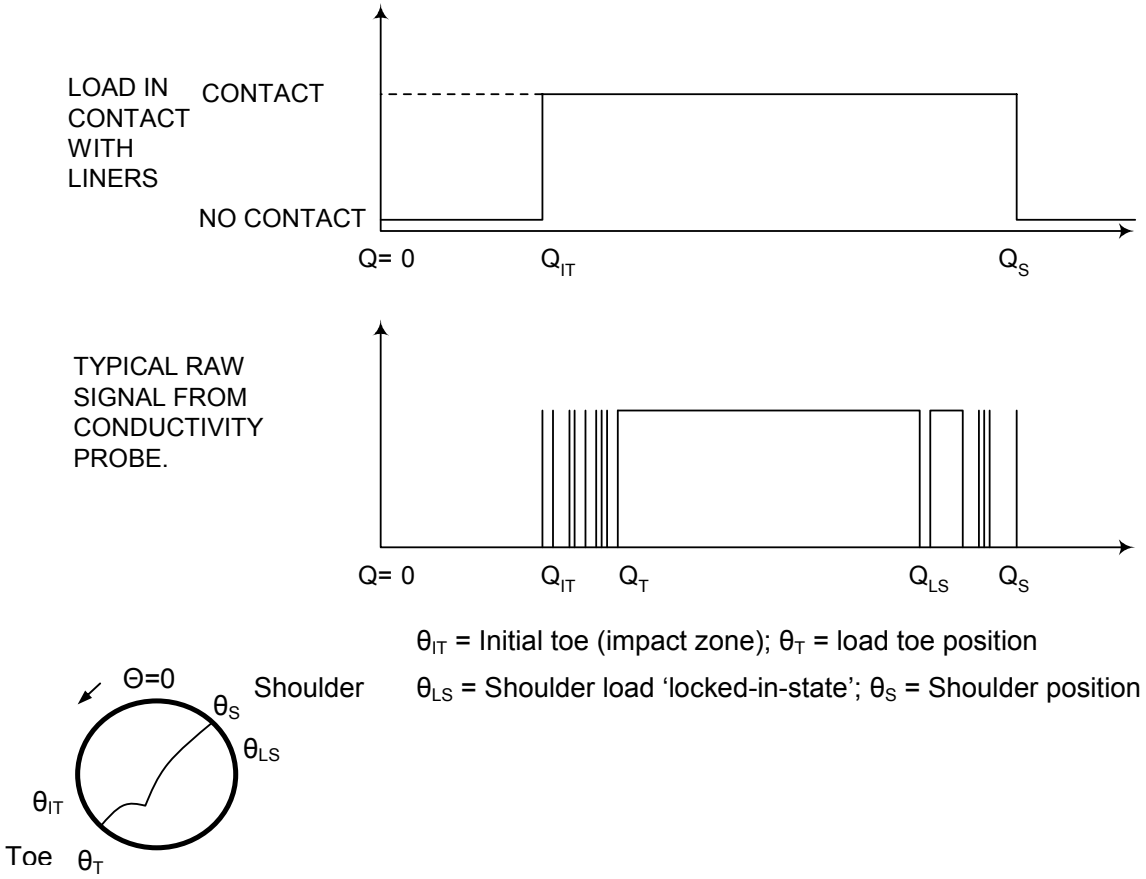
3.4 Data capturing apparatus: Sensor design

The electronic apparatus used to record the signals from the various probes included:

1. a control box consisting of an electronics circuit, a solid-state recording and storage device (Analogue Recording Module (ARM)) and four 12V batteries
2. an infra-red hand held module (used for downloading recorded data from ARM)
3. laptop computer.

In order to maximize the number of revolutions recorded as well as the amount of data that can be recorded per revolution, the ARM sampling rate was set at 5ms i.e. for the current mill speed of 15.5 RPM a signal would be recorded every 0.5 degrees, accumulating to 780 measurements per revolution. With this setting programmed into the ARM's 8 input channels, approximately 42 revolutions per channel (or per probe) were recorded per test i.e. 262080 measurements per test. To enhance the raw data received from the probes prior to them being recorded by the ARM, an electronics circuit was designed, unique for each probe type. Refer to Appendix 1 to review ARM and laptop specifications.

Analogue filters of the signal ensured data was reliably recorded by the ARM. When good contact between a ball, liner and the conductivity probe was made, a 0V output resulted; however in the absence of any contact a 5V signal resulted (Figure 3.5).



θ_{IT} = Initial toe (impact zone); θ_T = load toe position

θ_{LS} = Shoulder load 'locked-in-state'; θ_S = Shoulder position

Figure 3.5: Variation of key conductivity signals during a rotation in the mill.

In the case of the movement probe the raw data from the strain gauges was amplified prior to being recorded by the ARM.

3.5 Experimental Programs

Table 3.1 includes details of the two experimental programs conducted at Matimba's Mill 2C. The main difference between the two programs was the liner geometry i.e. the first experimental program was conducted with Mill-2C having worn internal liners, whereas in the second program the mill had been fitted with new liners. Mill operating conditions and charge composition remained constant i.e. mill speed, mill fill level, ball distribution and particle shape remained unchanged for both programs.

Table 3.1: Details of experimental programs.

	Experimental Program 1 (27 November 02 – 1 December 02)	Experimental Program 2 (30 March 03 – 5 April 03)
Liners	1. Worn shell and conical end liners 2. Rectangular liners located at the two feed ends of the shell incorporated a 'single diagonal lifter arrangement'.	1. New shell and conical end liners 2. Rectangular liners located at the two feed ends of the shell incorporated a 'dual diagonal lifter arrangement'.
Probes utilized	6 Conductivity probes 2 Laser signal probes	7 Conductivity probes 3 Laser signal probes 2 Movement probes 1 CCD camera 1 video camera
Tests completed	1 barring-mill test; 6 mill tests	3 barring-mill tests; 11 mill tests

3.6 First experimental program

This program made use of two types of probes, namely: conductivity and photo-detector signals to investigate Mill-2C's ball load behaviour.

This section consists of a description of: the equipment used and their position on the mill; method of installation of each type of probe; and a discussion of observations, problems and conclusions associated with this program.

3.6.1 Probe positions

Figure 3.6 illustrates the positioning of all the experimental apparatus used for the first experimental program.

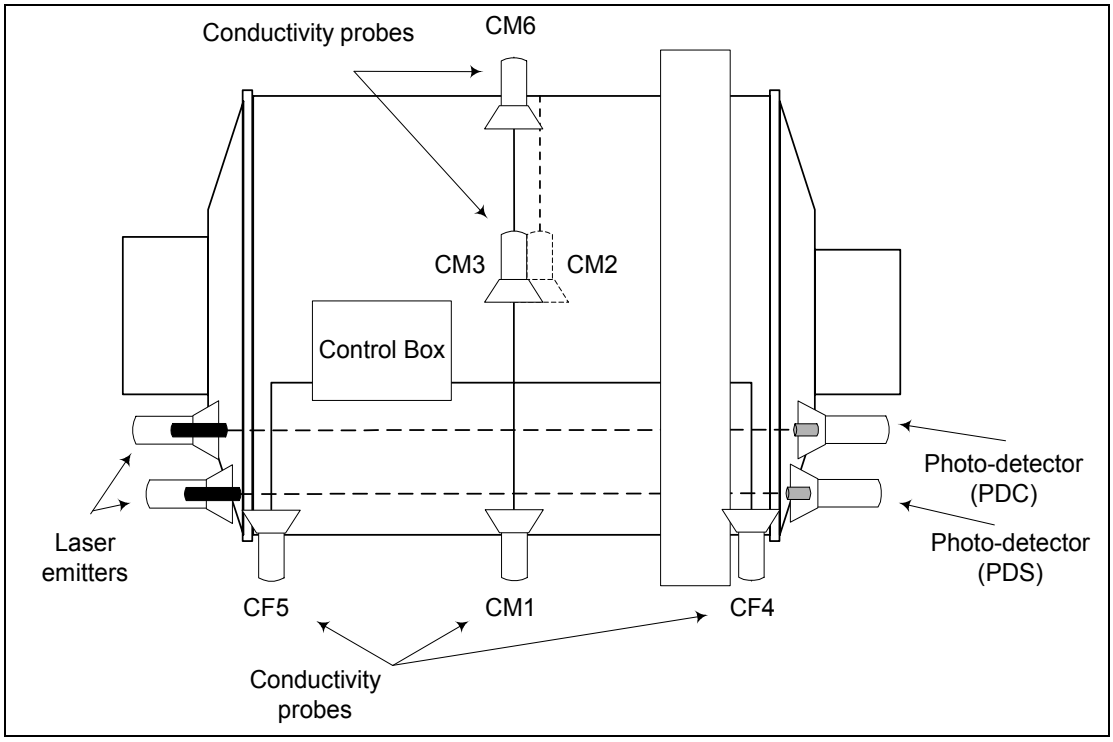


Figure 3.6: Diagram representing experimental apparatus positioning on mill 2C for the first experimental program.

3.6.1.1 Conductivity probes

Three conductivity probes were installed in one row at different positions i.e. the first conductivity probe CF4 was installed 1150mm from mill non-drive feed end[2], the next probe CM1 located towards the middle of the mill was installed 2400mm from CF4 and the third probe CF5, 2700mm from the previous. The remaining three conductivity probes (CM2, CM3 and CM6) were positioned around the circumference at the 'middle'[3] of the mill

[2] Length of 1150mm was measured from the shell non-drive end inner flange wall (facing the shell) to the centre of the first rectangular shell liner bolt.
[3] 'Middle' of the mill is referred to as the distance of 1150mm + 2400mm = 3550mm, measured from the non-drive end inner flange to the middle of the shell liner bolt. Due to the mill's liner bolt-hole arrangement, no probe could be installed at the exact middle distance of 3700mm (i.e. 7400mm/2).

length. This meant that there was a probe at 90 degree intervals around the mill circumference at this point on the mill length.

3.6.1.2 Photo-detector signal probes

Two sets of laser emitters and photo-detectors were used. They were positioned in line with the three conductivity probes (CF4, CM1, CF5) at different heights on the shell conical end liner (Figure 3.7). PDS (or photo-detector closer to mill shell) and corresponding laser were positioned directly opposite each other at a perpendicular height of 193mm from the mill shell (or radius of 2177mm from mill centre). PDC (or photo-detector closer to mill centre) set were also positioned directly opposite each other at a perpendicular height of 514mm from the mill shell (or radius of 1855mm from mill centre). Both the laser emitters were mounted at the non-drive end of the mill facing their corresponding photo-detectors mounted at the mill drive side.

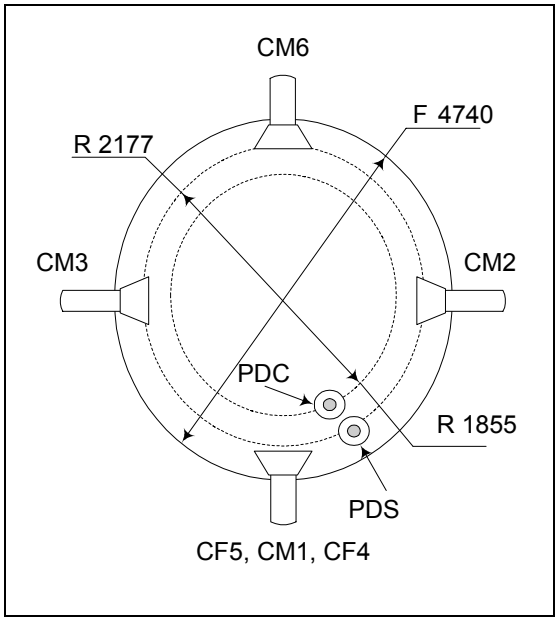


Figure 3.7: Experimental apparatus positioning on mill 2C for the first experimental program, indicating conductivity and photo-detector probe locations.

3.6.1.3 Marker Signal

The positioning and method used for locating a reference point per mill revolution was identical for both experimental programs. A laser emitter and photo-detector, identical to

that used for the laser signal probe were placed inside a PVC housing which was glued onto two steel plates. The steel plates (4mm thick, 30mm wide by 150mm long) had been pre-drilled to suit the mill's liner bolt-hole diameter of 27mm. The plates were then mounted onto two mill shell liner bolts, of the same row in such a way so that the laser emitter and photo-detector were facing each other. A steel plate (4mm thick, 80mm wide by 130mm long) was then permanently positioned between the laser set, so as to obstruct and effectively break the laser signal each time the mill completed a revolution. Refer to Appendix 3 to view pictures of the marker signal set-up on installation.

3.6.2 Electronics circuit

The circuitry was designed to transfer raw signals or raw-hold signals to the ARM device dependant on which signal or combination was required.

The raw signal refers to the signal as received by the ARM device. The raw-hold signal incorporated one mono-stable multi-vibrator which was used to hold any incoming raw signal for a 6ms period, thus minimizing the chances of missing instantaneous incoming signals. This way the raw-hold signal made it easier to interpret incoming data produced by the probes.

3.6.3 Installation of experimental equipment

The installation and commissioning of the experimental equipment took approximately 3.5 days to complete while testing and dismantling took approximately 8 and 5 hours, respectively (refer to Appendix 4 to review experimental program schedule).

The entire milling circuit was off line for the installation part of the experiment, however barring of the mill was permitted. Access to the mill was through the hot box's[4] inspection door. On entering the hot box area, entry to the mill was through the screw conveyor (810mm diameter by 3950mm long).

[4] Hot box refers to the raw coal feed compartment. When the mill is in full production coal and primary air are fed to the mil via the hot box.

3.6.3.1 Conductivity probe installation

Conductivity probe positions were identified and marked and existing liner bolts were removed. The mill was then inched to the most suitable position for probe installation and the brake was applied i.e. this method results in the ball load inside the mill to rest at an incline position, thus allowing access to the lower most point of the mill shell, and hence liner bolt. Conductivity probes were then inserted from inside the mill while the PVC locating washers were positioned in place from the outside of the mill. These washers were not only used to position the conductivity probes in position but ensured that they would be electrically isolated from the mill shell throughout the experimental process.

Probe steel spacers where then added to the top of the bolt so that the probe extended approximately 9mm above the lifter. Once in position, using a multi-meter, the probe was tested to determine whether it was electrically isolated from the shell and shell liner. Thereafter, a quick setting polyurethane surface casting resin elastomer (refer to Appendix 1 for specifications) was used to fill the gaps between the probe, the mill liner and mill shell. The resin took approximately six hours to cure and once it solidified, the resin overflow was ground off so as to maximize the probability of electrical conductivity. Similar process was performed on the remaining five conductivity probes.

3.6.3.2 Photo-detector and laser signal probe installation

The locations for the detectors and lasers were marked at each of the mill's conical ends; existing end liner bolts were removed and replaced with the laser emitter and photo-detector probes. Power was then supplied to the emitter in order to align its beam with the detector installed at the opposite end of the mill. Quickset Pratley epoxy putty was used to set and secure the transmitter in place. A similar process was performed on the other laser signal probe set.

To maximize the accuracy of the photo-detector return signals, high-quality shielded wire resistant to both heat and electrical noise was used for all photo-detectors connections.

3.6.3.3 Control box installation

The positioning of the control box was identical for both experimental programs. The control box was mounted to a steel base (4mm thick by 310mm wide by 388mm long) and thereafter secured on the mill shell via two liner bolts. Once the box was secured all signal wires from the various probes were connected to it.

3.6.4 Experimental procedure

On positioning of all probes and connection of all wiring to the control box, experimental test details (including configuration commands, recording start times etc.) were programmed into the laptop using ARM supplied software. During this time, power to the control box circuitry and ARM device was activated. Once programming was complete, program code was sent to the ARM device via a hand-held infra-red module which was connected to the laptop's serial port. On completion of this process, Mill 2C was started. Depending on the nature of the particular test, once the test details were sent to the ARM, recording of data from the ARM device would commence either immediately or after a pre-defined delay. Mill tests lasted between 3 to 6 minutes at a time, depending on whether a pre-programmed delay was set. Delays were set in some tests so that the ARM could log data once the mill had already reached steady state conditions.

On completion of a test, the mill was stopped and the ARM data was downloaded using the infra-red hand held module. Once downloading was complete, the ARM software allowed for a graphical display of the recorded data. This was not sufficient enough to analyse any of the data in detail, however it provide for a quick check on whether the pre-programmed data was recorded and that all the probes were operational.

The above routine was repeated for every test. This procedure was discussed prior to all the testing with Eskom project personnel.

3.6.5 Observations

3.6.5.1 Milling area

The milling area was neat and ordered, free of any grease and ore deposits. It was however quite dusty and noisy making communication and working conditions difficult at times. Matimba's ball mills were enclosed with noise absorbing panels, assembled together to form an acoustic hood, leaving only the drive arrangement uncovered. Access to the mill from ground level was via the 'mill room' doors. The mill room formed part of the base of the acoustic hood and proved highly beneficial as by closing the mill room's doors the noise from the power station was dampened.

The power station is geared at performing any task as safely as possible. Besides it being compulsory to wear safety gear at all times inside the station, permits were required for almost every task concerning the mill i.e. opening of hot box doors; barring of the mill etc.

3.6.5.2 Mill 2C

Prior to the installation of any experimentation equipment it was agreed with Matimba to remove as much PF from inside the mill as possible. Two important reasons supported this decision: firstly, experimental apparatus did not meet intrinsically safety standards; secondly, laser detectors could not operate effectively in dusty conditions.

Removal of the PF was carried out by operating the mill with primary airflow for approximately four hours. The primary air fed to the mill in this instance is not preheated it is simply drawn from the atmosphere. Even though most of the PF was removed from the mill load, a thick layer (approximately 15mm) of dust (Figure 3.8) was found below the screw conveyor proving that this method of PF removal was not very effective. Also, by running the mill to remove the PF, the temperature inside the mill increased to approximately 35°C. This temperature decreased slowly over the next 48hours, even with the hot box inspection door wide open. A short burst of air from each feed end (lasting 5 sec at a time) was pumped through the mill every 0.5 hours. This was done to improve air circulation while working inside the mill.



Figure 3.8: Picture of screw conveyor taken from inside the mill shell (mill rotates in an anti-clockwise direction). Picture indicates the approximately 15mm thick layer of coal dust present inside the mill.

3.6.5.3 Ball size distribution

During the installation of the probes the mill was constantly barred with the load either being at an incline (by applying the barring brake) or level (by allowing the mill to come to rest under the influence of gravity). At one of these instances while work was performed on the conductivity probes, the load distribution was observed at different areas of the mill. Figures 3.9 and 3.10 show two pictures of the ball load, 800mm from the feed drive end of the mill, at depths of approximately 100mm and 170mm, respectively. The top layer of balls was carefully removed each time until a 100mm, and thereafter 170mm depth was reached.

By closely inspecting the ball charge one can observe that the size distribution decreases at a decreasing rate from 40mm diameter balls to 10mm cubes. This behaviour was common at three different locations in the mill.

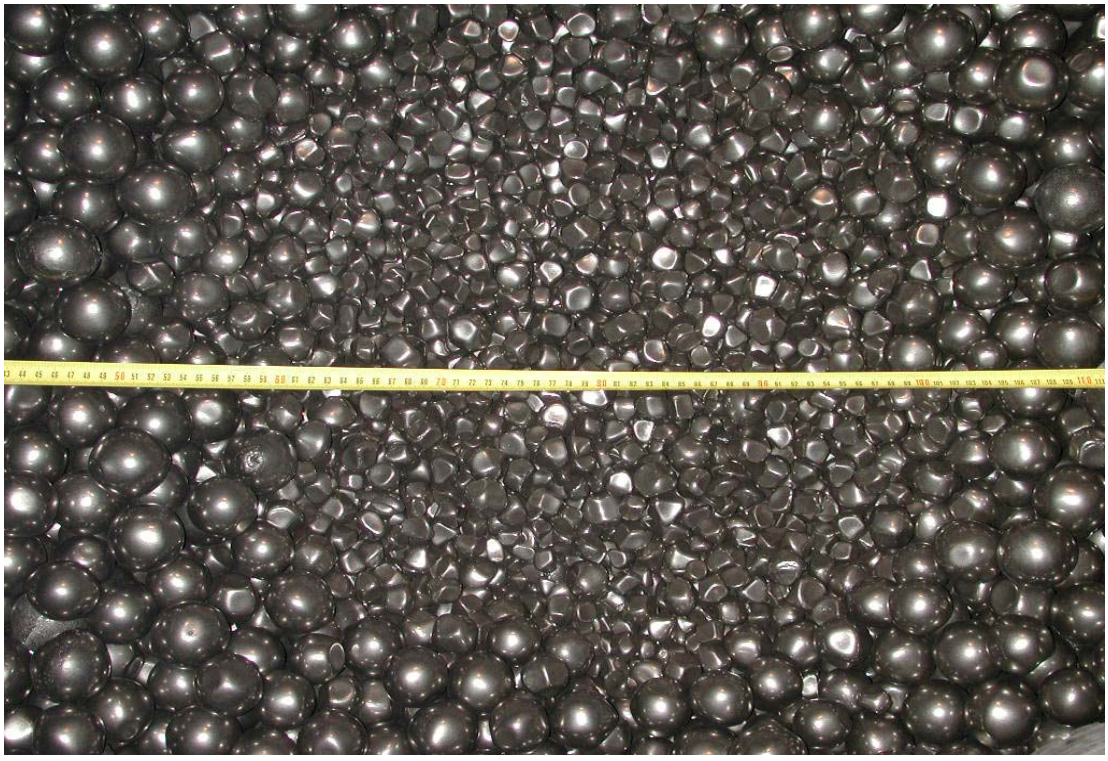


Figure 3.9: Ball load distribution at the surface; 800mm from mill feed drive end in a hole 100mm deep after barring.



Figure 3.10: Ball load distribution at the surface; 800mm from mill feed drive end in a hole 170mm deep after barring.

3.6.6 Problems

A number of technical problems were encountered in the installation, commissioning, operation and dismantling phases of the project. Furthermore, project allocated time was shortened to just under five days as opposed to the initially agreed to seven day period.

Problems were encountered in the installation of both the conductivity and laser signal probes. The wear pattern of the shell liners made the shell liner hole dimensions smaller, thus making it harder to electrically isolate the conductivity probes from the liner. Even though the wear pattern was similar for all shell liners, each shell liner hole dimension was unique, thus modifications needed to be performed per probe to ensure good electrical isolation.

Setting up of the laser and receiver units was also a time consuming task. Even though the bolts were machined to cater for the conical ends, positioning of each laser to focus on the receiver (approximately 7.4m away) proved to be quite challenging.

Once all the wiring was connected, prior to mill testing, the ARM device was programmed and a barring test was completed. The results of the test were graphically displayed using ARM software. The graph indicated that all the probes resulted in ‘on’ signals except for the laser signal data from the receivers (PDC and PDS) and the data from the conductivity probe located at the non-drive end (CF5). The connections corresponding to these probes were checked both on the probes and on the internal circuit board. Slight modifications were carried out on the circuitry resulting in CF5 producing ‘on’ signals for raw signals, however due to the time constraints on the project, no further barring tests were permitted to ensure all signals were operating satisfactory.

3.6.7 Conclusions

Six mill tests were carried out. Only six out of the eight probes installed resulted in significant data. Once the data was processed it was noted that the ‘raw-hold’ circuitry could be improved to better interpret the raw data.

Lessons learned from these experiences were used to better plan and improve the design of the probes as well as the electronics circuit to be used in the second experimental program.

3.7 Second experimental program

This program made use of three types of probes, namely: conductivity, laser signals and movement probes to investigate Mill-2C's ball load behaviour. A CCD camera and video camera were also used to record the mills behaviour. This section consists of a description of the equipment used and their position on the mill; method of installation of each type of probe; and a discussion of observations, problems and conclusions associated with this program.

3.7.1 Probe positions

Figure 3.11 illustrates the positioning of all the experimental apparatus used for the second experimental program.

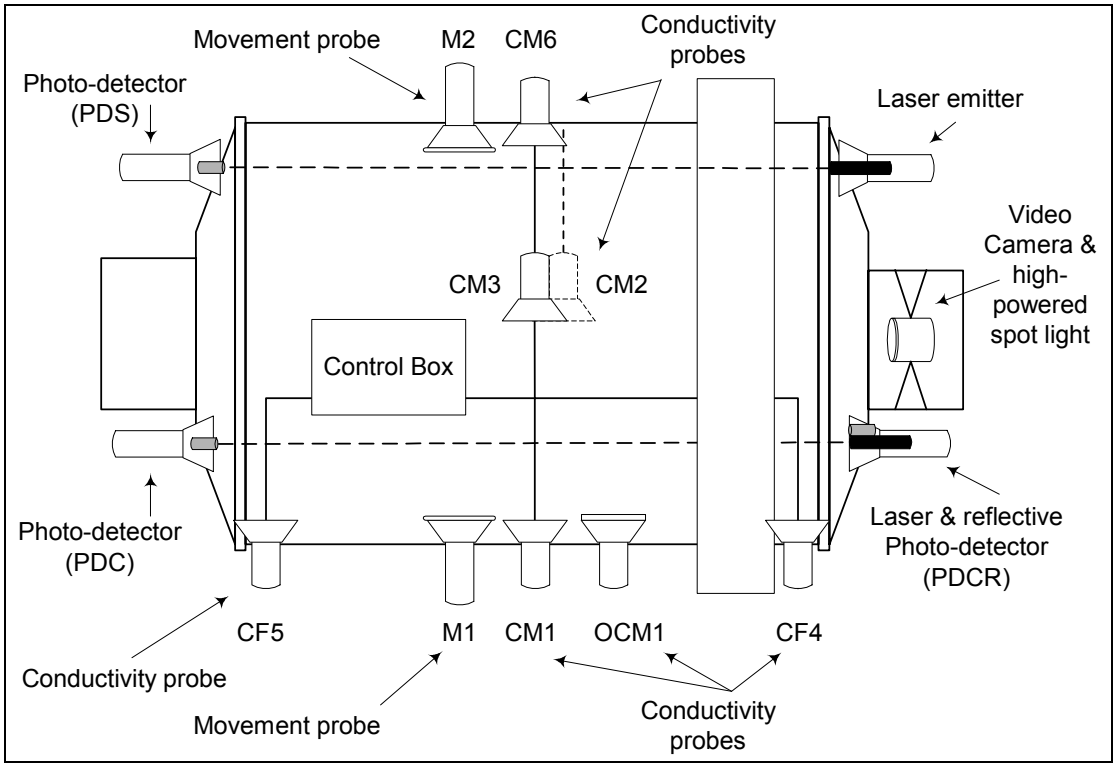


Figure 3.11: Experimental apparatus positioning on mill 2C for the second experimental program.

3.7.1.1 Conductivity probes

The location and positioning of the conductivity probes were altered slightly compared to the first program; the 'middle' conductivity probes positioned at 90 degree intervals remained unchanged; probes CF4 and CF5 however were installed closer to the feed ends of the mill i.e. each probe was installed approximately 300mm as oppose to 1150mm from the mill shell inner flange wall. An additional conductivity probe OCM1 was installed on the same row as CF4 and CF5 positioned next to CM1 (or 3842mm from the shell non-drive end inner flange wall to bolt centre).

3.7.1.2 Laser signal probes

The relative positions of the probes remained constant (Figure 3.12), however their locations were changed i.e. PDS was positioned diagonally across PDC with both detectors mounted at the mills non-drive conical end, capturing the same load paths as in the first program.

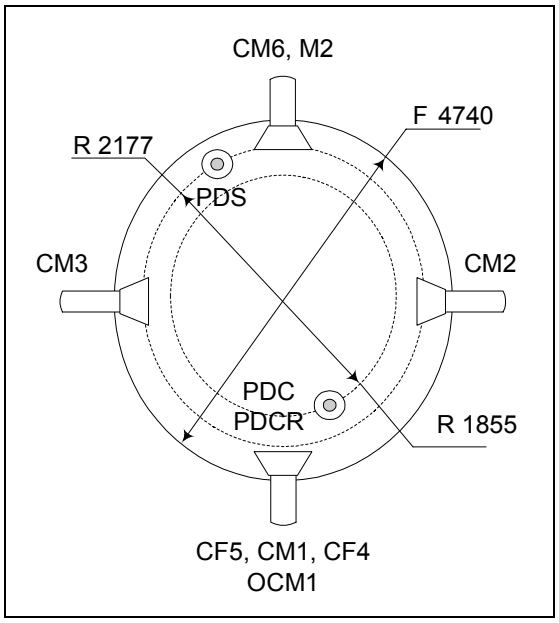


Figure 3.12: Experimental apparatus positioning on mill 2C for the second experimental program, indicating additional conductivity, photo-detector and movement probe locations.

An additional photo-detector was installed with PDC's laser emitter. The purpose of this probe was to detect ball reflection (PDCR).

3.7.1.3 Movement probes

No movement detection probes were used in the first program. Two movement probes (M1 and M2) were used in this program: one positioned in the same row as the four conductivity probes 4146mm from the mill non-drive end (or 596mm from CM1); and the other directly opposite the first (positioned next to CM6).

3.7.1.4 Camera

No cameras were used in the first experimental program. This program consisted of two different types of camera probes, used at two different instances. In both of these instances, the cameras were placed 1120mm away from the mill load, inside the mill's screw conveyor (measuring 810mm diameter by 3950mm long). Each camera was mounted at the cross-centre of two 810mm long, 20mm square tubes, wedged in place, positioned perpendicular to one another inside the screw conveyor. Refer to Appendix 3 to view camera installation pictures.

3.7.2 Electronics circuit

To increase the sensitivity of the probes, the raw signal from the probes was connected to a mono-stable multi-vibrator set at 6ms and thereafter an OR gate i.e. if an instantaneous contact was made lasting less than 6ms, the OR gate would select the multi-vibrators 6ms hold signal to send to the ARM, however if the signal lasted for more than 6ms, the longer signal would be sent to be recorded by the ARM (Figure 3.13). These circuits increased the accuracy of the data extracted from the probes and in turn minimized the chances of any data been 'lost'. The ARM would be progressively less likely to sense voltage spikes of less than 5ms, because it was preset to record signals every 5ms.

The circuitry also allowed for multiple signals to be recorded simultaneously from one probe i.e. the ARM would use three channels to simultaneously record conductivity probe raw, raw-hold and OR-Gate data signals.

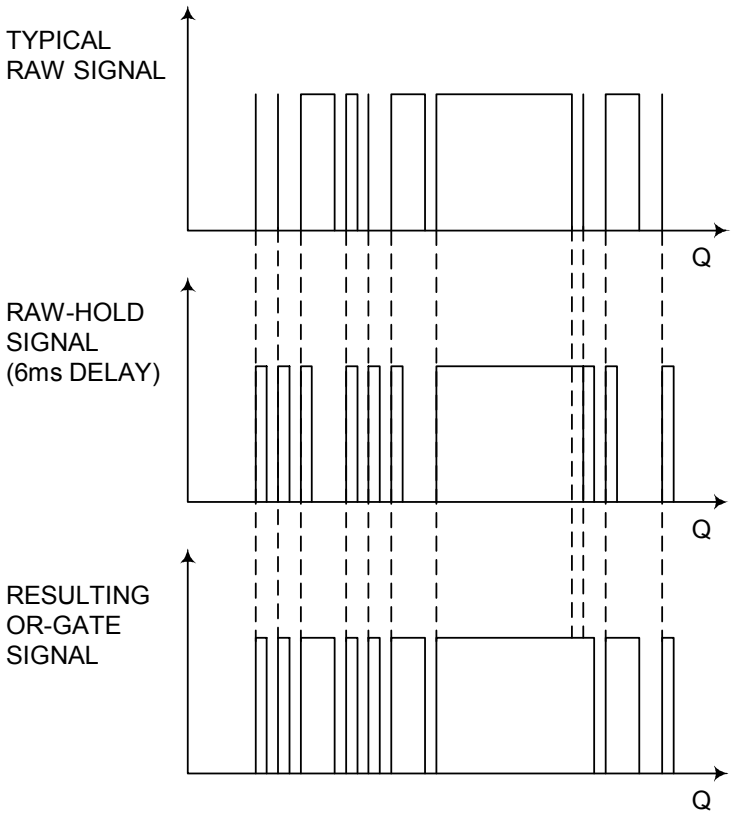


Figure 3.13: Graphical illustration indicating how a typical raw signal is transformed using raw-hold and OR-Gate signals.

3.7.3 Installation of experimental equipment

The installation and commissioning of the experimental equipment took approximately 4 days to complete while testing and dismantling took a further 2 days (refer to Appendix 4 to review experimental program schedule).

A similar approach was adopted in the installation of the probes as per the first experimental program. The sections below emphasize the differences in installation techniques carried out between the different experimental programs.

3.7.3.1 Conductivity probe installation

Two main differences existed between the two programs, namely: conductivity probe spacer height above liners and the insulation material used to electrically isolate the

probes from the liners. In the first program, the spacers protruded between 7-10mm above the liner. In the second program, all conductivity probes with the exception of OCM1, protruded between 2-4mm above the mill liner. OCM1 protruded approximately 9mm above the liner.

As a result of the long curing time required for the resin to solidify, quickset Pratley epoxy putty was used electrically isolate the conductivity probes from the shell liners. This process speeded up the installation process by approximately 4 hours per probe.

3.7.3.2 Movement probe installation

Only one movement probe M1 was installed. The existing shell liner bolt (lying 596mm from CM1) was removed and the movement probe bolt was inserted. A steel-to-rubber adhesive was used to glue the rubber washer to the steel disc and shell liner. The bolt and strain gauge was then secured in place from outside the mill. Quickset Pratley putty was used to secure the base to the mill shell.

3.7.4 Observations

3.7.4.1 Mill 2C

Liner replacement commenced on the 1st of December 2002. Five working days were required to replace the mills existing worn liners with new. The design and shape of the new shell liners were identical to that of the old ones except for the diagonal liners located at the ends of the mill shell. The new liner replacement included diagonal liners with a dual lifter arrangement as opposed to the single diagonal lifter arrangement previously used.

From time of liner replacement (December 2002) until the second experimental program (April 2003), the mill was on a maintenance program, this included barring the mill for a few hours every 2-4 weeks. No primary airflow was introduced into the mill while the mill was on set on barring. This resulted in a substantial build-up of PF inside the mill, as even though a liner change is performed on the mill, a small percentage of PF still exists within the ball load. To reduce the PF content in the mill, the mil was run at standard operating conditions for approximately three hours.

Contaminants were also found inside the mill, these included: used and new steel liner and end bolts; 10-pound hammers; and one screw conveyor drive rod (solid steel round bar measuring 100mm diameter by approximately 400mm long). It was important to rid the mill of these steel objects as any direct impact with the probes during mill operation would damage them.

3.7.5 Problems

3.7.5.1 Marker Signal

One main problem which consumed a large part of the testing phase was the marker signal. It is thought that the problem originated from the vibration generated from the ball load inside the mill at the toe position. These vibrations would cause the emitter and receiver to vibrate thus decreasing the chances of establishing a constant direct signal from the laser emitter to the photo-detector, thus instead of recording one sharp ‘on’ signal per mill revolution corresponding to the steel plate ‘breaking’ the constant ‘off’ signal (indicating the reference point), many random ‘on’ signals would result making it difficult to accurately identify the reference point. This problem was resolved by stiffening the base of both the laser emitter and receiver. Rigidity was achieved by utilizing quickset epoxy putty to act as a support structure at the ends of the emitter and receiver steel plates.

3.7.5.2 Conductivity probes

The quickset putty used to isolate the conductivity probes from the shell liners decreased the installation process significantly, however, because of its rough surface finish, small steel particles tended to collect between the probe and steel liner, resulting in constant ‘on’ signals recorded by several probes for various revolutions during a test. This phenomenon tended to increase as the testing continued and was not easily identified by the ARM graphical display which was observed after each test. Figure 3.14 shows small steel chips accumulating between the conductivity probe and steel liner resulting in a constant ‘on’ conductivity signals.



Figure 3.14: Steel particles collecting around conductivity probe (CM1).

3.7.5.3 Laser probes

Laser signal readings also proved to be problematic. Out of the five experiments set up to record laser signals only two were successful. Close inspection of the laser emitters during the tests indicated that both were focused directly onto their corresponding photo-detectors. This was strange as all three photo-detectors (PDS, PDC, PDCR) showed no activity during the first two experiments; it is thought that the dusty conditions inside the mill might have affected the detector performance as prior to initial mill testing all three detectors were functioning.

The detectors were inspected again on the second day of testing. The laser emitter positioned closer to the mill centre (focused on photo-detector PDC) had moved slightly as its beam was focused approximately 15 cm from PDC[5]. The second emitter focusing on PDS was not operational; it's thought that a ball must have impacted onto the face of the emitter.

[5] The laser emitters emit a laser signal approximately 7.4m away from the source, thus small changes on the emitter position result in large changes at the opposite mill end.

3.7.5.4 Movement probe

Besides the constant calibration that needed to be conducted prior to each test, the movement probe was successful at responding to the impacting ball load. Problem in the design of probe is that it detects movement for both lateral and axial directions, thus making it difficult to correctly interpret its data.

3.7.6 Conclusions

The load behaviour was once again successfully recorded from an industrial ball mill. Despite the problems encountered with the reference probe, sufficient data was recorded to study and compare the load behaviour results of the new and used liners.

CHAPTER 4

CONDUCTIVITY, MOVEMENT AND PHOTO DETECTOR DATA

4.1 Introduction

The methodology adopted to process the signal data from all the probes, as well as the results processed from the two experimental programs are presented in this chapter. A comparison of these results and discussion per test is also included.

The conductivity data was the most useful as it was successfully recorded in both programs. Movement and photo detector data signals were only recorded in the second program.

4.2 Data processing methodology

The data processing methodology for each probe type was similar. It consisted of the following three stages:

1. Data recorded from the ARM device was downloaded to the laptop via the portable handheld infra-red device connected to the laptop serial port. The data was in the form of voltage signals with their corresponding times. This was graphically displayed using the ARM supplied software (Figure 4.1). The software allowed for the data to be exported as text format, saved as 'Comma Separated Values' (CSV) suitable for importing into a spreadsheet type program.

2. The data was imported into a Microsoft Excel spreadsheet for processing. This included 8 columns i.e. one column per channel or probe, and approximately 32760 rows of data. In order to process the enormous amount of data recorded (262080 data points) per test, a program (written in Visual Basic version 6 (VB6)) was compiled by Ms. Anna Van Nierop, programmer in the Milling Research Group.

3. The data processing programs' main tasks were as follows:
    a. Find and reference all recorded consistent data from the ARM (probes) to the datum (or marker) signal. On mill start-up, where the mill speed is not constant, the first revolution is slightly slower resulting in an incrementally longer first cycle; in this case the program selects the constant cycle time as the initial datum signal. The constant cycle time is defined as the time

recorded per mill revolution at constant mill speed. The program thus allowed for inconsistencies in the datum signal and graphically displayed them per cycle.

b. Calculate the corresponding degree from each time allocated to a data point.
c. Generate plots of data versus degrees.
d. Perform statistical analysis of selected data points.

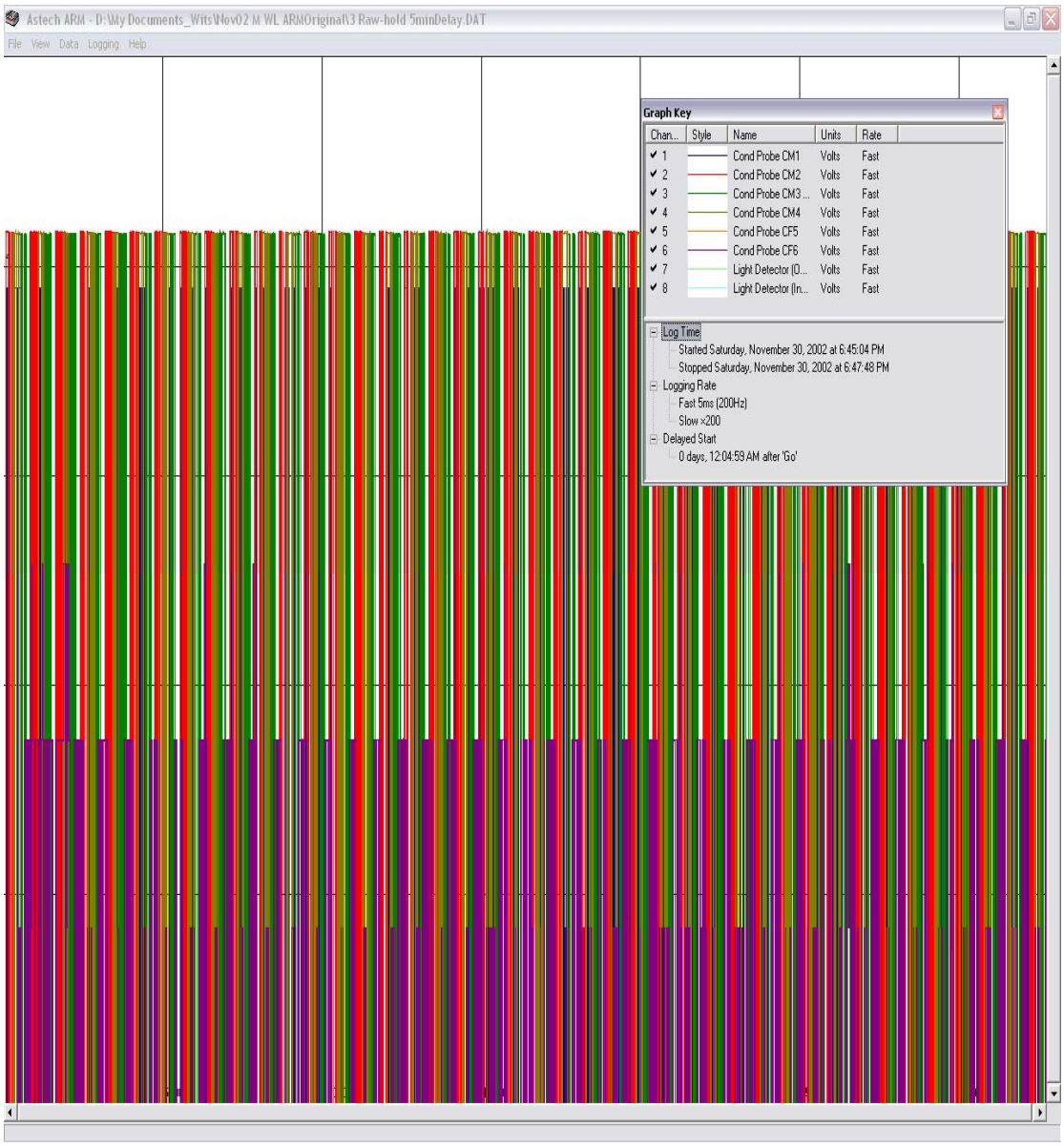


Figure 4.1: ARM graphical display of recorded data from first experimental visit (Nov02, Test 3 (Raw-hold 5minDelay) Cycles (1-42)).

4.3 Conductivity probe data analysis

Three types of electronic signals were used to record conductivity data, namely: raw, raw-hold and OR-Gate signals (as defined in section 3.6.2). The OR-Gate was only added in the second experimental program.

The procedure adopted to process the various conductivity signals was similar however data analysis differed slightly per data type.

4.3.1 Data analysis per cycle

Using the data processing program the recorded signals from the ARM device (per test) were plotted per cycle. Figure 4.2 displays conductivity data processed from the second experimental program; cycles 26 to 30; probe CM1 (positioned at the middle of the mill shell). This graphical display is typical of all the other conductivity type plots, once the mill load reaches steady state conditions.

The initial toe region defined between angular positions θ_{IT} and θ_T is indicated by the primary voltage spikes located between 109° up to 131° (cycle 30). These differed slightly from one probe to another as well as from cycle to cycle, as good contact is required between the balls and specific probe.

After this initial impact region, a constant ‘on’ signal begins to dominate the conductivity curve. This is due to the increasing pressure exerted by the load on the liners which initially increases to a maximum at approximately 180° and then slowly starts to decrease as the load enters the shoulder region (θ_{LS} to θ_S). This agrees with all of the above cycles, however sudden ‘off’ signals (or loss in electrical conductivity) in the data is evident in almost all the cycles, especially in cycle 30. This phenomenon can be attributed to movement of the load over the probe.

The shoulder position is not as turbulent and can thus (depending on signal data type) be more easily defined (Figure 4.2). It’s important however to note that due to the nature of conductivity measurement it’s possible that the ‘actual’ shoulder position lies a few degrees higher than indicated in the experimental data. This is because the resultant force exerted on the shell liners decreases asymptotically as the load reaches the shoulder

position, thus increasing the chances of losing good contact between the ball load and conductivity probes.

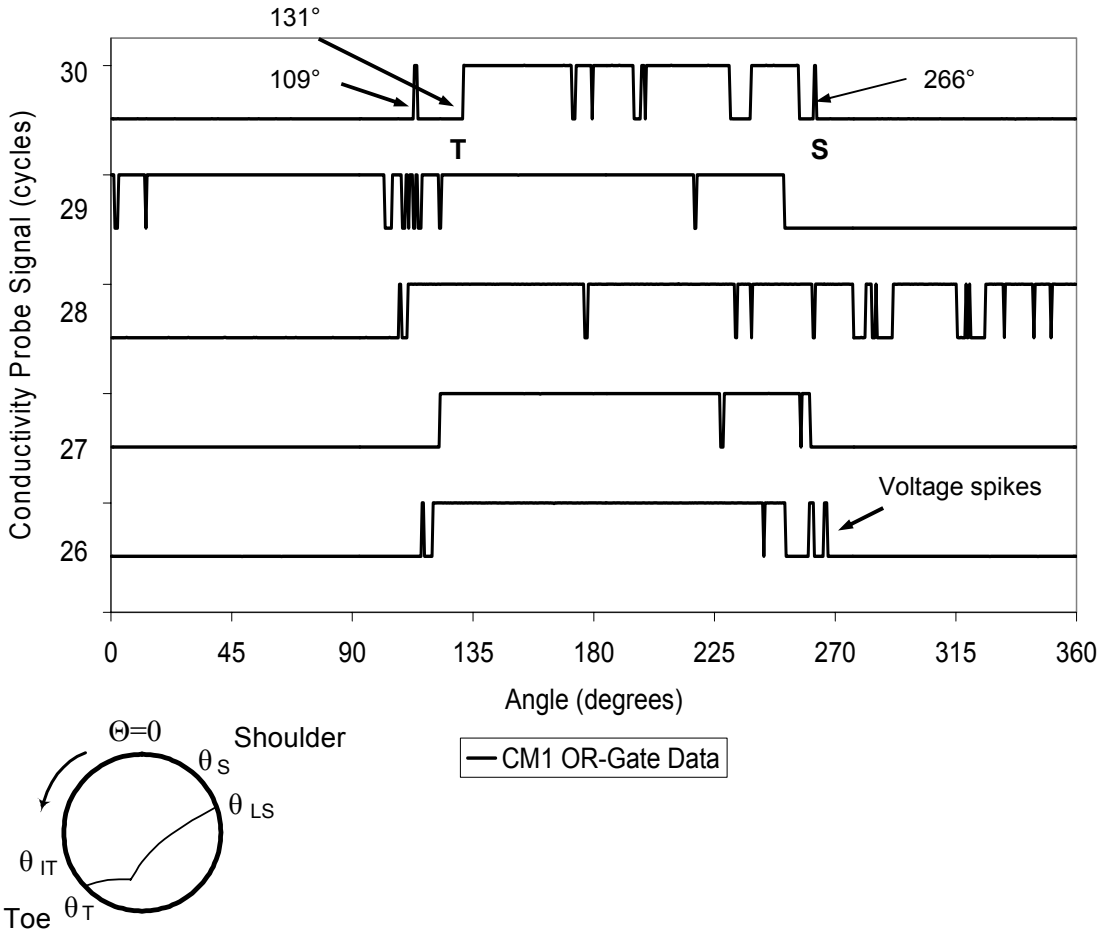


Figure 4.2: An example of typical conductivity probe data profiles from second experimental program (probe CM1, Test 3 (OR-Gate data), Cycles (26-30)). Profile indicates load toe (T) and shoulder (S) positions as well as other load shape characteristics.

A constant ‘on’ signal is observed towards the end of cycle 28 and beginning of 29. It is assumed that this phenomenon occurs due to small steel chip(s) temporarily getting stuck between the probe spacer and neighbouring liner. The design of the probe also plays a role, as the higher it protrudes from the shell lifter, the higher the chances of steel chips clinging on the head of the probe and thus resulting in a constant ‘on’ signal.

4.3.2 Selection of load toe and shoulder positions

The difficulties encountered in defining the initial angular positions (or toe) of the load are owed to the bias imposed per probe due to small difference in probe geometry as well as the fact that this is the most turbulent region of the load. These factors also affected the accuracy in defining the final angular position i.e. at the shoulder position the load pressure is at its lowest, thus decreasing the chances of establishing good electrical contact. This accounts for the voltage spikes arising at end of cycle 26 (Figure 4.2 and 4.3) which is also common with other conductivity signals.

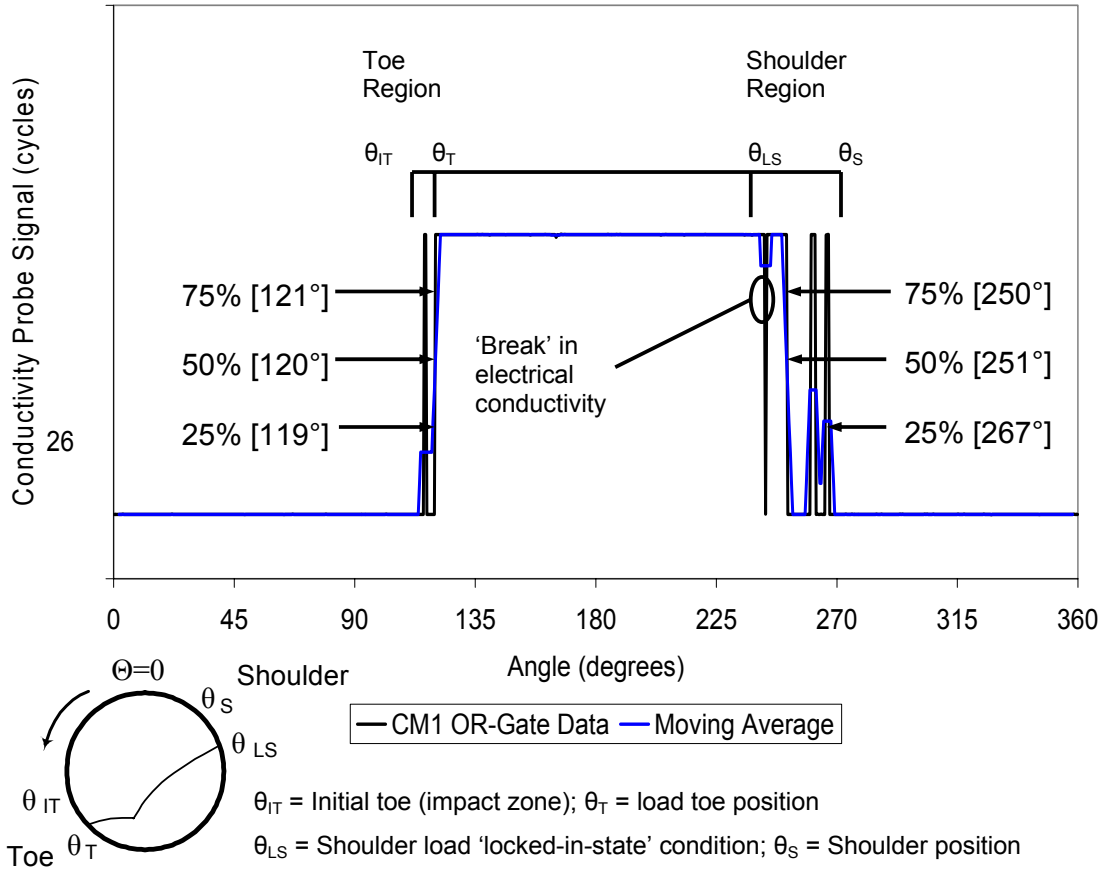


Figure 4.3: Detailed analysis of cycle 26 extracted from second experimental program (probe CM1, Test 3 (OR-Gatedata)). Profile indicates moving average analysis used in the selection of toe and shoulder positions.

To standardize the selection processes the moving average analysis was used i.e. this projects a value of a variable at a given time, based on the average value of the variable,

a specific number n (=4) of preceding and following readings. Nine periods (2n+1) were selected i.e. moving average of 20ms (1.84 degrees) was used to project a trend line over the original data. Figure 4.3 illustrates the moving average trend line projected over the original cycle 26 data curve.

Data collection process per cycle was then initiated. Beginning from the first cycle, the program would trace the moving average trend line and record degree measurements corresponding to 25, 50 and 75 per cent of the voltage signal i.e. two sets of degree measurements would be recoded per 25 per cent increment, one representing the toe and the other the shoulder position.

The recording process per cycle starts from left to right (or from 90° to 180°) for toe positions and from right to left (315° to 180°) for shoulder positions. Based on the mill's operating parameters and hence internal load behaviour characteristics, signals lying between angles 315° forwards to the next 90° were not accounted for in the load toe and shoulder statistical analysis. In addition the program rejected 'breaks' in conductivity signals (Figure 4.3) which are assumed to have occurred due to a reduction in load pressure and hence a loss in electrical contact.

Table 4.1 presents toe and shoulder position results corresponding to Figure 4.2 conductivity data profiles.

Table 4.1: Toe and shoulder results produced from the data processing program using moving average analysis. Data used for the analysis was extracted from the second experimental program, probe CM1 (Test 3 (OR-Gatedata), Cycles (26-30)).

	Toe			Shoulder		
Cycle No.	25%	50%	75%	75%	50%	25%
26	119.25	120.17	121.09	250.32	251.24	267.81
27	121.89	122.80	123.72	259.53	260.45	261.37
28	109.00	110.83	111.75	-	-	-
29	-	-	-	249.86	250.78	251.70
30	112.21	131.55	132.47	255.34	256.26	257.18

Even though the data processing program allowed for the moving average data points to be automatically selected, this method was not fool-proof i.e. a constant 'on' signal (as at the shoulder region of cycle 28 and toe region of cycle 29 (Table (4.1)) results in either the toe, the shoulder or entire cycle to be considered invalid. Thus, prior to statistically analyzing the results all data produced via the program would need to be verified against their corresponding plots.

Approximately 42 cycles were recorded per test. The first seven cycles were omitted from the statistical analysis, as at times the ARM would initiate logging several seconds prior to mill start-up. Incorporation of this data would result in an inaccurate analysis. The main statistical tools used to compare the different tests included calculation of the arithmetic mean, variance, standard deviation and coefficient of variation.

4.4 Conductivity probe results and discussion: First program

Apart from the mill barring test, six other tests were conducted in this program: three tests used raw-hold type signaling; while the remaining three used raw type filtering to capture probe data (Table 4.2).

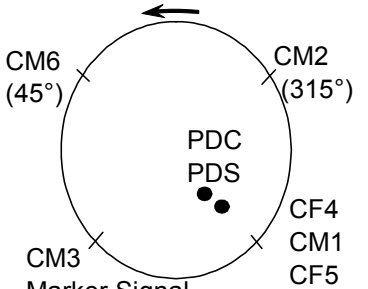
For four of these tests, data logging was initiated from mill start-up whereas in the remaining two tests, data was recorded after a pre-defined time delay. The test schedule (Table 4.2) allowed for comparative analysis between tests 1 (or 2) with test 4 and between test 3 and test 5.

Each probe signal per test was also graded. Grading was primarily based on the amount of complete cycles recorded per test; this was broken up into three main categories:

1. Good test data: Indicates that greater than 70 per cent of its data was processed and used in the statistical analysis i.e. recorded numbers of cycles lie between 24 up to 37 cycles per test.
2. Average test data: Indicates that 40 to 70 per cent of data could be processed.
3. Poor test data: Indicates that less than 40 per cent of the data was processed.

Thus, the lower the number of quality cycles recorded, the higher the uncertainty of the resulting statistical data.

Table 4.2: First experimental program (worn liner) test schedule, indicating: conductivity probe and signal type used per test; quality of recorded data; and test details.



		TenMin Barring Filtered Data No delay	Raw-holdNoDelay	Raw-holdNoDelay	Raw-hold5minDelay	RawNoDelay	Raw5minDelay	Raw 2minDelay High-Speed sampling
	Test No.	0	1	2	3	4	5	6
Conductivity Probes								
End probes								
CF4 Conductivity/Feed (225 degrees)			RH	RH	RH	R	R	
CF5 Conductivity/Feed (225 degrees)			RH	RH	RH	R	R	
Middle probes								
CM6 Conductivity/Middle & Datum (45 degrees)			RH	RH	RH	R	R	RH
CM3 Conductivity/Middle (135 degrees)			RH	RH	RH	R	R	
CM1 Conductivity/Middle (225 degrees)			RH	RH	RH	R	R	
CM2 Conductivity/Middle (315 degrees)			RH	RH	RH	R	R	
Additional test data	Units							
Logging rate	freq.	50	200	200	200	200	200	200
Logging rate	ms	20	5	5	5	5	5	500
Mill 2C Operating Duration	min	11:25	3:00	3:30	8:45	3:30	8:45	4:00
ARM - Delayed Start	min	0	0	0	5	0	5	2
ARM - Logging Start	time	16:32:30	17:50:49	18:09:32	18:45:04	20:12:19	20:47:57	21:15:22
ARM - Logging Finish	time	16:43:25	17:53:33	18:12:15	18:47:48	20:15:02	20:50:41	21:16:06
ARM - Logging Time	time	0:10:55	0:02:44	0:02:43	0:02:44	0:02:43	0:02:44	0:00:44

Key

1. Filtering method used for recording data	R	Raw
	RH	Raw-hold
2. Quality/Consistancy of data		Good (> 70% of useful data)
		Average (between 40-70% of useful data)
		Poor (< 40% of useful data)

Tests 1, 2, 3, 4 and 5 were processed, statistically analysed and discussed. Test 1 is of identical nature to test 2, this was specifically carried out to determine the reproducibility of the raw-hold signal results. Test 6 measured laser signal data.

Table's 4.3, 4.4 and 4.5 present statistical results of the load toe and shoulder positions. Table 4.3 and 4.4 present data processed from the raw-hold signal (tests 1, 2 and 3), while Table 4.5 presents data processed from the raw signal (tests 4 and 5).

4.4.1 Analysis of experimental data and results

Two sets of probe results were excluded from the statistical analysis, namely probes CM1 (located at centre of mill shell) and CF5 (located at the non-drive end of the mill).

Graphical representation of CM1's test 1 (raw-hold) results showed minor voltage spikes occurring at the early stages of each cycle between 45 and 115 degrees. Because of the low magnitude and short duration of these voltage spikes, the moving average trend line would seldom reach the 25 per cent mark of the accumulated voltage signal and hence these signals would not be recorded in tests 1 and 2 results (Appendix 5, Figure A5.1).

The magnitude and duration however increased per test resulting in a large concentration of voltage spikes at the early stages of each cycle in test 3 (Appendix 5). This high voltage concentration affected the moving average calculations and in turn the data selection process resulting in the overall sample number and hence the amount of quality cycles to less than half of the 37 cycles analysed. CM1's probe results for test 3 were omitted from Table 4.3. Two explanations thought to describe this phenomenon: either the electronics circuit was faulty or an accumulation of small pieces of worn steel particles clinging between the probe and steel liner caused the voltage spikes. CM1's raw data plots (tests 4 and 5) displayed no irregular voltage spikes at the initial stage of each cycle, thus it is believed that the fault lay with the electric circuitry.

A problem with the electric circuitry resulted in no data being recorded by probe CF5 for the first three tests (raw-hold data type), Tables 4.2 and 4.3. The fault was later rectified allowing for probe CF5 data to be recorded for tests 4 and 5 (Table 4.4).

Table 4.3: First experimental program conductivity toe and shoulder position statistical results. Raw-hold signal (Tests 1 and 2).

	First Program: Test 1 Raw-holdNoDelay						First Program: Test 2 Raw-holdNoDelay					
	Toe (degrees)			Shoulder (degrees)			Toe (degrees)			Shoulder (degrees)		
	25%	50%	75%	75%	50%	25%	25%	50%	75%	75%	50%	25%
End probe data CF4 (225 degress)												
Minimum	137.99	151.34	156.95	236.97	237.89	238.81	140.29	156.41	164.23	238.81	239.73	242.03
Maximum	166.61	177.64	179.02	257.23	258.15	274.20	171.14	176.20	177.12	254.89	263.62	265.92
Sample Number	36	36	36	36	36	36	36	36	36	36	36	36
Arithmetic Mean	158.80	162.45	165.09	248.54	250.18	253.32	162.11	165.62	169.02	246.39	249.24	253.19
Arithmetic Mean AVERAGE		162.11			250.68			165.58			249.60	
Midrange	14.31	13.15	11.03	10.13	10.13	17.69	15.42	9.90	6.45	8.04	11.94	11.94
Range	28.62	26.30	22.07	20.26	20.26	35.38	30.84	19.80	12.89	16.07	23.89	23.89
Variance	31.75	27.13	25.66	25.38	25.32	40.85	31.19	12.50	11.27	15.05	21.73	35.92
Standard Deviation	5.63	5.21	5.07	5.04	5.03	6.39	5.58	3.54	3.36	3.88	4.66	5.99
Middle probe data CM6 (45 degrees)												
Minimum	138.91	141.09	154.43	251.24	252.16	254.00	134.20	144.44	147.20	254.27	256.57	259.71
Maximum	161.32	163.31	166.99	269.19	271.50	282.08	165.15	166.07	166.99	266.25	269.19	309.83
Sample Number	36	37	37	36	36	36	36	36	36	36	36	36
Arithmetic Mean	151.46	155.40	160.15	260.82	262.63	264.96	153.64	157.43	160.52	260.39	262.87	270.53
Arithmetic Mean AVERAGE		155.67			262.81			157.20			264.60	
Midrange	11.20	11.11	6.28	8.98	9.67	14.04	15.48	10.82	9.90	5.99	6.31	25.06
Range	22.41	22.22	12.57	17.95	19.34	28.08	30.96	21.64	19.80	11.98	12.62	50.11
Variance	37.75	28.64	11.12	20.25	24.22	35.05	54.51	26.91	14.22	8.76	8.14	124.60
Standard Deviation	6.14	5.35	3.33	4.50	4.92	5.92	7.38	5.19	3.77	2.96	2.85	11.16
Middle probe data CM3 (135 degrees)												
Minimum	137.76	150.19	151.11	245.34	249.02	249.94	149.27	154.80	158.02	253.46	254.69	256.99
Maximum	161.70	165.80	167.64	266.66	267.87	270.17	169.57	170.49	171.41	267.29	269.14	279.28
Sample Number	37	37	37	37	37	37	36	36	36	36	36	36
Arithmetic Mean	154.40	158.97	160.81	260.13	261.46	263.71	158.86	161.12	163.06	260.49	261.82	264.15
Arithmetic Mean AVERAGE		158.06			261.77			161.01			262.16	
Midrange	11.97	7.81	8.27	10.66	9.43	10.11	10.15	7.85	6.70	6.91	7.22	11.14
Range	23.94	15.61	16.53	21.32	18.85	20.23	20.30	15.70	13.40	13.83	14.44	22.28
Variance	34.12	10.66	10.79	32.23	27.56	25.87	12.23	8.30	9.36	9.54	9.79	14.74
Standard Deviation	5.84	3.27	3.29	5.68	5.25	5.09	3.50	2.88	3.06	3.09	3.13	3.84
Middle probe data CM1 (225 degrees)												
Minimum	101.16	136.72	140.86	245.23	250.29	253.97	139.37	145.92	153.64	257.64	258.56	262.75
Maximum	157.41	161.01	163.31	271.50	284.39	285.31	161.93	162.85	164.23	274.72	275.64	282.16
Sample Number	29	36	36	36	36	36	36	36	36	36	36	36
Arithmetic Mean	141.30	151.54	155.42	264.61	267.41	270.55	152.78	156.92	159.38	265.16	266.83	269.61
Arithmetic Mean AVERAGE		149.42			267.52			156.36			267.20	
Midrange	28.13	12.14	11.22	13.13	17.05	15.67	11.28	8.47	5.29	8.54	8.54	9.70
Range	56.25	24.29	22.45	26.27	34.10	31.34	22.56	16.93	10.59	17.07	17.08	19.41
Variance	192.88	46.05	30.19	32.33	43.62	34.97	28.39	11.92	6.22	16.05	13.15	16.21
Standard Deviation	13.89	6.79	5.49	5.69	6.60	5.91	5.33	3.45	2.49	4.01	3.63	4.03
Middle probe data CM2 (315 degrees)												
Minimum	136.38	137.30	138.22	252.47	254.31	255.23	136.38	139.84	143.29	258.38	260.29	262.59
Maximum	156.64	161.44	162.36	277.76	278.68	282.82	155.46	160.78	161.70	271.27	273.11	280.93
Sample Number	36	36	36	36	36	36	36	36	36	36	36	36
Arithmetic Mean	144.02	146.80	150.63	266.11	267.79	270.20	145.49	150.30	154.26	264.48	266.42	270.27
Arithmetic Mean AVERAGE		147.15			268.03			150.01			267.05	
Midrange	10.13	12.07	12.07	12.64	12.18	13.79	9.54	10.47	9.21	6.45	6.41	9.17
Range	20.26	24.13	24.13	25.29	24.37	27.59	19.08	20.94	18.41	12.89	12.82	18.35
Variance	39.71	46.61	52.81	35.53	35.97	45.19	32.43	30.98	23.18	12.57	11.50	19.27
Standard Deviation	6.30	6.83	7.27	5.96	6.00	6.72	5.69	5.57	4.81	3.55	3.39	4.39

Table 4.4: First experimental program conductivity toe and shoulder position statistical results. Raw-hold signal (Test 3).

	First Program: Test 3 Raw-hold5minDelay						First Program: Test 3 Raw-hold5minDelay					
	Toe (degrees)			Shoulder (degrees)			Toe (degrees)			Shoulder (degrees)		
	25%	50%	75%	75%	50%	25%	25%	50%	75%	75%	50%	25%
	End probe data CF4 (225 degress)						Middle probe data CM6 (45 degrees)					
Minimum	155.03	158.25	160.17	236.49	240.63	241.55	138.45	139.37	143.06	254.27	257.96	259.99
Maximum	173.90	174.82	178.91	253.54	258.61	267.76	159.63	162.85	164.85	277.02	280.70	286.23
Sample Number	36	36	36	36	36	36	36	36	36	36	36	36
Arithmetic Mean	164.18	166.88	170.77	244.69	247.40	250.47	148.89	154.45	158.28	259.97	263.01	266.63
Arithmetic Mean AVERAGE		167.28			247.52			153.87			263.20	
Midrange	9.44	8.29	9.37	8.52	8.99	13.10	10.59	11.74	10.90	11.38	11.37	13.12
Range	18.87	16.57	18.73	17.05	17.97	26.21	21.18	23.48	21.79	22.75	22.75	26.24
Variance	23.53	20.32	18.45	19.02	18.93	29.54	44.81	34.47	19.66	16.57	21.26	29.25
Standard Deviation	4.85	4.51	4.30	4.36	4.35	5.44	6.69	5.87	4.43	4.07	4.61	5.41
	Middle probe data CM3 (135 degrees)						Middle probe data CM2 (315 degrees)					
Minimum	137.76	154.80	156.61	253.77	256.38	257.30	135.92	138.00	142.13	258.84	259.76	263.90
Maximum	161.24	167.18	168.10	265.57	286.00	286.92	148.35	152.75	156.64	270.81	272.19	277.71
Sample Number	36	36	36	36	36	36	36	36	36	36	36	36
Arithmetic Mean	157.54	160.09	161.23	259.05	261.71	263.52	141.75	144.41	146.94	263.98	266.40	268.71
Arithmetic Mean AVERAGE		159.62			261.43			144.36			266.36	
Midrange	11.74	6.19	5.75	5.90	14.81	14.81	6.21	7.38	7.26	5.98	6.21	6.91
Range	23.48	12.39	11.49	11.80	29.62	29.62	12.43	14.75	14.51	11.97	12.43	13.81
Variance	15.11	4.62	4.54	8.02	24.95	27.01	6.65	11.81	17.00	9.15	10.11	10.28
Standard Deviation	3.89	2.15	2.13	2.83	5.00	5.20	2.58	3.44	4.12	3.02	3.18	3.21

In order to maximize the ARM operational efficiency and make use of all eight channels for recording probe data, one of the conductivity probes was permanently connected to the ARM with the datum signal. Conductivity probe CM6 was selected as it was located 90° from the datum signal (Table 4.2) i.e. the datum signal would be activated approximately 90° before the conductivity signal. The electrical circuit was designed to transmit different output voltages when the probe or datum signals were activated i.e. conductivity produced a high signal (1.74V) and datum a lower signal (0.84V). Due to this output voltage differentiation, raw-hold type signals (tests 1, 2 and 3) allowed for good data interpretation (Figure 4.5).

The additional (0.84V) voltage spikes occurring after the sequential sharp datum signal (located at 45°) are thought to have been caused by a malfunction of the datum sensor (discussed in section 3.7.5.1). It is assumed that these interruptions occurred due to vibrations inflicted onto the mill shell i.e. the datum measurement devise was located and hence activated at the 135° mark which coincided with the load toe region (also defined as the most turbulent region in the mill), thus resulted in vibrations and hence voltage spikes.

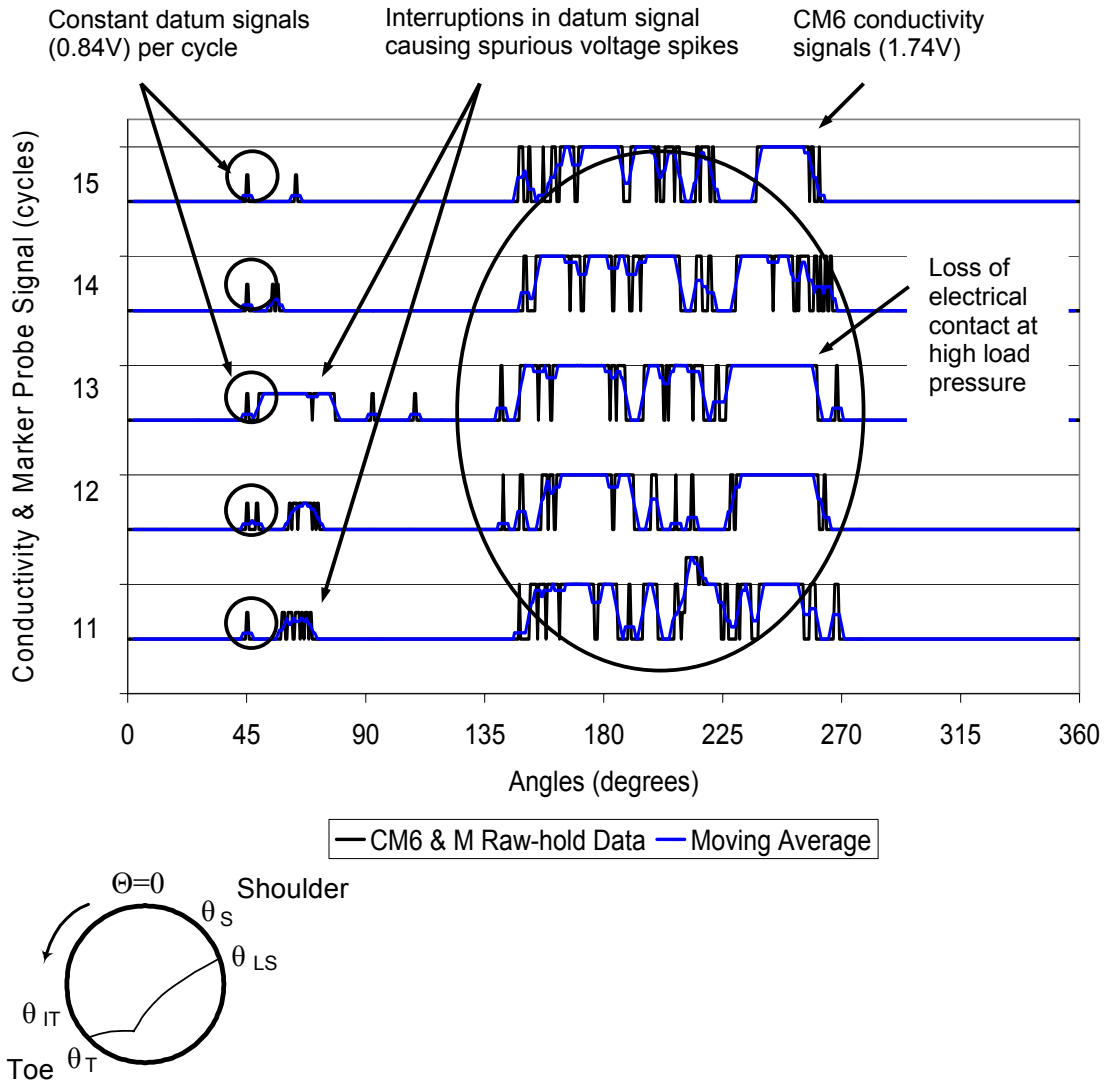


Figure 4.4: Conductivity probe data profiles from first experimental program (probe CM6 and datum signal, Test 3 (Raw-hold5minDelay), Cycles (11-15)). Profile indicates datum signals; voltage spikes; and probe CM6 conductivity signals per cycle.

Also evident from Figure 4.4 is the loss of electrical contact occurring between the load toe and shoulder positions indicating that physical contact of the load onto the probe did not result in a constant electrical output signal. This phenomenon is common to all recorded conductivity probe data. Figure 4.4 also demonstrates how unlikely it is to achieve constant electrical contact between the load toe and shoulder positions.

Table 4.5: First experimental program conductivity toe and shoulder position statistical results. Raw signal (Tests 4 and 5).

	First Program: Test 4 RawNoDelay						First Program: Test 5 Raw 5minDelay					
	Toe (degrees)			Shoulder (degrees)			Toe (degrees)			Shoulder (degrees)		
	25%	50%	75%	75%	50%	25%	25%	50%	75%	75%	50%	25%
End probe data CF5 (225 degrees)												
Minimum	148.83	156.20	158.51	214.74	217.05	223.96	138.80	159.08	163.69	216.70	222.23	230.53
Maximum	180.17	194.92	199.99	249.78	251.16	258.99	173.83	194.12	198.33	236.95	242.03	248.97
Sample Number	36	36	36	36	36	36	36	36	36	34	35	35
Arithmetic Mean	164.48	171.26	176.75	238.02	240.58	247.34	162.91	171.74	177.82	229.46	233.27	239.94
Arithmetic Mean AVERAGE		170.83			241.98			170.82			234.22	
Midrange	15.67	19.36	20.74	17.52	17.06	17.52	17.52	17.52	17.32	10.13	9.90	9.22
Range	31.34	38.72	41.49	35.03	34.11	35.03	35.03	35.03	34.64	20.25	19.80	18.44
Variance	63.27	78.61	98.68	58.95	57.54	35.90	39.53	53.70	70.84	27.35	23.66	15.51
Standard Deviation	7.95	8.87	9.93	7.68	7.59	5.99	6.29	7.33	8.42	5.23	4.86	3.94
Middle probe data CM3 (135 degrees)												
Minimum	156.55	163.46	166.69	218.78	219.70	220.62	147.45	154.82	156.20	222.12	230.42	232.26
Maximum	174.99	183.75	186.05	252.43	254.73	258.88	169.94	171.37	177.41	252.54	254.85	257.61
Sample Number	36	36	36	36	36	36	36	36	36	36	36	36
Arithmetic Mean	167.05	171.21	175.08	236.63	242.16	245.24	158.37	162.71	167.59	238.49	241.60	245.47
Arithmetic Mean AVERAGE		171.11			241.34			162.89			241.85	
Midrange	9.22	10.14	9.68	16.82	17.52	19.13	11.25	8.27	10.60	15.21	12.22	12.68
Range	18.44	20.28	19.36	33.65	35.03	38.26	22.50	16.55	21.20	30.42	24.43	25.35
Variance	16.66	24.33	25.09	71.84	62.51	71.55	22.26	17.89	35.85	43.61	34.19	31.80
Standard Deviation	4.08	4.93	5.01	8.48	7.91	8.46	4.72	4.23	5.99	6.60	5.85	5.64
Middle probe data CM1 (225 degrees)												
Minimum	153.90	156.20	162.20	225.35	231.34	236.87	137.42	148.02	149.40	238.37	239.29	243.90
Maximum	166.81	173.26	176.02	253.46	254.85	259.92	162.31	164.15	171.53	253.97	255.80	268.68
Sample Number	36	36	36	36	36	36	37	37	37	36	36	36
Arithmetic Mean	159.85	165.06	169.69	241.93	245.95	250.51	151.53	157.11	161.26	244.74	247.71	252.39
Arithmetic Mean AVERAGE		164.87			246.13			156.63			248.28	
Midrange	6.45	8.53	6.91	14.06	11.75	11.52	12.45	8.07	11.06	7.80	8.26	12.39
Range	12.91	17.06	13.83	28.12	23.51	23.05	24.89	16.13	22.13	15.60	16.52	24.78
Variance	11.62	13.32	15.36	52.63	44.19	42.84	28.38	20.86	31.84	13.65	14.71	25.35
Standard Deviation	3.41	3.65	3.92	7.25	6.65	6.55	5.33	4.57	5.64	3.69	3.84	5.03
Middle probe data CM2 (315 degrees)												
Minimum	148.02	153.55	154.94	215.32	216.24	217.16	133.39	144.91	149.98	234.33	235.26	242.63
Maximum	165.54	174.76	179.83	252.66	253.58	256.34	156.90	165.19	168.42	248.79	252.01	258.76
Sample Number	37	37	37	37	37	37	37	37	37	37	37	37
Arithmetic Mean	159.13	165.39	168.94	237.45	240.51	246.48	148.10	154.90	158.69	242.19	245.84	251.31
Arithmetic Mean AVERAGE		164.49			241.48			153.90			246.45	
Midrange	8.76	10.60	12.45	18.67	18.67	19.59	11.75	10.14	9.22	7.23	8.38	8.07
Range	17.52	21.20	24.89	37.34	37.34	39.18	23.51	20.28	18.44	14.46	16.76	16.13
Variance	16.94	20.78	22.93	103.71	95.70	77.65	25.42	17.09	16.23	13.43	13.67	23.02
Standard Deviation	4.12	4.56	4.79	10.18	9.78	8.81	5.04	4.13	4.03	3.66	3.70	4.80

CF4's and CM6's raw data signal statistical results were poor and hence omitted from Table 4.4. This is thought to have occurred because the raw signal outputs (being prone to

a higher degree of irregularity[1]) result in irregular voltage signals; thus reducing the effectiveness and hence accuracy of the data collection process.

Figure 4.5 illustrates two cycles, namely cycle 4 (extracted from test 2 raw-hold signal data) and cycle 25 (extracted from test 4 raw signal data); both cycles including the moving average trend line and data processing results at different 25 per cent increments corresponding to the relative degree values. Further discussion between the effectiveness of each signal type is discussed in section 4.4.2.3.

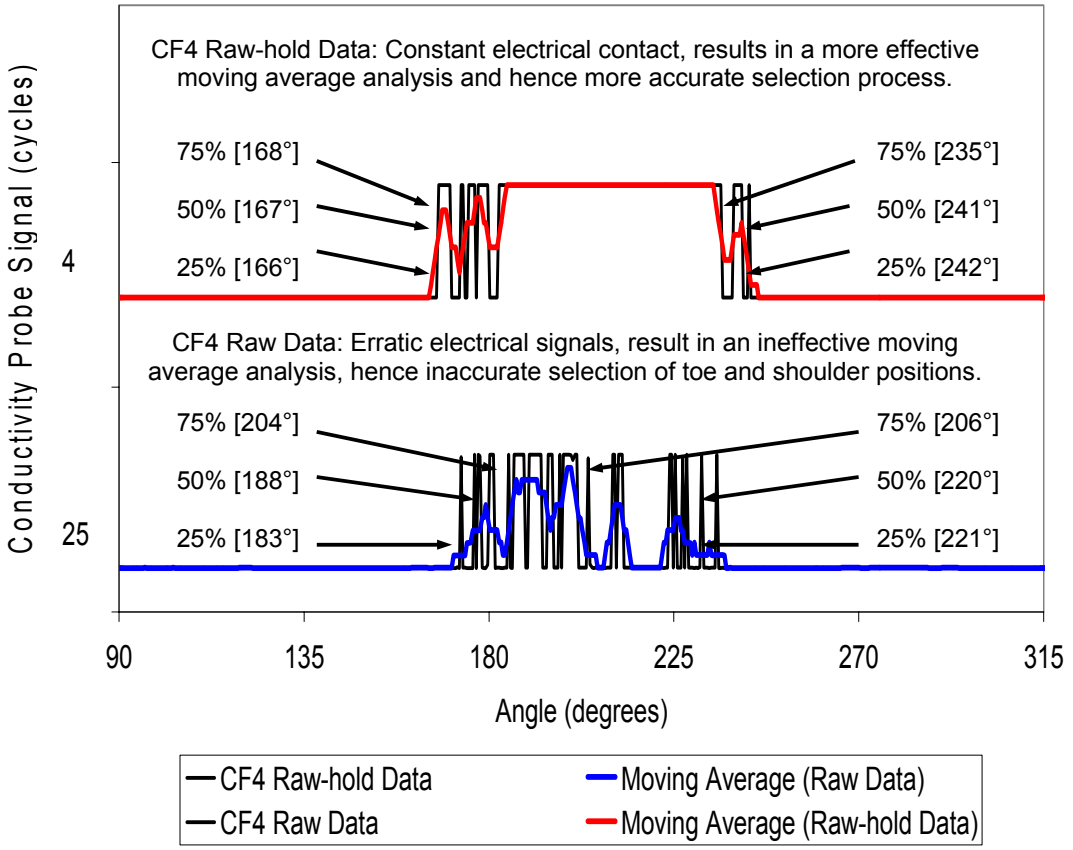


Figure 4.5: Conductivity probe data profile from first experimental program (probe CF4: Test 2 (Raw-holdNoDelay), Cycle (4) and Test 4 (RawNoDelay), Cycle (25)). Figure compares the raw-hold to raw signal electrical conductivity signal and affect these signals have on the moving average trend line and hence data selection process.

[1] As discussed in section 3.6.2, the raw signal refers to the signal as received by the ARM device, whereas the raw-hold signal incorporates a hold of 6ms on the incoming raw signal, resulting in a more constant output.

4.4.2 Discussion of first experimental program results

4.4.2.1 Data reproducibility

Tests 1 and 2 were selected to investigate data reproducibility because these tests are of identical nature i.e. both tests recorded raw-hold conductivity data from mill start-up and their useful data per test is the greatest.

The arithmetic mean results for tests 1 and 2 (Table 4.3) per middle probe show a large consistency both at the toe and shoulder positions, indicating a high degree of reproducibility for raw-hold signal tests. The arithmetic mean average[2] results show maximum deviations of approximately 1 degree at the shoulder and 3 degrees at the toe, except for probe CM1 where the difference between the two arithmetic mean average toe positions is just below 7 degrees. CM1's large deviation is attributed to voltage spikes occurring at the beginning of each cycle (section 4.4.1); this behaviour exacerbated after each test right up to test 3. Thus, besides probe CM1, raw-hold signals are reproducible.

End probe (CF4) arithmetic mean average toe and shoulder positions differ from the middle probe toe and shoulder positions i.e. for both tests 1 and 2, toe and shoulder positions tend to rise marginally higher towards the middle of the mill and sink slightly lower at the mill ends. The diagonal mill shell liners positioned at either end of the mill influence this type of behaviour i.e. the lifters are positioned in such a way so that they act as shovels, throwing the load portion located at the shell ends to the centre of the mill. This contrasts with the result of Moys and van Nierop (1996) who found the shoulder position to be higher at the feed and discharge ends of the mill (in a wet gold mill which did not have diagonal liners, so the end liners of the mill caused a greater lift of the load and hence a higher shoulder position).

4.4.2.2 Effect of delay on Raw-hold signal results

Tests 2 and 3 (Tables 4.3 and 4.4) are used to determine the effect that the 5 minute delay has on the raw-hold signal results.

[2] Arithmetic mean average value is calculated by adding the corresponding degree values at the 25, 50 and 75 per cent positions and dividing their result by three.

End probe CF4 demonstrates small changes of 2 degrees at the toe and shoulder. This behaviour is similar to that of tests 1 and 2, thus tests 1, 2 and 3 display a high degree of reproducibility, indicating that the 5 minute delay period has no large effect on the load toe and shoulder positions. These results are to be expected as the mill reaches its constant rotating speed (15.35 RPM) within the second or third revolution; it is also believed that equilibrium is also reached during this time period.

A common factor affecting the toe position in all three tests is the decrease in the standard deviation values from the 25 to 75 per cent values. This is thought to be attributed to the load leaving the very random and turbulent 'initial toe' region and entering the more deterministic load 'locked' condition where it is accelerated to the shoulder position. In contrast the increase in the standard deviation values from the 75 to the 25 per cent degree value (common to the shoulder positions of the probes) is attributed to the load losing electrical contact at the shoulder region as the pressure of balls on the probe decreases to zero in a variable asymptotic fashion.

4.4.2.3 Effect of delay on Raw signal results

Tests 4 and 5 (Table 4.5) were selected to compare the effect that the 5 minute delay had on the raw conductivity data. Raw data at the toe and shoulder positions per middle probe differ on average by 9 and 2.5 degrees, respectively; conversely end probe (CF5) toe and shoulder positions differ by 0.5 and 7.5 degrees, respectively.

It is thought that, the high inconsistency (of 7.5 degrees) in shoulder position occurred because the probe failed to establish constant electrical contact at the shoulder region. As a result, the moving average analysis and hence, data collection process was not as effective in collecting data at any of the 25 per cent incremental shoulder positions (Figure 4.5) thus it is believed that CF5's shoulder values do not define the actual load shoulder positions.

It is thus difficult to establish a pattern or relationship between raw signal tests.

4.4.3 First experimental program conductivity data conclusions

Achieving constant electrical contact (or conductivity) between the load toe and shoulder positions (even though it is known that physical contact does indeed exist), proved to be very difficult. The few cycles which did manage to capture constant electrical contact were the raw-hold data signals.

Raw-hold data showed good reproducibility for all three tests i.e. the 5 minute delay appears to have not had a major effect on the load toe and shoulder positioning. Arithmetic mean average toe and shoulder results[3] are 154 and 265 degrees, respectively.

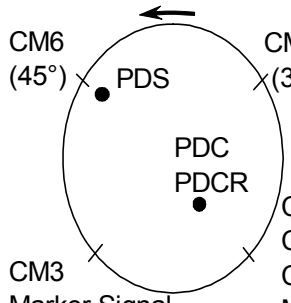
Raw data signals very seldom recorded constant electrical contacts between the load toe and shoulder position. This is primarily because of the nature of the signal i.e. raw signals comprised of more erratic 'breaks' throughout the conductivity signal, when compared to the raw-hold signal, which holds the signal for a pre-defined period (of 6ms) and ensures that any minor contact is sensed by the ARM. For this reasoning, raw data is defined as being unreliable and thus cannot be used for further comparative analysis.

4.5 Conductivity probe results and discussion: Second program

Out of the eleven tests conducted, six were directed at measuring conductivity data (Table 4.7). Tests 3, 4 and 5 recorded primarily OR-Gate data; test 8 recorded raw and raw-hold data; test 10 recorded raw data and test 11 recorded OR-Gate data. Tests 10 and 11 were recorded at high-speed sampling rates[4].

[3] Results are calculated by calculating the arithmetic mean average raw-hold signal of each middle probe for worn liner tests 1, 2 and 3 at the toe and shoulder positions.
[4] The default sampling rate that the ARM was set at 5ms (or every 0.5 degrees). High-speed sampling refers to a sampling rate of 2ms (or every 0.2 degrees). Using a higher sampling rate, increased the amount of data points recorded per degree, hence increased the accuracy of the results.

Table 4.6: Second experimental program (new liner) test schedule, indicating: conductivity probe and signal type used per test; quality of recorded data; and test details.

		ORGateNoDelay	ORGate2minDelay	ORGateNoDelay	Raw and Raw-holdNoDelay	Raw NoDelay High-Speed Sampling	ORGate NoDelay High-Speed Sampling
	Test No.	3	4	5	8	10	11
Conductivity Probes							
End probes							
CF4 Conductivity/Feed (225 degrees)		OR	OR			R	OR
CF5 Conductivity/Feed (225 degrees)							
Middle probes							
CM6 Conductivity/Middle & Datum (45 degrees)		OR	OR	OR	RH		
CM6 Conductivity/Middle (45 degrees)		not connected	not connected	not connected	not connected	R	OR
CM3 Conductivity/Middle (135 degrees)		OR	OR	OR	R and RH	R	OR
CM1 Conductivity/Middle (225 degrees)		OR	OR	OR	R and RH	R	OR
OCM1 Conductivity/Middle (225 degrees)		OR	OR	not connected	not connected	not connected	OR
CM2 Conductivity/Middle (315 degrees)		OR	OR	OR	R and RH	R	OR
Additional test data	Units						
Logging rate	freq.	200	200	200	200	500	500
Logging rate	ms	5	5	5	5	2	2
Mill 2C Operating Duration	min	3:30	5:30	3:30	3:30	2:00	2:00
ARM - Delayed Start	min	0	2	0	0	0	0
ARM - Logging Start	time	21:31:33	21:56:59	22:29:01	15:52:31	17:11:12	17:41:40
ARM - Logging Finish	time	21:34:17	21:59:53	22:31:44	15:55:15	17:12:27	17:42:45
ARM - Logging Time	time	0:02:44	0:02:54	0:02:43	0:02:44	0:01:15	0:01:05

Key

1. Filtering method used for recording data	R	Raw
	RH	Raw-hold
	OR	OR-Gate
2. Quality/Consistancy of data		Good (> 70% of useful data)
		Average (between 40-70% of useful data)
		Poor (< 40% of useful data)

During tests 4, 5 and 6, problems were encountered with the datum signal (refer to section 3.7.5.1). This led to inaccurate results for several tests, as all conductivity (movement and photo-detector) data recorded from the ARM is referenced using the datum signal data. A close examination of the datum data using the ARM graphical display (Appendix 5, Figure A5.2) together with its corresponding voltage signals resulted in the following tests being affected: isolated stages of test 4; tests 5, 6; and the last quarter of tests 7 (Appendix 5, Figure A5.3) and 9. For this reasoning tests 5 and 6 will not be used in the analyses.

Data recorded from tests 3, 4 and 8 were processed and statistically analysed. Remaining conductivity tests were also processed however a statistical analysis could not be effectively performed due to the low number of effective cycles that were recorded per probe i.e. less than 30 per cent (or less than 10 out of 37 cycles) of recorded data per test proved to be useful. Furthermore, this small percentage of useful data usually occurred randomly within the 37 cycle range, resulting in inaccurate toe and shoulder positions.

It is evident (Table 4.7) that as the tests progressed, the quality of conductivity data available for processing and analysis decreased.

4.5.1 Analysis of experimental data and results

The conductivity results processed from tests 3 and 4 are displayed in Table 4.7. In test 3 data logging was initiated on mill start-up, whereas in test 4 data logging was initiated after a 2 minute delay period.

No useful data was recorded from conductivity probe CM2 for any of the tests; hence its results are excluded from Table 4.7. Test 4 CM1 was also omitted from the statistical analysis due to the low number of effective toe positions.

Table 4.7: Second experimental program conductivity toe and shoulder position statistical results. OR-Gate signals (Tests 3 and 4).

	Second Program: 3 ORGateNoDelay						Second Program: 4 ORGate2minDelay					
	Toe (degrees)			Shoulder (degrees)			Toe (degrees)			Shoulder (degrees)		
	25%	50%	75%	75%	50%	25%	25%	50%	75%	75%	50%	25%
End probe data CF4 (225 degress)												
Minimum	141.68	145.00	149.96	259.53	264.13	265.97	120.36	121.75	131.43	225.46	226.38	236.06
Maximum	161.01	166.61	170.68	275.18	284.77	287.53	162.47	164.77	173.51	277.09	278.47	279.39
Sample Number	36	36	36	36	36	36	35	35	35	36	36	36
Arithmetic Mean	153.51	158.18	162.26	267.74	270.73	273.87	143.36	146.51	149.87	250.37	252.93	256.40
Arithmetic Mean AVERAGE		157.98			270.78			146.58			253.23	
Midrange	9.67	10.80	10.36	7.83	10.32	10.78	21.05	21.51	21.04	25.81	26.04	21.66
Range	19.34	21.61	20.72	15.65	20.64	21.56	42.11	43.02	42.08	51.63	52.09	43.33
Variance	26.24	23.28	20.54	10.99	24.48	30.37	132.35	100.48	107.12	110.32	120.15	125.92
Standard Devaition	5.12	4.83	4.53	3.32	4.95	5.51	11.50	10.02	10.35	10.50	10.96	11.22
Middle probe data CM6 (45 degrees)												
Minimum	94.66	96.03	96.95	252.62	254.92	259.25	Poor (< 40% of useful data)					
Maximum	160.09	171.44	173.28	286.69	289.45	296.82						
Sample Number	27	27	27	29	29	29						
Arithmetic Mean	132.76	144.66	152.32	262.67	265.31	271.12						
Arithmetic Mean AVERAGE		143.25			266.37							
Midrange	32.72	37.70	38.16	17.03	17.26	18.78						
Range	65.43	75.40	76.32	34.07	34.53	37.56						
Variance	277.14	393.62	387.48	99.02	103.08	118.42						
Standard Devaition	16.65	19.84	19.68	9.95	10.15	10.88						
Middle probe data CM3 (135 degrees)												
Minimum	96.79	98.63	101.85	246.41	247.33	248.25	98.12	99.05	99.97	224.88	225.81	226.73
Maximum	163.08	164.92	167.69	287.84	288.76	290.60	157.59	158.51	163.58	276.51	277.43	278.35
Sample Number	29	29	28	33	33	33	29	29	29	30	30	30
Arithmetic Mean	128.94	130.51	137.38	259.20	261.38	264.23	126.23	129.58	133.60	247.73	249.71	251.54
Arithmetic Mean AVERAGE		132.28			261.60			129.80			249.66	
Midrange	33.15	33.15	32.92	20.72	20.72	21.18	29.73	29.73	31.81	25.81	25.81	25.81
Range	66.29	66.29	65.83	41.43	41.43	42.35	59.46	59.46	63.61	51.63	51.63	51.63
Variance	326.73	344.82	394.54	57.52	49.76	66.06	355.70	394.07	396.28	119.58	142.10	136.80
Standard Devaition	18.08	18.57	19.86	7.58	7.05	8.13	18.86	19.85	19.91	10.94	11.92	11.70
Middle probe data CM1 (225 degrees)												
Minimum	96.10	97.02	97.94	249.86	250.78	251.70	Poor (< 40% of useful data)					
Maximum	127.99	131.55	132.47	294.43	295.34	296.26						
Sample Number	19	19	19	25	25	25						
Arithmetic Mean	113.51	117.43	118.67	270.24	271.77	275.56						
Arithmetic Mean AVERAGE		116.54			272.52							
Midrange	15.94	17.26	17.26	22.28	22.28	22.28						
Range	31.89	34.53	34.53	44.57	44.56	44.56						
Variance	67.24	83.20	85.96	211.92	206.48	147.74						
Standard Devaition	8.20	9.12	9.27	14.56	14.37	12.15						
Middle probe data OCM1 (225 degrees)												
Minimum	96.56	97.94	98.86	254.00	256.72	257.64	90.86	92.25	93.63	236.06	236.98	240.21
Maximum	156.41	159.71	163.85	286.23	291.67	292.59	153.74	156.49	159.25	291.84	292.76	293.68
Sample Number	19	19	19	26	26	26	29	29	29	26	26	26
Arithmetic Mean	135.97	140.82	145.73	267.48	271.42	275.55	117.92	122.09	125.65	258.60	260.76	262.57
Arithmetic Mean AVERAGE		140.84			271.48			121.89			260.64	
Midrange	29.92	30.89	32.49	16.11	17.47	17.47	31.44	32.12	32.81	27.89	27.89	26.73
Range	59.85	61.77	64.99	32.23	34.94	34.94	62.87	64.25	65.62	55.77	55.77	53.47
Variance	261.73	266.36	289.85	105.54	121.51	95.36	216.89	269.23	234.00	190.63	194.06	177.17
Standard Devaition	16.18	16.32	17.02	10.27	11.02	9.77	14.73	16.41	15.30	13.81	13.93	13.31

4.5.2 Discussion of second experimental program results

4.5.2.1 Data reproducibility

Tests 3 and 4 conductivity data are used for data reproducibility. Besides probe OCM1, probes CM3 (middle) and CF4 (end) were the only conductivity probes which recorded useful data for these tests. Also important to note is that test 3 initiated data capture from mill start-up, whereas test 4 recorded data 2 minutes after mill start-up.

CM3 arithmetic toe and shoulder positions decrease by 2 and 12 degrees, respectively from test 3 to test 4. CF4 toe and shoulder arithmetic mean positions show a higher decrease of 11 and 18 degrees, respectively.

These differences are excessive when compared to the slight 1-3 degree differences encountered in the first experimental program (section 4.4.2.1). Also, the fact that both probes CF4 and CM3 protruded 2-4mm above the liner and that they were mounted inside each of the liners in an identical fashion makes it difficult to understand or explain these large differences between tests 3 and 4. These results are thus not reproducible and due to the problems encountered with the datum signal, there are no additional tests available for further comparative analysis.

4.5.2.2 Load positioning at middle and end of mill

The arithmetic mean toe values (for both tests 3 and 4) are approximately 15 degrees greater at the mill end (CF4) than at the mill centre (CM3 and OCM1) indicating that the toe rises higher towards the centre of the mill than at its ends. In tests 3 and 4, the arithmetic mean shoulder values at the mill centre decrease at a similar rate to that at the mill ends, however the shoulder positions at the mill centre remain marginally higher than at the ends.

The new set of dual diagonal end liners (designed to throw the load towards the centre of the mill) are thought to have influenced this behaviour.

4.5.2.3 Analysis of OCM1 data

Probe OCM1 (positioned 292mm across from middle probe CM1) was purposely installed to protrude approximately 9mm above the liner, whereas all other conductivity probes protruded between 2-4mm above the liner. This was done in order to: determine the effect that the additional 5-7mm would have on the probes behaviour and to compare its results to the first experimental program results where all the probes were installed to protrude approximately 9mm above each liner (section 3.6.3.1).

Test 4s' arithmetic mean shoulder position for probe OCM1 (Table 4.7) is greater by approximately 10 degrees when compared to test 3 i.e. this shows that OCM1 follows a similar decreasing trend as CM3 and CF4 from test 3 to test 4. OCM1's arithmetic mean shoulder values are greater than CM3's at the toe and shoulder by precisely 10 degrees. It is thus thought that the additional 5-7mm protrusion increased the sensitivity of the probe and hence OCM1 started recording data before CM3.

4.5.2.4 Analysis of Raw-hold results and comparison to OR-Gate results

Test 8 (Table 4.8), was the only test that recorded raw and raw-hold signals. This was performed specifically in order to compare raw-hold results (used in the first experimental program) to OR-Gate results (second experimental program). Unfortunately insufficient quality data resulted in only probe CM3 raw-hold data to being analysed.

Table 4.8: Second experimental program conductivity toe and shoulder position statistical results. Raw-hold signals (Test 8).

	Second Program: 8 Raw-holdNoDelay					
	Toe (degrees)			Shoulder (degrees)		
	25%	50%	75%	75%	50%	25%
Middle probe data CM3 (135 degrees)						
Minimum	96.33	98.12	99.05	262.98	263.90	264.82
Maximum	156.18	164.43	167.23	300.27	301.19	302.11
Sample Number	22	25	26	29	29	29
Arithmetic Mean	119.35	121.76	127.49	275.08	277.01	278.65
Arithmetic Mean AVERAGE		122.87			276.91	
Midrange	29.92	33.15	34.09	18.64	18.64	18.64
Range	59.85	66.30	68.18	37.29	37.29	37.29
Variance	304.08	381.57	439.75	91.68	101.74	101.60
Standard Devaition	17.44	19.53	20.97	9.57	10.09	10.08

CM3s raw-hold arithmetic mean toe position (Test 8) is approximately 10 degrees less than test 3 and 4's OR-Gate toe positions, implying that the raw-hold signal recorded conductivity data further up the down coming side of the mill. The shoulder position differs by approximately 15 degrees (between tests 8 and 3), and 27 degrees (between tests 8 and 4), suggesting that the raw-hold signal recorded conductivity data further up the shoulder. This behaviour is surprising as the OR-Gate signaling was designed to be more sensitive in comparison to the raw-hold signaling (section 3.7.2).

4.5.3 Second experimental program conductivity data conclusions

OR-Gate data was not reproducible, yet it did display a level consistency between tests 3 and 4.The problem with the datum signal resulted in only having two tests (tests 3 and 4) for analysis of conductivity data. The arithmetic mean average toe and shoulder results[5] are 131 and 256 degrees, respectively.

Only one test (test 8) and only one probe (CM3) successfully recorded data using raw-hold signaling.

Besides the datum signal problems, the lack of enough useful data due to electronic circuitry problems and inherent difficulty in establishing good electrical contact, resulted in most of the data analysed in this program to be defined as unreliable and questionable.

4.6 Conductivity probe data conclusions

Measurement of the load behaviour of a dry industrial ball mill using the conductivity probes (defined in Chapter 3), does not result in accurate toe and shoulder position data.

The main factor contributing to this is the inherent difficulty in establishing good electrical contact. This problem was anticipated prior to both experimental programs, hence the sensitivity of the capturing electronic signals was increased; this however still did not result in reliable load position data.

[5] Results are calculated by calculating the arithmetic mean average raw-hold signal of each middle probe for worn liner tests 1, 2 and 3 at the toe and shoulder positions.

4.7 Movement probe data analysis, results and discussion

The movement probe was only used in the second experimental program. Even though two movement probes (M1 and M2) were mounted onto the mill shell, data was only recorded from probe M1. The methodology used to process, analyse and discuss the recorded data is presented in this section.

4.7.1 Data analysis per cycle

Raw signals from the movement probe were fed directly to the ARM device i.e. no additional filtering was performed. To standardize the amount of statistically analysed data per test and insure that the data recorded reflected mill steady state conditions, the first seven cycles (out of the approximately forty recorded cycles) were omitted. The data processing program was then used to process and display the data into graphical format. A typical movement probe data plot is illustrated in Figure 4.6.

By closely examining the movement probe curve from left to right (Figure 4.6), it is evident that as the toe region is approached, the signals start becoming more erratic (probably from the increasing vibration of the shell as the probe approaches the toe region), and in most cases prior to reaching the high amplitude toe movement signal, instantaneous impacts are recorded. These are not referred to as the initial toe positions; the initial toe (θ_{IT}) is assumed to be where the high amplitude signal commences. These impacts were not evident in each and every cycle nor are they systematic, they occur randomly (probably due to direct ball collisions onto the face of the movement probe).

Continuing dynamic vibration is evident up to approximately 195 degrees; thereafter the vibration decreases before leveling-out as the load reaches the shoulder position (θ_S). The decrease in vibration signifies that the load is moving out of the turbulent toe region and is passing under the ‘locked-in’ load. Also, as the probe approaches the shoulder (between 220 to 250 degrees), the movement undergoes a slight dip. This ‘dip’ is typical of almost all movement probe curves, stretching over different areas before reaching the shoulder position.

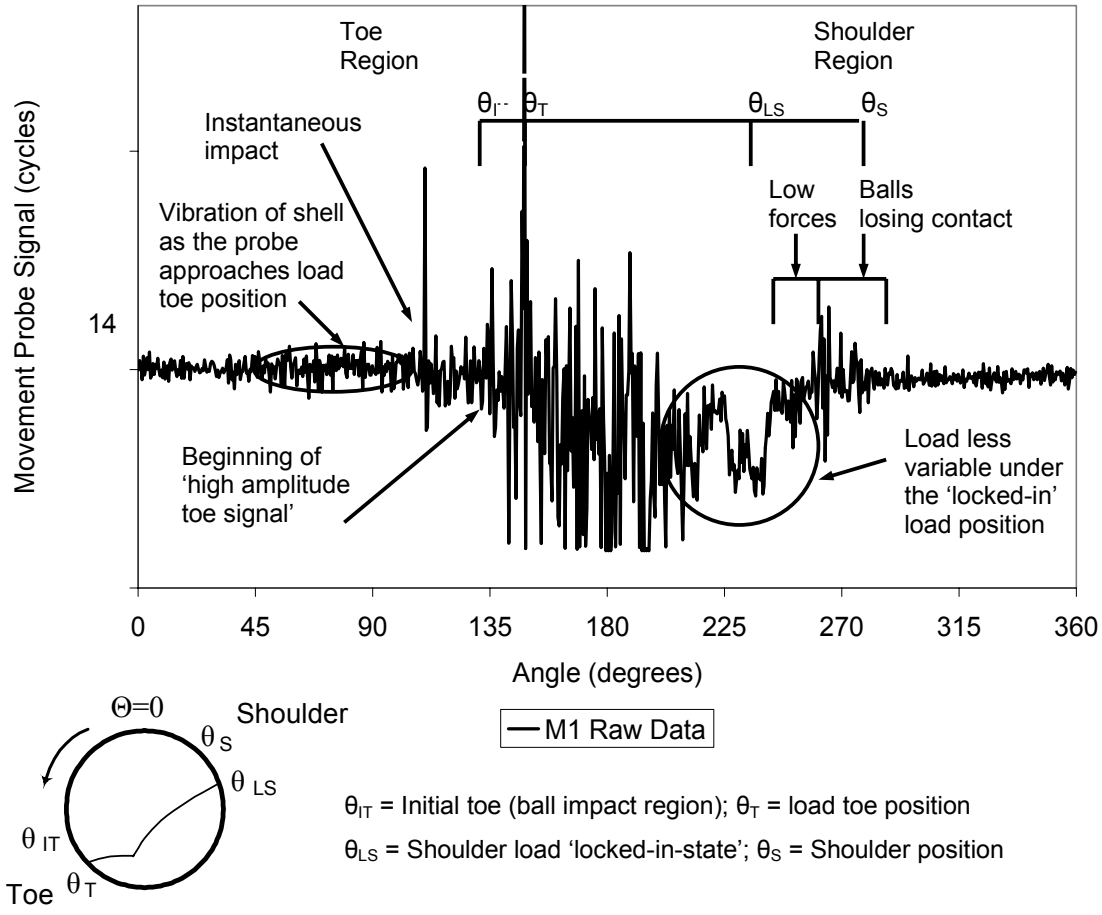


Figure 4.6: Typical movement probe profile, indicating toe and shoulder region characteristics (second experimental program, Test 3 (OR-Gatedata), Cycle 14).

By closely examining the last part of the signal from right to left the first erratic impact is assumed to signify the end of the shoulder region (θ_S). It is also evident that the movement signal after θ_S (towards 360 degrees) is more stable than and less erratic as from (0 to 90) degrees, thus making it easier to accurately identify the shoulder in comparison to the toe position.

4.7.2 Selection of toe and shoulder positions

Due to the complex response of the probe to ball impacts (discussed further in section 4.7.3), sharp increases and decreases made it difficult to define the load toe and shoulder positions. To overcome this problem, a moving variance was used to analyse the probe

data rather than the moving average. Nine periods (as per the moving average curve) were used in the moving variance analysis (implying a moving average range of 20ms or 1.84 degrees). Figure 4.7 illustrates the moving variance trend line and base line over the original M1 cycle 14, as analysed in Figure 4.6.

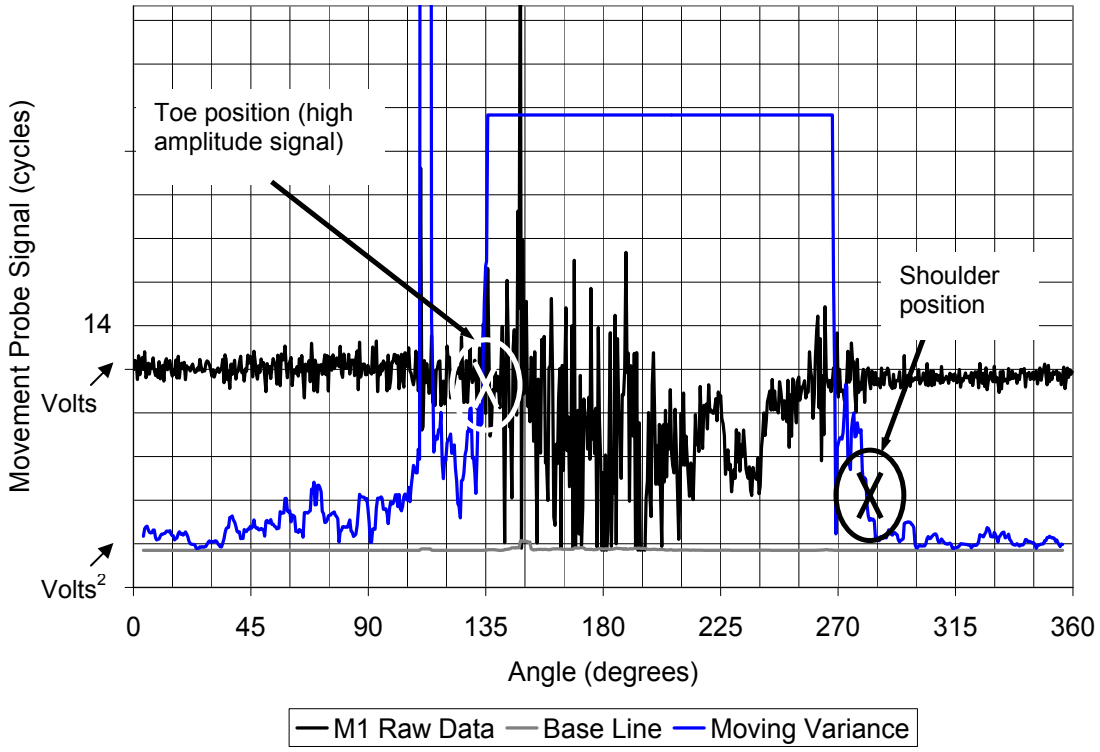


Figure 4.7: Processed movement probe data profile (M1), using moving variance analysis. Second experimental program, Test 3 (OR-Gatedata), cycle (14). Moving variance graph is truncated for clarity purposes.

The two 'X' symbols (Figure 4.7) encompass the complete load cycle (excluding the random instantaneous impact) and are the two points selected per cycle to be used in the movement probe analysis. The high amplitude signal (or toe position) measures 134 degrees, just before the beginning of the dynamic turbulent toe region. The shoulder position (located at 280.63 degrees) is defined as the point where the moving variance curve first intersects the volts^2 grid line (from right to left) as this denotes the last ball movement on the curve.

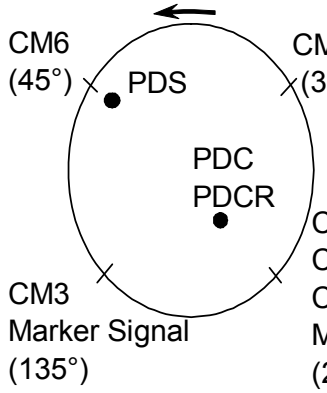
This method for selecting the toe and shoulder positions was used to analyse all the movement probe data. Unlike the automated program used to select various toe and

shoulder positions for the conductivity signals, toe and shoulder locations for the movement data was recorded manually per cycle.

4.7.3 Analysis of experimental data and results

The movement probe was integrated in nine tests; only five out of these were processed and analysed (Table 4.11); the remaining four were negated due to problems encountered in calibrating the strain-gauge circuitry.

Table 4.9: Second experimental program (new liner) test schedule, indicating movement probe (M1) experimental test details.



	Test No.	3	4	5	6	7
		ORGate NoDelay	ORGate 2minDelay	ORGate NoDelay	DatumTest 2minDelay	DatumTest NoDelay
Movement probe						
M1 Movement/Middle		R	R	R	R	R

Additional test data	Units					
Logging rate	freq.	200	200	200	200	200
Logging rate	ms	5	5	5	5	5
Mill 2C Operating Duration	min	3:30	5:30	3:30	5:30	5:30
ARM - Delayed Start	min	0	2	0	2	1
ARM - Logging Start	time	21:31:33	21:56:59	22:29:01	11:54:35	14:04:27
ARM - Logging Finish	time	21:34:17	21:59:53	22:31:44	11:57:18	14:07:10
ARM - Logging Time	time	0:02:44	0:02:54	0:02:43	0:02:43	0:02:43

Key

1. Filtering method used for recording data	R	Raw
	RH	Raw-hold
	OR	OR-Gate logic
2. Quality/Consistancy of data		Good (> 70% of useful data)
		Average (between 40-70% of useful data)
		Poor (< 40% of useful data)

Of the five that were processed (Table 4.11), only tests 3 and 7 were selected for further processing. The selection was based on two criterions, namely: datum functionality per test; and movement probe signal plot.

4.7.3.1 Datum Functionality

By referring to test 3's datum plot[6] for cycles 11 to 20 (Appendix 5, Figure A5.2), it is clear that most periods are clear, consistent and well defined, however a slight deviation is evident for a small percentage of the cycles. This is because the mill speed varies slightly between 15.34 and 15.32RPM, hence affecting the timing per revolution between 3.911 and 3.916 seconds, respectively. The heavy data datum signals is owed to the method of detection per revolution i.e. a steel plate was permanently placed between the datum emitter and receiver in order to 'break' the signal; this measured 171mm which equates to 4.06 degrees (or 43.44ms).

Tests 4, 5 and 6 datum signal plots are similar to that of test 3 as their datum signal was also connected with conductivity probe CM6, however the consistency and accuracy of the well defined datum periods decreased (at an increasing rate) as the tests progressed. This datum malfunction resulted in the datum tests consisting of extremely heavy data strands making detection of the datum signals a difficult task. In turn, this resulted in highly inaccurate results for tests 4, 5, 6 and the last quarter of test 7 (appendix 5, Figure A5.3), as all movement data recorded from the ARM is referenced using the datum signal data. For this reasoning tests 4, 5 and 6 are discarded from the analyses.

4.7.3.2 Movement probe signal

Besides the datum functionality, a problem also existed with the movement probe design (refer to section 3.7.5.4). The objective of the movement probe was to detect the load positioning per mill revolution i.e. detect only normal forces from the mill ball load, not tangential forces; the problem lay in that the way the movement probe was designed made it susceptible to both normal and tangential forces. This influenced the results and hence the accuracy of the load position. Figure 4.8 illustrates the influence that the different loading had on the strain bridge and hence the movement probe results.

[6] In order to make efficient use of all available channels, for test 3, the datum was connected to one of the conductivity probes (CM6).

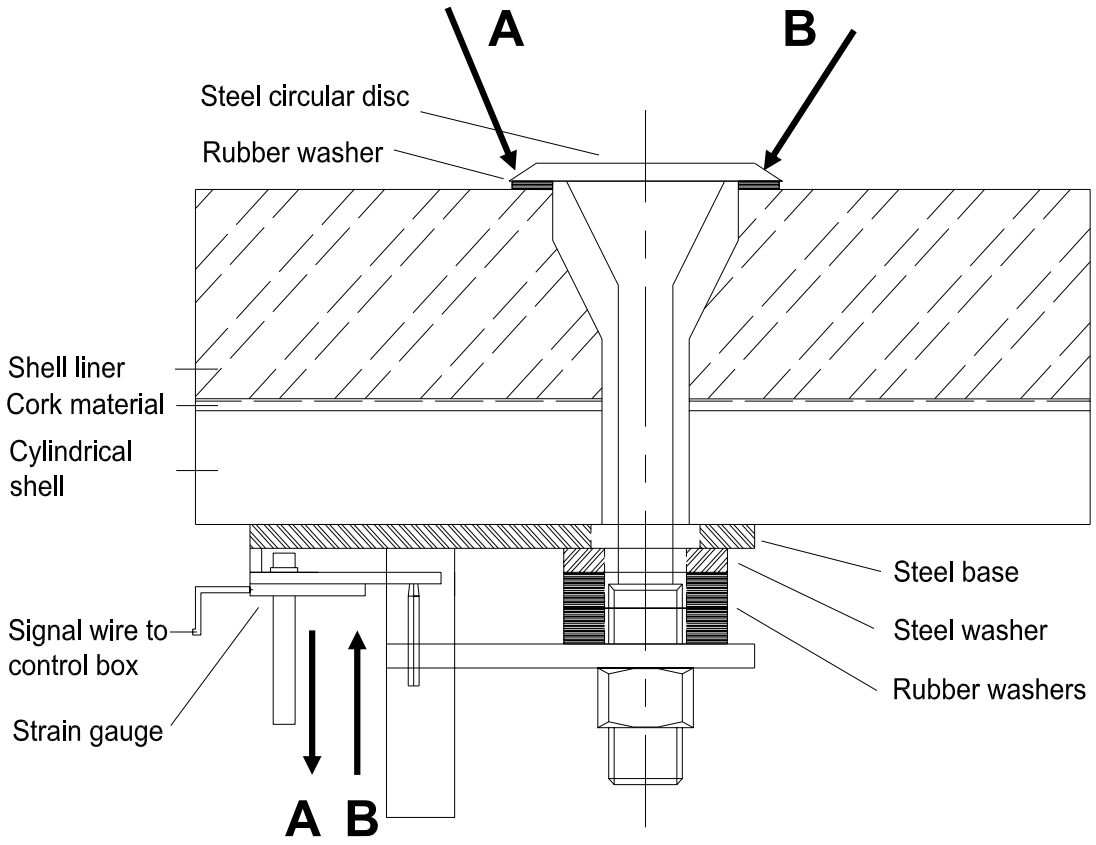


Figure 4.8: Diagram illustrating movement probe installation and effect of different forces on the strain bridge and in turn movement probe results. Force A tends to bend the probe downwards, while force B bends the probe upwards.

4.7.4 Discussion of experimental results

4.7.4.1 Data reproducibility

Tests 3 and 7 experimental results were selected for further analysis and discussion. Table 4.12 displays the measured results of the movement probe toe and shoulder positions for tests 3 and 7.

The arithmetic mean toe and shoulder results for tests 3 and 7 are comparable; this is expected as the nature of each experiment was identical (both tests were recorded from mill start-up) and no operational changes were performed on the mill between the two tests.

It's thought that the overall statistical deviation is greater at the toe than the shoulder largely because the shoulder region experiences less turbulence (and hence less instantaneous impacting axial forces) than the toe region. Thus, the types of forces active on the probe have a direct effect on the movement probe results.

Table 4.10: Second experimental program movement probe toe and shoulder position statistical results for: Test 3 (ORGateNODelay) and Test 7 (DatumTestNoDelay).

Raw data (No delay)	Test 3	Test 7	Deviation	Test 3	Test 7	Deviation
	Toe (degrees)			Shoulder (degrees)		
Minimum	121.40	130.17	8.77	268.21	272.02	3.81
Maximum	137.07	143.06	5.99	298.65	294.89	-3.76
Sample Number	36.00	36.00	-	36.00	36.00	-
Arithmetic Mean	129.83	135.56	5.73	284.52	280.30	-4.22
Midrange	7.83	6.45	-1.39	15.22	11.43	-3.79
Range	15.67	12.89	-2.78	30.44	22.87	-7.57
Standard Deviation	14.83	8.21	-6.62	46.92	30.35	-16.57
Variance	3.85	2.87	-0.99	6.85	5.51	-1.34

4.7.4.2 Data analysis and discussion

Figure 4.9 represents a plot of test 3 and 7 toe and shoulder positions from cycle 7 to 42. Test 7's toe positions remain approximately 5 degrees higher than test 3's throughout the 35 cycles; this 5 degree difference is noted at several instances in Figure 4.9.

It's known that the toe region is more turbulent than the shoulder, however the toe position plot appears more consistent and controlled when compared to the noisier shoulder data. It's believed that the design and hence resulting high sensitivity to both normal and tangential forces of the movement probe may have affected this irregularity. This behaviour could also be attributed to the asymptotic decrease in forces at the shoulder.

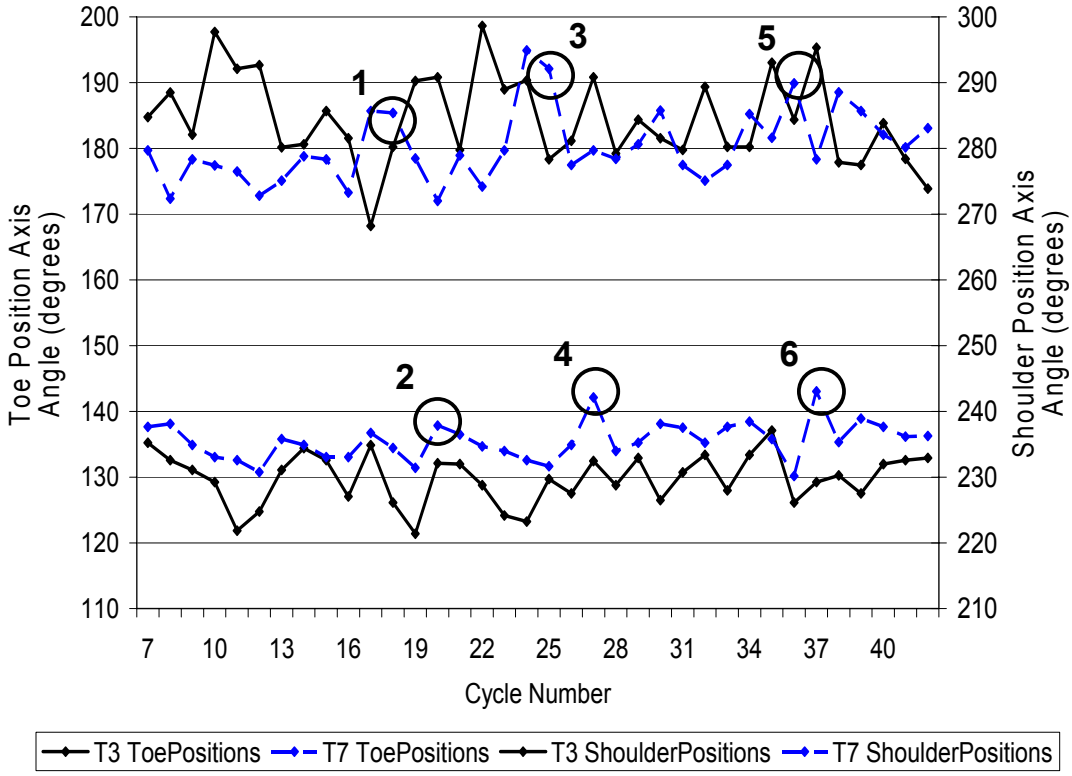


Figure 4.9: Movement probe (second experimental program) toe and shoulder position plots (cycles 7-42) for: Test 3 (ORGateNODelay) and Test 7 (DatumTestNoDelay).

Points 1 and 2 marked on Figure 4.9 represent the effect that a sudden rise in shoulder position has on the toe position; point 1 (test 7 data curve) indicates a shoulder reading of 290 degrees (cycle 18) and corresponding toe reading (point 2) of 138 degrees (cycle 20). This trend is observed again at points 3 and 4, and 5 and 6. Besides movement probe design, sensitivity (and hence signal capturing); many other variables such as surrounding ball positioning and speed; liner profile; instant of ball projection etc. effect this shoulder to toe relationship, hence this trend is not as recurrent as expected.

4.7.5 Movement probe data conclusions

The movement probe data does not accurately measure the load behaviour of a dry industrial ball mill; primary reason being that the movement probe was subject to forces from different directions, thus producing an ambiguous signal.

Due to problems associated with the datum signal, only two tests were used for data analysis. The arithmetic mean average toe and shoulder results[7] are 133 and 282 degrees, respectively.

4.8 Photo detector probe data analysis, results and discussion

Photo detector probes were used in both experimental programs; however photo detector data was only successfully recorded in the second experimental program. OR-Gate signals were used to record photo detector data. The methodology used to process the data was identical to that of the conductivity probes. Detailed analysis and discussion of the results are presented in this section.

4.8.1 Data analysis per cycle and selection methodology

Out of the three detectors (PDC, PDCR and PDS) mounted on the mill in the second program, only photo-detector probe measuring ball reflection from a laser mounted approximately 2mm from the receiver (or PDCR) transmitted data successfully to the ARM device.

The PDCR was mounted on one of trunnion liners positioned closer to the mill shell, measuring a distance of 514.64mm from the mill inner shell wall to the detector probe (Figure 4.10). Its data path thus lies along a diameter of 3710mm (or radius of 1855.36mm) as oppose to the conductivity and movement probe data path which lies along the mill inner liner diameter of 4620mm.

[7] Results are calculated by calculating the arithmetic mean average between tests 3 and 7.

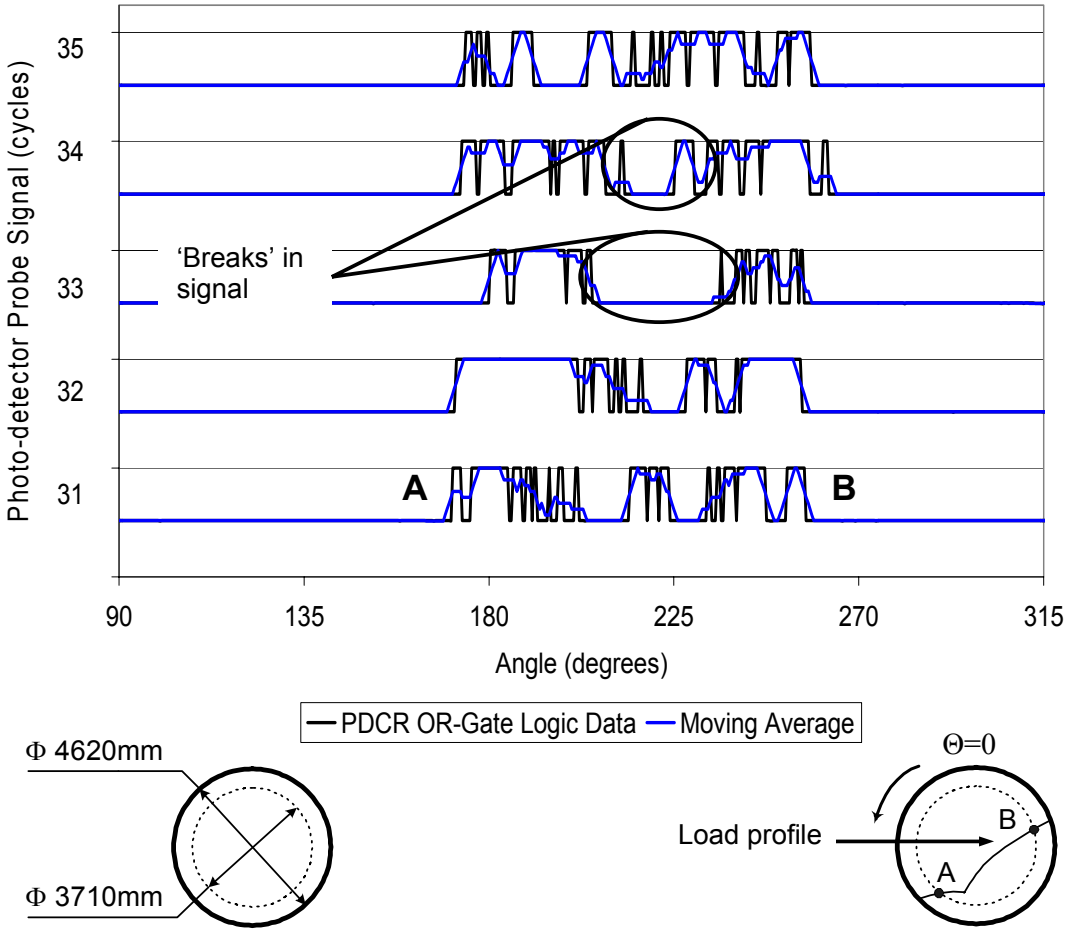


Figure 4.10: Typical (PDCR) photo-detector probe profile, including moving average analysis, indicating positions A and B (second experimental program, Test 3 (OR-Gatedata), cycles (31-35).

The PDCR probe OR-Gate signal recorded by the ARM was processed and graphically displayed (Figure 4.10) using the data processing program. This graphical display is typical of the recorded reflective photo detector OR-Gate type plots (once the mill load reaches steady state conditions). The marked letters 'A' and 'B' on cycle 31 correspond to the points where PDCR probe intersected the mills load profile. Even though these positions are well defined, the data curve is very erratic displaying numerous 'breaks' in signal throughout each cycle. This erratic nature of the data is typical as good ball reflection is a function of various factors such as: ball surface curvature and overall size; dust level etc. The larger 'breaks' in the signal (as shown in cycles 33 and 34, Figure 4.10) located in the middle or towards the end of certain cycles are thought to occur due to reduction in load pressure within the load (as the shoulder position is reached), causing

the balls facing the photo-detector to shift slightly, resulting in a break in reflection. It is likely that the 'breaks' could also be caused by ball positioning reflecting light away, or balls being to close to the detector.

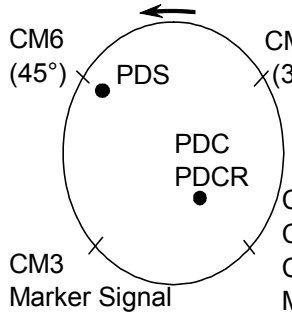
The degree values corresponding to the foremost positions were captured using the moving average analysis and thereafter the 25 per cent incremental data collection process. Nine periods (or 20ms) were used to project a trend line over the original photo-detector data. To standardize the amount of data to be statistically analysed per test, the first seven cycles were omitted. This allowed for the mill to reach steady state conditions and improved the accuracy of the results.

4.8.2 Analysis of experimental data and results

Photo detector probes were included in six out of the eleven tests conducted in the second experimental program. The only two tests that successfully recorded ball reflection data (using probe PDCR) were tests 3 and 4. Test 3 recorded data from mill start-up whereas in test 4 the mill operated for 2 minutes prior to data capture.

Table 4.11 represents a summary of the test schedule and grading of all probe photo detector data recorded.

Table 4.11: Second experimental program (new liner) test schedule, indicating three types of photo-detector probes and experimental test details per probe.



		Photodetector AllSignals	Photodetector RawSignals High-Speed Sampling	ORGate NoDelay	ORGate 2minDelay	ORGate NoDelay	ORGate NoDelay
	Test No.	1	2	3	4	5	9
Photo detectors							
PDC Photo-detector positioned close-to-mill-Centre (225 degrees)		R - OR	R			R - OR	OR
PDCR Photo-detector positioned close-to-mill-Centre (Reflection type) (225 degrees)		R - OR	R	OR	OR	OR	
PDS Photo-detector positioned close-to-mill-Shell (45 degrees)		R - OR	R				
Additional test data	Units						
Logging rate	freq.	200	500	200	200	200	200
Logging rate	ms	5	2	5	5	5	5
Mill 2C Operating Duration	min	3:30	3:00	3:30	5:30	3:30	3:30
ARM - Delayed Start	min	0	0	0	2	0	0
ARM - Logging Start	time	19:10:26	19:44:34	21:31:33	21:56:59	22:29:01	16:19:24
ARM - Logging Finish	time	19:13:10	19:45:07	21:34:17	21:59:53	22:31:44	16:22:08
ARM - Logging Time	time	0:02:44	0:00:33	0:02:44	0:02:54	0:02:43	0:02:44

Key

1. Filtering method used for recording data	R	Raw
	RH	Raw-hold
	OR	OR-Gate logic
2. Quality/Consistancy of data		Good (> 70% of useful data)
		Average (between 40-70% of useful data)
		Poor (< 40% of useful data)

4.8.3 Discussion of experimental results

The reflective probe toe and shoulder results are illustrated in Table 4.12. These results were calculated by computing the average values from the 25, 50 and 75 per cent data generated from the moving average curves.

The reflective probe results for test 3 indicate that position A data is concentrated over a concise data range, spread over approximately 17 degrees suggesting that it took the ball load approximately 17 degrees (or 0.2 seconds) to settle in front of the detector. Between positions A and B a number of signal 'breaks' were recorded and the load 'locked-in-state' condition lasted for just under 1 second. The data distribution at position B is concentrated over a 30 degree region (approximately double that of position A).

Table 4.12: Photo-detector probe results (PDCR): Test 3 (ORGateNoDelay) and Test 4 (ORGate2minDelay), calculated by calculating the average values from the 25, 50 and 75 per cent data generated from the moving average curves.

	Test 3	Test 4	Deviation	Test 3	Test 4	Deviation
	Position A (degrees)			Position B (degrees)		
Minimum	168.84	142.95	-25.88	236.05	218.55	-17.50
Maximum	185.89	186.38	0.49	265.92	257.70	-8.22
Sample Number	35.00	34.00	-	36.00	35.00	-
Arithmetic Mean	175.00	163.41	-11.59	256.55	240.07	-16.48
Midrange	8.52	21.71	13.19	14.94	19.58	4.64
Range	17.05	43.43	26.38	29.87	39.15	9.28
Standard Deviation	19.06	141.54	122.48	46.29	124.32	78.02
Variance	4.31	11.90	7.59	6.78	11.15	4.37

Test 4's reflective probe results deviate significantly from test 3's results. Position A's data is spread over a 43 degree range (or 0.5 seconds), exceeding double that of test 3's position A. Position B's test 4 data range exceeds test 3's by 10 degrees. It is believed that the key reason for these large reflective probe differences is the malfunctioning of the datum signal during test 4.

A close examination of several cycles of test 4's datum data using the ARM graphical display (Figure 4.11) demonstrates the extent of the datum malfunction. From Figure 4.11 it is evident that the consistency and accuracy of the datum signal decreased per cycle i.e. out of the ten cycles displayed, only cycles 5, 8 and 14 demonstrate well defined datum signals. This malfunctioning of the datum signal data had a direct effect on the validity of test 4's reflective probe data as its data was referenced from the datum signal.

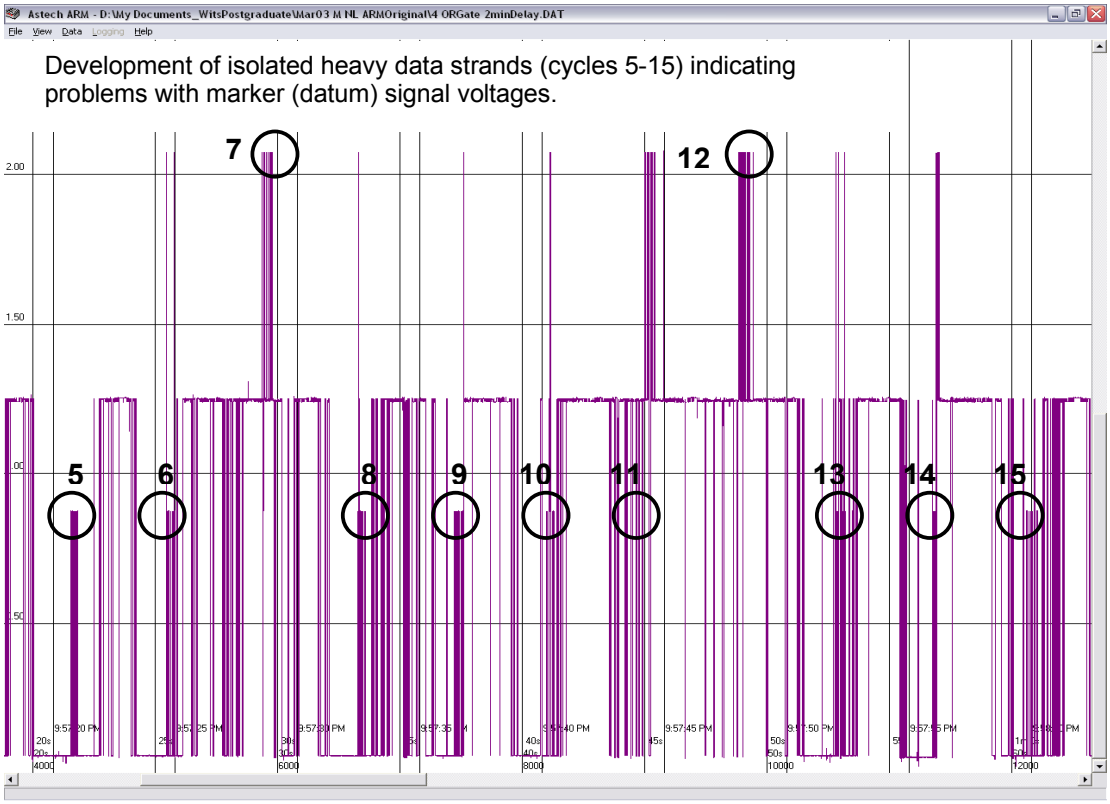


Figure 4.11: ARM graphical display of conductivity probe CM6 and datum signal data from second experimental program. X and Y scales represent time and voltage, respectively. Test 4 (ORGate2minDelay) Cycles (5-15).

Figure 4.12 is a plot comparing test 3 and 4's 75 per cent degree values for positions A and B, starting from cycle 7 through to 42. It is clear that test 4's A and B data curves converge; this unexpected behaviour is thought to be primarily owed to the malfunctioning of the datum signal. Several attempts were made at modifying test 4's datum's signal by altering the mills speed between -2 and +2 per cent to account for speed variations (this would allow the data processing program to search for an alternative repetitive voltage trend and hence result in a different datum signal). These attempts were unsuccessful, as they resulted in irregular datum curves and in turn irregular reflective probe results.

Points 1 and 2 (Figure 4.12), cycles 15 and 34, respectively, denote two extreme points on test 4's position B data curve. Their corresponding cycles where inspected however besides a slightly extended load cycle, no other erratic signal was present. Points 3 and 4 however were eliminated from tests 4's curves as erratic signals were present in their corresponding cycles. Besides unidentified faults in the electronics and/or sensing

equipment, there are various reasons, which might be the cause of these erratic voltage signals (refer to section 4.8.1).

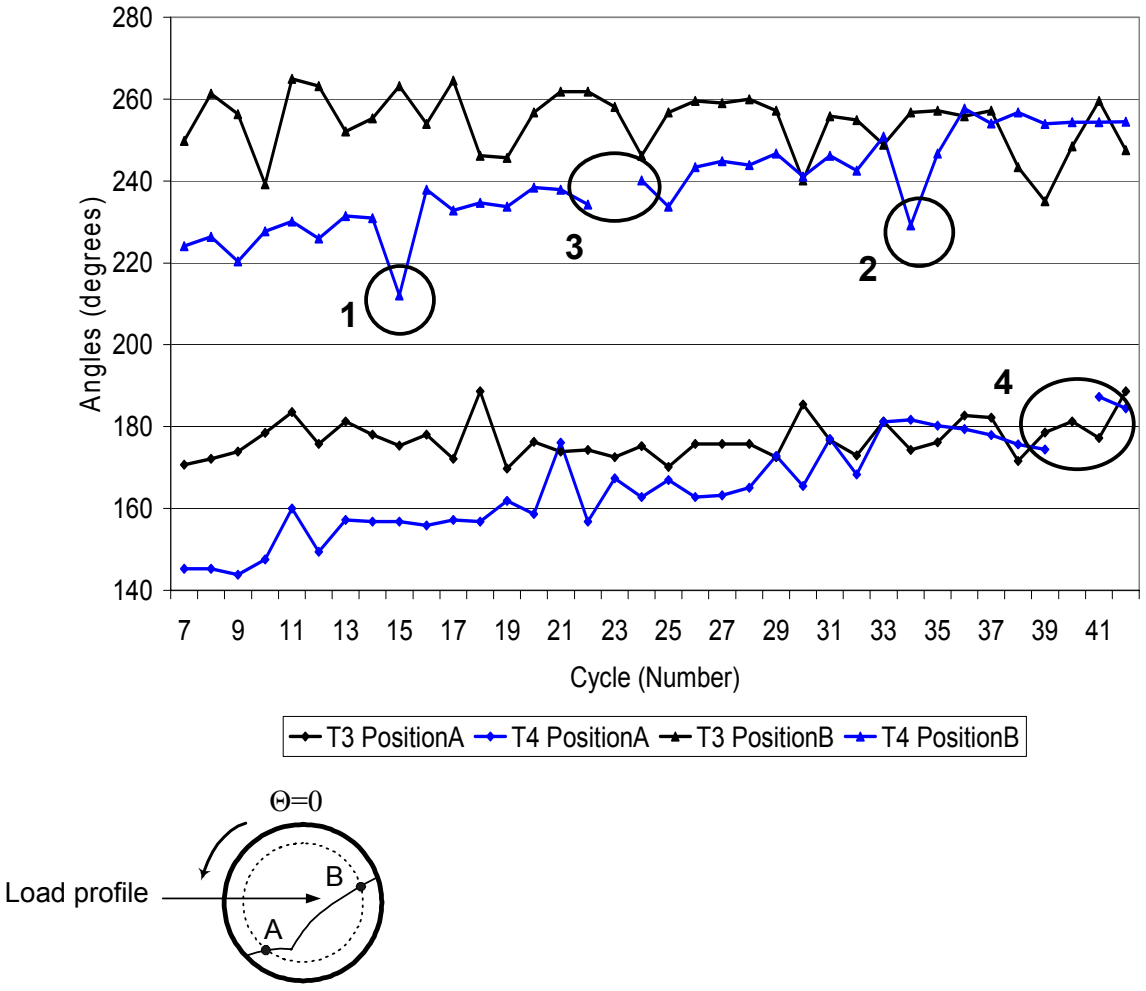


Figure 4.12: Photo-detector (PDCR) plot comparing test 3 (ORGateNoDelay) and test 4 (ORGate2minDelay) 75 per cent degree values for positions A and B, between cycles 7 - 42.

4.8.4 Photo detector probe data conclusions

Only two tests where used in the analysis: test 3 (recorded data from rest) and test 4 (recorded data after a 2 minute delay period); test 4's reflective probe data is questionable and thus discarded from further analysis primarily because of problems encountered with the datum during that test.

Test 3's results are concentrated over a shorter range at position A (17 degrees) compared to position B's (30 degrees). Their arithmetic mean is 175 and 256 degrees at positions A and B, respectively.

Several cycles displayed erratic voltage signals for both positions A and B; especially at the early cycles of test 3. These erratic signals can be attributed to ball behaviour and positioning especially on mill start-up and throughout the 2 minute duration of the experiment.

Due to the insufficient number of recorded test data (and high unreliability thereof), no further analysis will be performed on the photo detector probe data.

4.9 Worn and new liner simulation results

Simulations for both worn and new liners were conducted using Mishra and Rajamni's (1994) computer-simulation 2D package (Millsoft Version 1.1). The simulation is based on the discrete element method (DEM) of particle flows inside ball mills.

4.9.1 Millsoft simulation setup

Mill design and operating parameters used to conduct the Millsoft simulations included: mill diameter; length; speed; charge density and size distribution; lifter material and geometry. In addition, Millsoft also required the user to input the following parameters: normal Stiffness (K_N); shear Stiffness (K_S); ball to ball coefficient of restitution and friction; and ball to wall coefficient of restitution and friction. Table 4.13 displays pertinent data used in the simulation. Altering any of these parameters has a direct effect on the load behaviour and hence simulation results.

Millsoft outputs three types of data, namely: a visual animation of grinding charge motion; prediction of mill power (discussed in Chapter 5); and a distribution of the impact energy.

The visual animation of the load may be displayed as: continuous play; one time display; or frame by frame. A frame by frame type display was selected, from which two types of plots were generated, namely: particle density plot; and a ball path distribution plot.

Two simulations (of twelve revolutions each) were executed using Millsoft. A single class of 50mm diameter balls was used for each simulation. The first simulation was performed using worn liner data (measured off Mill 2Cs removed worn liners), while the second used new liner measurements (refer to Appendix 5, Figure A5.4 for dimensioned cross-sectional view of worn and new liner profiles). The simulations generated 120 frames per revolution, resulting in a total of 1440 frames available for toe and shoulder position analysis.

Table 4.13: Millsoft contact parameters used for both worn and new liner simulations

Normal Stiffness (KN)	400000
Shear Stiffness (KS)	300000
Coefficient of Restitution:	
Ball-ball impact	0.66
Ball-Wall impact	0.36
Coefficient of Friction:	
Ball-ball impact	0.142
Ball-Wall impact	0.389
Mill effective diameter (New/Used liners)	4642/4656mm
Mill length	7320mm
Mill filling	19.4%
Mill rotational speed	15.32 RPM
Critical speed	19.74 RPM
Number of lifters	40
Ball density	7800kg/m^3
Ball size (diameter)	50mm
Voidage (ε)	0.4

4.9.2 Simulation analysis and selection of toe and shoulder positions

Only revolution 11 (120 frames) out of the total twelve revolutions recorded for worn and liners was used in the load positioning analysis.

The following system was implemented to ensure consistent, accurate recording of load toe and shoulder positions for each of the 120 frames recorded per mill revolution. The toe position was defined as the degree value at the point where initial constant contact was established between the ball and down coming mill shell; whereas the shoulder position was defined as the degree value were the contact between the ball and rising mill shell was lost. Figures 4.13 and 4.14 represent the position density plots generated by Millsoft for worn and new liners, respectively.

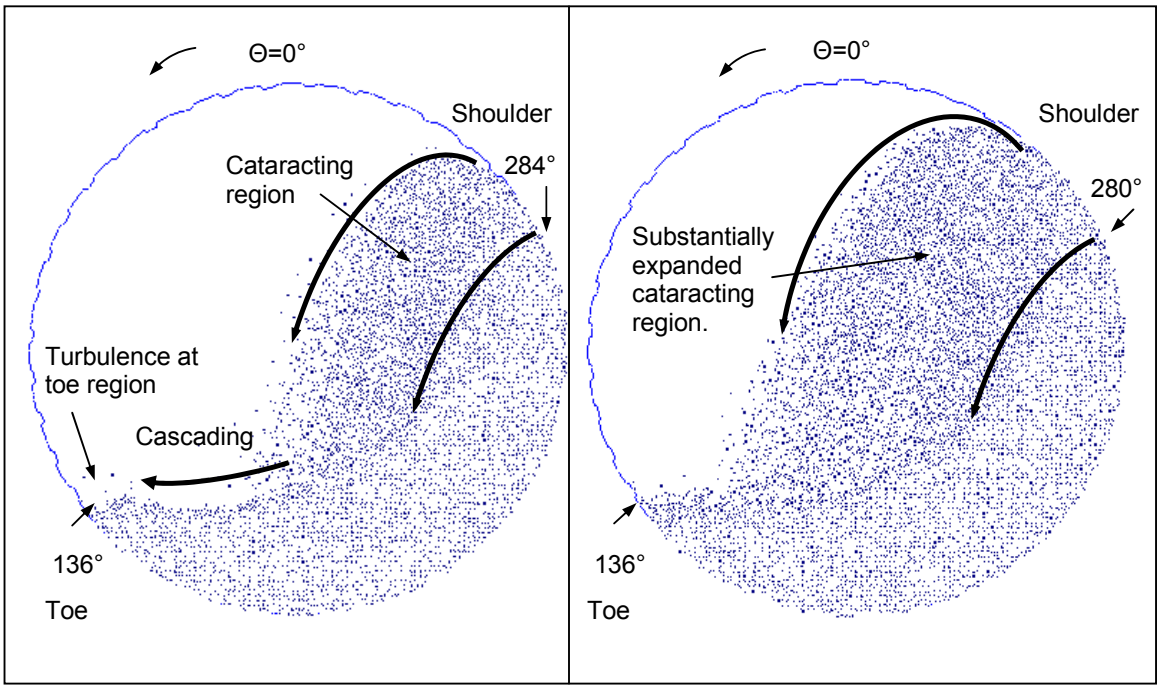


Figure 4.14: Ball density plot representing worn liner load behaviour for a Φ4.74m ball mill (effective diameter Φ4.656m); 19.4% load volume; 50mm balls. Display indicates turbulent toe region thought to have been caused by the cascading ball action rushing towards the toe.

Figure 4.144: Ball density plot representing new liner load behaviour for a Φ4.74m ball mill (effective diameter Φ4.642m); 19.4% load volume; 50mm balls. Display a substantially expanded cataracting region resulting in a similar toe value to that of Figure 4:13. Shoulder position is slightly lower than that of the worn liners (this unexpected behaviour is thought to have occurred due to the more aggressive new liner profile).

4.9.3 Discussion of simulation results

Using the selection methodology defined in section 4.9.2, a statistical analysis (Table 4.14) together with a plot of the toe and shoulder data (Figure 4.15) were produced.

The arithmetic mean results for the toe positions for both worn and new liners are identical at 135.6 degrees (Table 4.14) with a standard deviation of approximately 5 degrees.

Shoulder arithmetic mean positions between worn and new liners differ by 4.6 degrees (Table 4.14). Two fundamental differences thought to have contributed to this lower shoulder position between the worn and new liners are: the more aggressive new liner profile, which resulted in greater cataracting ball action; and the lower ball concentration at

the shoulder region, resulting in greater ball cascading action at early stages in the shoulder region.

Table 4.14: Millsoft simulation toe and shoulder statistical analysis results for worn and new liners (revolution 11).

Millsoft recorded data Revolution 11	Worn	New	Deviation	Worn	New	Deviation
	Toe (degrees)			Shoulder (degrees)		
Minimum	132.00	131.00	-1.00	279.00	274.00	-5.00
Maximum	141.00	141.00	0.00	289.00	286.00	-3.00
Sample Number	120.00	120.00	-	120.00	120.00	-
Arithmetic Mean	135.59	135.67	0.07	284.69	280.07	-4.63
Midrange	4.50	5.00	0.50	5.00	6.00	1.00
Range	9.00	10.00	1.00	10.00	12.00	2.00
Standard Deviation	4.43	4.95	0.52	5.53	3.74	-1.78
Variance	2.10	2.22	0.12	2.35	1.93	-0.42

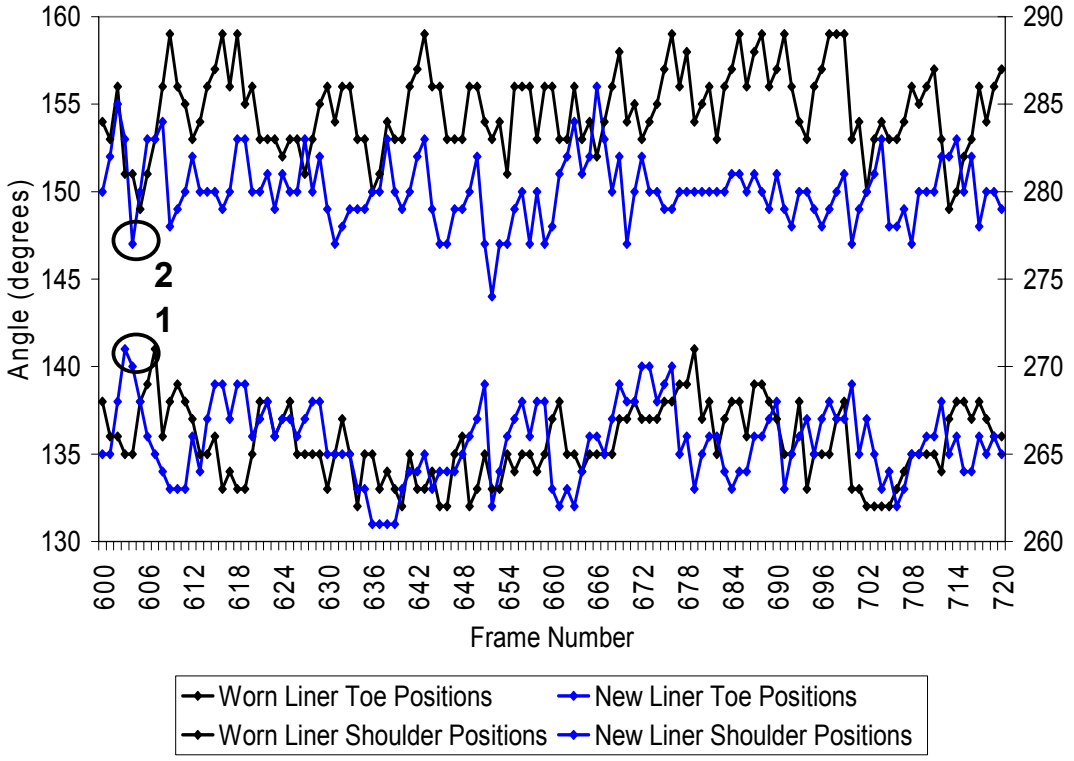


Figure 4.15: Millsoft plot comparing simulation results selected from worn and new liners simulations (revolution 11, 121 frames (frame no. 600 -720). Plot indicates similarity in toe positions and a higher shoulder position for worn liners, implying more cataracting ball action

It is clear from Figure 4.15 that both toe and shoulder results are constantly oscillating over an approximately 10 degree range. Also evident for several cycles is the recurring pattern that exists between the toe and shoulder positions of each cycle i.e. points 1 and 2 on the new liner data curve, indicate that a high toe position (141 degrees, cycle 603) results in a corresponding low shoulder position (277 degrees, cycle 604), or vice-versa.

4.9.4 Millsoft simulation conclusions

Two simulations were conducted, the first made use of worn liner geometrical data, while the second used new liner data. Of the 12 revolutions performed per liner configuration, 120 frames of each 11^{th} revolution where analysed.

The results showed identical toe arithmetic mean values (of 135.6 degrees) for both worn and new liners, indicating that the different liner configuration did not have a great effect on the toe position. The worn liner shoulder arithmetic mean results differed to that of the new by 5 degrees i.e. physical contact between the ball and liner was lost at 284.7 and 280 degrees for the worn and new liner configurations, respectively (this unexpected behaviour is thought to have occurred due to the more aggressive new liner profile).

Note that the mill load behaviour for worn and new liners did differ, however the scope of this report focuses only on the analysis of the load toe and shoulder positions for the worn and new liners.

4.10 Comparison of experimental data with Millsoft results

Experimental data for both worn and new liners are compared to Millsoft 2D mill simulation program.

4.10.1 Millsoft comparison to conductivity and movement probe results

Table 4.15 presents the Millsoft simulation load toe and shoulder position results for worn and new liners together with the conductivity and movement probe arithmetic mean average results calculated from the first and second experimental programs.

Millsoft results represent the load toe and shoulder positions more accurately than the conductivity results because of the difficulties encountered by the conductivity probes in achieving good electrical contact (section 4.4.3). It is thought that the conductivity results (recorded for both worn and new liners) represent only the load 'locked-in-state' or the period where maximum pressure is applied to the mill walls. Worn (or smooth) liners are known to reduce the load 'locked-in-state' period (Moys et al, 1993), as particle slippage is common with worn profiles; hence conductivity probe load cycle for worn liners is 38 degrees less to that of Millsoft load cycle.

Table 4.15: Millsoft worn and new liner load toe and shoulder results compared to conductivity and movement probe experimental program results.

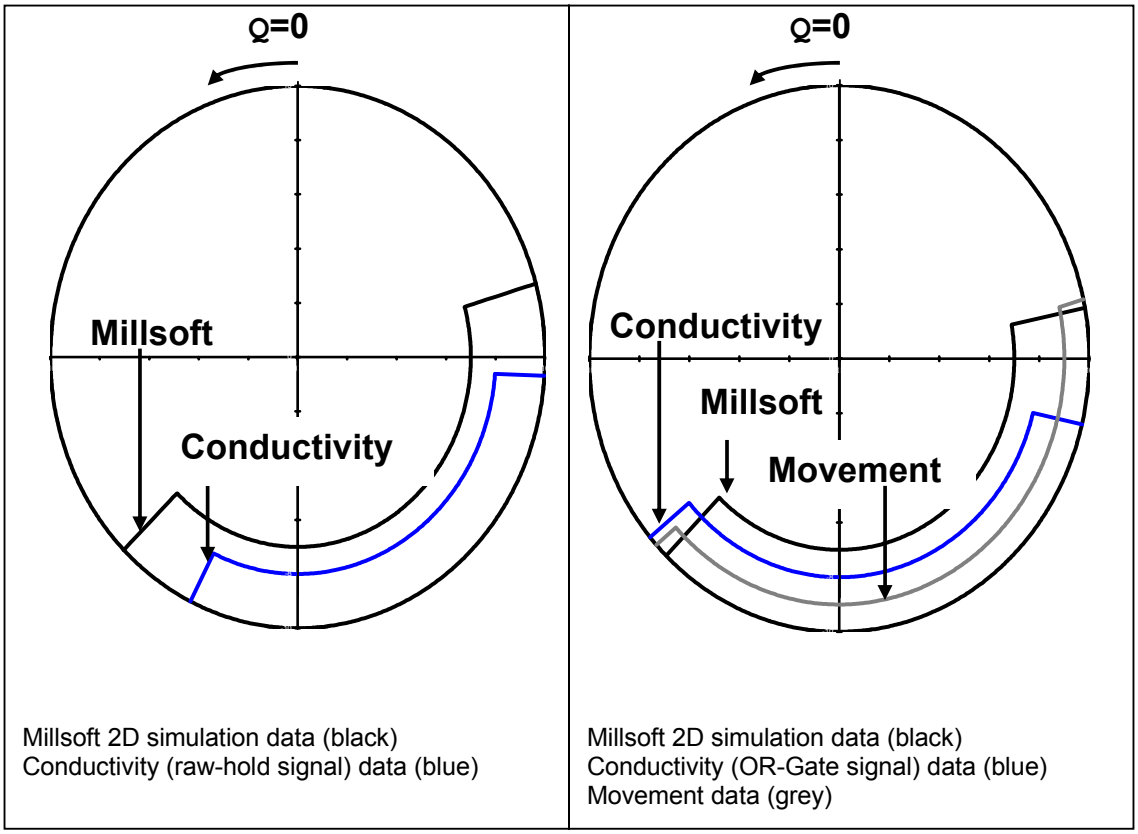
Source data	Load arithmetic mean average results		Load Cycle (degrees)
	Toe (degrees)	Shoulder (degrees)	
First Experimental Program (Worn Liners)			
1. Millsoft simulation results	136	285	149
2. Conductivity probe results (Raw-hold signal)	154	265	111
Second Experimental Program (New Liners)			
4. Millsoft simulation results	136	280	144
5. Conductivity probe results (OR-Gate signal)	131	256	125
6. Movement probe results (Raw signal)	133	282	149

The load cycle difference between Millsoft and new liner conductivity results, is half (19 degrees) compared to that of worn liner deviation. Two factors thought to have contributed to better electrical contact are: the improvement in the conductivity data capturing signal (OR-Gate signal); and less ball slippage occurs with new liners, resulting in a longer load cycle.

A common trend noted between the Millsoft simulation and conductivity experimental results is the drop in shoulder position between the worn and new liner experiments. Factors thought to have contributed to this is the new, more aggressive liner profile and resulting increase in cataracting ball action at the shoulder (refer to section 4.9.3).

The movement probe toe and shoulder results in the second experimental program are almost identical to that of Millsoft's simulated results, with the movement probe experimentally recorded load cycle being only 5 degrees greater to that of predicted load cycle.

Figures 4.16 and 4.17 represent a comparison between the first and second program experimental and Millsoft simulation results.



Millsoft 2D simulation data (black)
Conductivity (raw-hold signal) data (blue)

Figure 4.16: First experimental program (worn liner) load arithmetic mean toe and shoulder results indicated along the mill shell

Millsoft 2D simulation data (black)
Conductivity (OR-Gate signal) data (blue)
Movement data (grey)

Figure 4.17: Second experimental program (new liner) load arithmetic mean toe and shoulder results indicated along the mill shell

4.10.2 Conclusions of Millsoft comparison

Second experimental program compared better to the Millsoft simulation results, than the first program.

Conductivity results dramatically improved at the toe region between the first and second programs, implying that the OR-Gate signal electronic configuration is more sensitive to data capture, especially at the toe region. No improvement was noted at the shoulder position; it is believed that the probe design limits accurate recording of the ball trajectory positions. Also noted is that conductivity results are thought to represent only the load 'locked-in-state' or the period where maximum pressure is applied to the mill walls (section 4.10.1).

Movement probe data paralleled Millsoft simulation results, thus increasing our confidence in the reliability of this probe for recording load toe and shoulder positions.

CHAPTER 5
MILL POWER

5.1 Introduction

Comminution equipment is considered to be one of the highest energy consuming and hence costly processes in most processing plants. Grinding mills consume most of this energy and usually incur the highest capital costs; hence accurate prediction of mill power plays a vital role in the design and control of grinding mill circuits. Power draft is also related to milling capacity as the mill should draw the maximum power possible to achieve the highest production rate. Based on this reasoning, mill power is considered by most researches to be one of the most important parameters when comparing performance for different mills.

This chapter compares the measured experimental power for both worn and new liners to power calculated from published power prediction models and Millsoft (DEM software). Prediction models used include that of Bond (1962), Harris et al (1985) and Morrell (1993).

5.2 Experimental measurement of power: Mill 2C

The mill input (or metered) power was recorded for each experimental program. This was done using an electronic device (connected to the mill main motor switchgear), constantly monitoring mill power during the mill test programs (refer to Appendix 1, Table A1.5 to review details of power monitoring device).

The following methodology was adopted in calculating the mill average power for the first and second experimental programs:

1. Three tests were selected from each program, with each test including a complete trace of the power signal.
2. The average power per test was then calculated. Only the power measurements recorded after a 30-45 second time lapse (or after the first 7-11 revolutions) per test where accounted for. This procedure ensured that all power readings selected reflected mill equilibrium conditions.

The average of the three tests thus reflects the measured power draw per experimental program.

The average power calculated for all three tests for the first and second experimental programs is 1863kW and 1936kW (Table 5.1), respectively i.e. the new liner instalment draws approximately 70kW (or an additional 4 per cent of mill motor power).

Table 5.1: First and second experimental program calculation of average mill powers.

	Test 1	Test 2	Test 3	Average (kW)
First experimental program tests	Test 4 RawNoDelay	Test 5 Raw5minDelay	Test 6 Raw 2minDelay	
Average measured power (kW)	1868.75	1857	1864	1863
Second experimental program tests	Test 6 DatumTest 2minDelay	Test 7 DatumTest NoDelay	Test 9 ORGate NoDelay	
Average measured power (kW)	1933.75	1928	1945	1936

5.3. Power model definitions

5.3.1 Bond

Bond's most recent equation (1962) for mill input power for 'conventional wet-grinding ball mills using make-up balls larger than about one-eightieth of the mill diameter' is defined as:

$$kW = 12.262\ D^{2.3}\ L\ \rho\ \phi\ J\ (1 - 0.937J)\ (1 - 0.1 / 2^{9-10\phi}) \qquad (5.1)$$

where, D is mill interior diameter (m), L is the mill internal length (m), ρ is defined as the bulk density of steel balls (tones / m^3), Φ is the fraction of critical speed, and J is defined as the volume fraction of ball charge. Bond (1962) added that for dry-grinding grate discharge mills the input mill power must be multiplied by a factor of 1.08. Since mill power is directly proportional to the filling term J (1 – 0.937J); differentiating this term and solving results in a filling volume of 0.53 i.e. indicating that the maximum mill power is drawn at 53 per cent of ball charge volume.

5.3.2 Harris, Schnock and Arbiter

Harris, Schnock and Arbiter (1985) semi-empirical equation, applied to a ball mill application is defined as:

$$kW = 10.76\ D^{2.5}\ L\ \phi\ \rho\ (1-\varepsilon)\ J\ (1.05-1.13J)\ (1-0.1/2^{9-10\phi}) \quad (5.2)$$

where, where, D is mill diameter (m), L is the mill length (m), ρ is defined as the bulk density of steel balls (tones / m^3), Φ is the fraction of critical speed, ε is the porosity of the ball bed and J is defined as the volume fraction of ball charge.

5.3.3 Morrell

Two of the three power prediction models presented by Morrell (1993) are used in the present investigation, namely the 'C-Model' and 'E-model'. Equation 5.3 defines Model-C's underline structure:

$$P_{Gross} = P_{No-Load} + kP_{Net} \quad (5.3)$$

where, P_{Gross} is the power input to the mill motor (or metered power), $P_{No\text{-}Load}$ is the power input to the motor when the mill is empty and P_{Net} is the theoretical power (dependant on the design characteristic of the mill) transmitted to the charge to provide motion. K factor is a calibration factor which accounts for heat losses due to internal friction, energy for attrition/abrasion breakage and rotation of the grinding media.

Morrell defined No-Load power as:

$$P_{No-Load} = 2.62\ (D^{2.5}L\ \phi)^{0.804} \quad (5.4)$$

where, D is the diameter of the cylindrical section of the mill inside liners (m), L is the length of the cylindrical mill inside liners (m) and Φ is the fraction of critical speed.

Morrell defined P_{Net} to consist of both a cylindrical and conical end component as defined by equations 5.5 and 5.7, respectively.

$$P_{Net} = \frac{\pi\ g\ L\ N_m r_m}{3(r_m - z\ r_i)}\left[2r_m{}^3 - 3zr_m{}^2 r_i + r_i{}^3(3z-2)\right]\left[\rho_c(\sin\theta_S - \sin\theta_T) + \rho_p(\sin\theta_T - \sin\theta_{TO})\right] + L\rho_c\left[\frac{N_m r_m \pi}{(r_m - z\ r_i)}\right]^3\left[(r_m - z\ r_i)^4 - r_i{}^4(z-1)^4\right] \quad (5.5)$$

and $$z = (1 - J_t)^{0.4532} \quad (5.6)$$

where,

g	=	acceleration due to gravity (m/sec^2)
N_m	=	mill rotational speed (revs/sec)
r_m	=	radius of the mill inside liners (m)
r_i	=	radial position of the charge inner surface (m)
ρ_c	=	density of the total charge (t/m^3)
ρ_p	=	discharge slurry density (t/m^3)
θ_S	=	angular displacement of the shoulder position at the mill shell (rads.)
θ_T	=	angular displacement of the toe position at the mill shell (rads.)
θ_{TO}	=	the angular displacement of surface of slurry pool at the toe (rads.)
J_t	=	fraction of mill balls occupied by balls and coarse ore charge (including voids)

$$P_c = \frac{\pi\ g\ L_d\ N_m}{3(r_m - r_t)}\left[(r_m{}^4 - 4r_m r_i{}^3 + 3r_i{}^4)(\rho_C(\sin\theta_S - \sin\theta_T) + \rho_p(\sin\theta_T - \sin\theta_{TO}))\right] + \frac{2\pi^3 N_m{}^3 L_d \rho_c}{5(r_m - r_t)}(r_m{}^5 - 5r_m r_i{}^4 + 4r_i{}^5) \quad (5.7)$$

where,

L_d	=	length of cone end (m)
r_t	=	radius of discharge trunnion (m)

Morrell's semi-empirical E-Model is defined by equation 5.8. Its response to changes in speed and mill filling were based on that of the C-Model. Morrell found E-Model power predictions to be marginally less precise than the C-Model.

$$P_{Gross} = P_{No-Load} + (kD^{2.5}L\rho_c\gamma\delta) \tag{5.8}$$

where,

$$\gamma = J_t(\beta - J_t) / \beta^2 \tag{5.9}$$

$$\beta = 2(2.9863\phi - 2.2129\phi^2 - 0.49267) \tag{5.10}$$

$$\delta = \phi(1 - (1 - \phi^*_{max})e^{-19.42(\phi^*_{max} - \phi)}) \tag{5.11}$$

$$\phi^*_{max} = 0.954 - 0.135J_t \tag{5.12}$$

$$\rho = 0.8\rho_o + (0.6J_B(\rho_B - \rho_o)) / J_t + 0.2 \tag{5.13}$$

where, γ and β are non-linear functions of speed and mill filling, respectively; and k is 7.66 for overflow discharge mills, and 8.81 for grate discharge mills.

5.3.4 The Discrete Element Method (DEM)

DEM is a numerical tool that models the motion of individual particles in rotary grinding mills by applying the fundamental laws of physics to individual collisions between balls, rock particles and mill shell. In the present investigation, the ball-to-ball and ball-to-liner collisions are modeled by a linear spring-slider-dashpot model, where: the spring provides the repulsive force depending on the material stiffness (where K_n and K_t represent the stiffness coefficients for normal and shear directions, respectively); the slider accounts for any surface motion that takes place (determined by the coefficient of friction μ); and the dashpot dissipates a portion of the relative kinetic energy in each collision (where C_n and C_t represent the damping coefficients for normal and tangential directions, respectively).

During a collision the particles are allowed to virtually overlap Δx, and the normal v_n and tangential v_t relative velocities determine the collision forces. A linear relationship between particle overlap and force was used in the simulation code. The normal (F_n) and tangential (F_t) forces for each interaction are given by equations 5.14 and 5.15, 5.16, respectively.

$$F_n = K_n \Delta x + C_n v_n \tag{5.14}$$

$$F_t = \mu F_n (F_t > \mu F_n) \tag{5.15}$$

$$F_t = K_t \int v_t dt + C_t v_t (F_t \leq \mu F_n) \tag{5.16}$$

where, dt represents the timestep of the simulation (which is a measure of the time interval between any two successive calculations). The damping coefficient in the normal direction (C_n) depends on the coefficient of restitution, ε, which is defined as the ratio of the velocity of a particle before and after a collision.

$$C_n = -2 \ln \varepsilon \frac{\sqrt{K_n \, m^*}}{\sqrt{(\ln \varepsilon)^2 + \pi^2}} \tag{5.17}$$

Where m* is the reduced mass of two particles m_1 and m_2 defined by:

$$m^* = \frac{m_1 m_2}{m_1 + m_2} \tag{5.18}$$

5.4 Power comparisons and discussion

Mill motor power calculated from power prediction models (defined in section 5.3) are compared to Mill 2C's measured motor power (Table 5.2). For the reason that Bond's and Harris's equations calculate mill power at the pinion shaft, an additional seven per cent was added to their resulting power values. This percentage incorporates all losses associated with a 2MW mill drive motor (4 per cent) and a double reduction gearbox (3 per cent), together with all the interconnecting couplings. Morrell's power model is related to mill input power, hence no added drive train loss percentages are required.

The relative error value (Table 5.2) is calculated using the following equation:

$$\text{Error}(\%) = (P_{\text{Gross (Measured)}} - P_{\text{Gross (Model)}}) / P_{\text{Gross (Measured)}} \quad (5.19)$$

where,

$P_{\text{Gross (Measured)}}$ = measured (or metered) mill power

$P_{\text{Gross (Model)}}$ = model mill input or (drive) power

Table 5.2: Input values used for both worn and new liner power calculations

Decription	Matimba Measured mill power	Semi-Emprical Models				DEM Model
				Morrell Models		
		Bond	Harris	C-Model	E-Model	MillSoft-2D
Worn Liners						
Cylindrical power (kW)		1704	2066	1432	1728	1515
Conical power (kW)		-	-	77	-	-
Morrel's no-load power (kW)		-	-	233	233	233
K-factor (kW)		-	-	324	-	-
Drive-train losses (kW)		119	145	-	-	122
Gross Power (kW)	1863	1704	2066	2066	1961	1871
Relative Error (%)		8.6	-10.9	-10.9	-5.3	-0.4
New Liners						
Cylindrical power (kW)		1692	2051	1430	1715	1531
Conical power (kW)		-	-	76	-	-
Morrel's no-load power (kW)		-	-	232	232	232
K-factor (kW)		-	-	324	-	-
Drive-train losses (kW)		118	144	-	-	123
Gross Power (kW)	1936	1692	2051	2062	1947	1887
Relative Error (%)		12.6	-6.0	-6.6	-0.6	2.5
Power difference (New-Worn) (kW)	72	-12	-15	-4	-14	16

Mishra's Millsoft-2D program predicted a Gross power of 1871kW, just 8kW short of Mill 2C's first experimental (worn liner) measured mill power. Following this prediction was Morrell's 'E-Model' at 1961kW resulting with a relative error of 5.3 per cent (or an over-prediction of 98kW).

In the second experimental program (new liners) Morrell's 'E-Model' over predicted mill power by 11kW, followed by Mishra's Millsoft-2D program which under predicted mill power by 49kW resulting with a relative error of 2.5 per cent.

Harris's and Morrell's 'C-Model' both over-predicted mill 2C's measured power. Worn liner predictions resulted in a relative error of approximately 11 per cent (equivalent to an additional 203kW) for both models; new liner predictions resulted in Harris's power results being slightly less than Morrell's 'C-model' at approximately 115 and 127kW (or 6 and 6.5 per cent relative error), respectively as compared to mill 2C's measured power.

Bond's magnitude of the relative percentage error increased from worn to new liners from 8.6 to 12.6 per cent (or from 160 to 244kW); resulting in Bond's model under-predicting Mil 2C's measured power the greatest for both the worn and new liners.

All power prediction models besides Mishra's Millsoft-2D program showed a decrease in mill power between the first and second experimental program. Morrell's 'E-Model' and Harris's power model decreased by 14 and 15kW, respectively, whereas Mishra's DEM model showed an increase of 16kW, proving that only Mishra's DEM model shows the correct trend between the first and second program.

5.5 Conclusion

A primary evaluation of how common published equations and a 2D simulation package (Millsoft) compare with measured mill power has been performed. Only Mishra's Millsoft-2D program exhibits the correct trend between new and worn liners.

CHAPTER 6

CONCLUSION AND RECOMMENDATIONS

6.1 Summary of experimental test work

The importance for better understanding grinding mill behaviour and its effect on grinding efficiency and mill power is emphasized in the literature review; also emphasized is the importance of raw data extracted from industrial type grinding mills as this can be used to validate and compare various published power prediction and numerical simulation models.

Experimental test work was carried out in a dry, industrial type ball mill in order to investigate the dynamic behaviour of the ball load (more specifically the load toe and shoulder positions) inside the mill. This was recorded using specifically designed experimental probes, positioned at strategic locations onto the mill shell and conical ends. The probes were inserted in the mill via the liners in such a way as to extract data from inside the rotating mill. Three different types of probes where used, namely: electrical conductivity, movement and photo-detector type probes. All three types were constructed by modifying original mill shell and end liner bolts where the modification of each bolt was based on nature of specific measurement.

Two experimental programs were conducted to measure the ball behaviour inside the mill; the first measured the behaviour as a function of worn liners, while the second measured the behaviour as a function of new shell and conical end liners. Mill operating conditions and charge composition remained constant i.e. mill speed, mill fill level, ball distribution and particle shape remained unchanged for both programs.

6.2 Summary of probe effectiveness, load behaviour results and simulation comparativeness

Accurate, reliable measurements of load toe and shoulder positions of a dry industrial ball mill using conductivity probes proved to be a difficult task. The main factor contributing to this was the inherent difficulty in establishing good electrical contact (even though it was known that physical contact did indeed exist). In attempt to overcome this problem the sensitivity of the capturing signals (in the second experimental program) were increased; this however still did not result in reliable load position data. When compared to Millsoft's 2D theoretical numerical simulation model (version 1.1), only the second programs load

toe positions were comparable. It was thus deduced that the conductivity probe design and electronics data capturing system limited accurate recording of the ball trajectory positions and tended to represent more of the load 'locked-in-state' region (or the period where maximum pressure is applied to the mill walls) instead of the load toe and shoulder positions.

The movement probe did not accurately measure Mill 2C's load behaviour because its design subjected it to forces from different directions, however its resulting load position data proved to be highly comparable with Millsoft's results, displaying small deviations in the load toe and shoulder positions.

Of the two photo detector probes installed in the mill ends, none recorded photo detector data in the first experimental program. In the second program only one probe (measuring ball reflection) out of the three probes installed managed to record detector data. Of the only two tests (tests 4 and 3) successfully recorded and processed; test 4's reflective data was discarded due to the effect that the inaccurate datum signal had on its results, while test 3's displayed high variances in its results, resulting in its data defined as unreliable.

6.3 Summary of Mill-2C's measured versus calculated mill input power results

Measured experimental power for both worn and new liners was compared to power calculated from three published power prediction models (Bond (1962), Harris et al (1985) and Morrell (1993)), and Mishra's Millsoft-2D simulation program.

Based on the relative error percentages, only Millsoft-2D program was found to best predict mill input power for both the worn and new liners.

6.4 Recommendations

6.4.1 General project recommendations

All probe designs, experimental procedures and problems encountered in recording the load positioning must be thoroughly studied and investigated; this way when re-designing

of experimental probes and test-procedures for future investigations of load behaviour, the entire process may be expedited with higher efficiency, probe accuracy and reliability.

The following is recommended should further investigation be conducted on similar dry industrial type ball mills:

1. Complete re-design of the datum signal. Datum signal must be clear and distinct from all other inputs. This is important as all other data captured is referenced to this signal.
2. Review design of movement probe and ensure that it is susceptible to only normal forces. Mount two or three along the same row, as close a possible to each other; this way the accuracy and reliability of the load position results may be substantially increased.
3. Refrain from using electrical conductivity for accurately locating the load toe and shoulder positions. If conductivity probes are to be used, ensure that: at least two are positioned along the same row; all probes to protrude the same distance above the liners (this way any inherent bias associated with each probe is minimised); study recorded data carefully after each test and if necessary enter the mill and inspect the probes to ensure no steel particles are collected around each probe.
4. Use more robust, industrial type photo detector receiver sensors and laser emitters; this type proved to be problematic for this harsh environment experienced in the industrial mill.
5. Design a simpler more reliable electronics circuit.
6. Photograph and label each probe used after installation and after each test.

An improved data processing program with additional processing mathematical tools and graphical presentation options would greatly assist in decreasing processing time, better presenting and hence interpreting the data recorded from the experimental probes.

A more in-depth analysis of each power model is necessary to better understand the reasoning and relationship of each, as compared to Mill 2C's measured power.

6.4.2 Recommendations specific to sensor selection

Over the past few years extensive testing has been conducted in small scale laboratory type mills using different methods and hence various sensors in measuring the mill load

toe and shoulder positions. Non-intrusive mill methods such as non-contact acoustics measurements (Pax et al, 2003), and more traditional methods where inductive proximity sensors are placed inside the mill shell liner bolts.

A series of load behaviour experiments conducted in a dry pilot mill by Kiangi et al (2006) have shown that the inductive proximity probes detect ball load positions far better to that of force probes. Inductive and capacitive type proximity sensors have several advantages over the electrical conductivity sensors in that, not only are they easier to install in industrial mills, but are more reliable and accurate as they can detect the presence of metallic objects (as well as other objects in the case of the capacitive sensors) in the proximity of the sensing face. A relationship also exists between the distance the measured object lies from the sensing face of proximity sensor to the sensor outlet signal. This way one can accurately measure the load and shoulder positions for when the mill is loaded with a metallic ball load only and when loaded with a metallic and non-metallic load (Kiangi et al).

REFERENCES

Austin, L.G., Klimpel, R.R. and Lickie, P.T., 1984, Process engineering of size reduction: ball milling, Guinn Printing Inc, New Jersey.

Djordjevic, N., 2003, Discrete element modelling of the influence of lifters on power draw of tumbling mills, *Minerals Engineering*, **16**:331-336.

Kelly, E.G., and Spottiswood, D.J., 1982, Introduction to mineral processing, John Wiley & Sons, New York.

Kiangi K. K. and Moys, M.H., 2006, Measurement of the load behaviour in a dry pilot mill using an inductive proximity probe, Minerals Engineering **19**:1348–1356.

Kiangi K. K. and Moys, M.H., Experimental study on the effect of particle filling and size on the ball load behaviour and power in a dry pilot mill. (To be submitted to Minerals Engineering).

Morrell, S., 1993, Prediction of power draw in wet tumbling mills, PhD. Thesis, University of Brisbane.

Moys, M.H., 1993, A model of mill power as affected by mill speed, load volume and liner design, *J.S. Afri. Inst. Min. Metall.*, **93** (6):135-141.

Moys, M.H. and Liddell, K.S., 1988, The effects of mill speed and filling on the behaviour of the load in a rotary grinding mill, *J.S. Afri. Inst. Min. Metall.*, **88** (2):49-57.

Moys, M.H. and Skorupa, J., 1992, Measurement of the radial and tangential forces exerted by the load on a liner in a ball mill, as a function of load volume and mill speed, *Int. J. Miner. Process.,* **37**:239-256.

Moys, M.H., Van Nierop, M.A. and Smit, L., 1996, Progress in measuring and modelling load behaviour in pilot and industrial mills, *Minerals Engineering*, **9** (12):1201-1214.

Mular, A.L., and Bhappu, R.B., 1980, Mineral processing plant design, Second edition, Society of Mining Engineers of the American Inst. of Mining, Metallurgical and Petroleum Engineers, New York.

Napier-Munn, T.J., Morrell, S., Morrison, R.D. and Kojovic, T., 1996, Mineral comminution circuits: Their operation and optimisation, JKMRC, Queensland.

Pax, R. A. and Djordjevic, N., 2003, Non contact acoustics measurement and validation of SAG mill operation, Proceedings of the XXII International Mineral Processing Congress **1**:371-377 SAIMM.

Stein, K.H., Robinson, A.N. and Pitman, B.L., 2002, Coal milling plant (selection, maintenance, operation and performance), Coal Milling Projects CC, Bryanston.

Van Nierop, M.A., 2001, Characterisation of the load behaviour of an industrial grinding mill, PhD. Thesis, University of the Witwatersrand.

Van Nierop, M.A. and Moys, M.H., 2001, Exploration of mill power modeled as function of load behaviour, *Minerals Engineering*, **14** (10):1267-1276.

White, H.A., 1904, The theory of the tube mill, *J. of the Chem. Metall. and Min. Society S. Afri.,* 290-304.

Wills, B.A., 1992, Mineral processing technology, Fifth edition, Pergamon Press, Oxford.

Internet Addresses used:

a. An energy overview of the republic of South Africa, 2002, http://www.fossil.energy.gov/international/safrover.html,

b. Alstom Air Preheater Company, Power Generation Products BBD “Ball Tube” Horizontal mill, 2003, http://www.airpreheatercompany.com/ballracemill.asp.

APPENDIX 1

BALL MILL AND APPARATUS TECHNICAL SPECIFICATIONS

Table A1.1: Mill 2C Main Motor, Gearbox and Barring gear nameplate details

Main Drive motor nameplate details:	
Manufacturer:	Brown Boveri
Model number / Drive Type / Duty:	No ZSM0254 / OLJ1710196 / S1
Rated power:	2150kW
Speed:	993 RPM
Stator voltage:	6600V
Mass:	11.4 tons
Frequency & Connection type:	50Hz & λ connection Cos φ 0.87
Gearbox nameplate details:	
Manufacturer:	David Brown
Gearbox output speed:	118.535 RPM
Model/Order number:	910164
Barring gear nameplate details:	
Manufacturer:	David Brown
Model/Order number / Type:	15882 / H3T2153 1988
Rated power:	27kW
Input Speed:	1480RPM
Output Speed:	13.07 RPM

Table A1.2: 1/3” COLOUR CCD camera details

Specification:	
Type:	Cone Pinhole lens 3.7mm STD – Indoor Type
Weight (approximately):	300g
Operating current:	90mA w/regulated power input
Power Source:	DC 12V (Tolerance:8V - 15V)
MTBF:	80000 hours
Video output:	1Vp-p 750hm composite
Dimensions:	Φ21mm x 63mm L

Table A1.3: Video camera details

Specification:	
Type:	SONY NP-98 (Handycam Video 8)
Model/Serial Number:	CCD-TR420E / 83333
Power Source:	DC 6V 3-971-656-01

Table A1.4: Polyurethane surface casting elastomer specifications

AXSON - UR 3569 Polyurethane surface casting elastomer Hardness 70 D Shore – RT Curing; Very good abrasion resistance			
Applications:	Polyurethane surface casting resin designed for foundry tools (patterns, core boxes) on aluminium performs, concrete resin etc.		
Properties:	- Good abrasion resistance - Excellent impact and shock resistance - MDA free (Methylene-bis aniline) - Quick hardening		
UR 3569 – Physical Properties			
	PART A	PART B	MIXING
Composition	ISOCYANATE	POLYOL	
Mixing ratio by weight Mixing ratio by volume @ 25°C	100 100	40 39	
Aspect	thick liquid	liquid	liquid
Colour	White	dark amber	light beige to yellow
Brookfield LVT viscosity @ 25°C (mPa.s)	7500	190	3500
Specific gravity @ 25°C Specific gravity of the cured product @ 23°C	1.03 -	1.04 -	- 1.03
Pot life @ 25°C on 500g (min.)			15 - 23
UR 3569 - Mechanical (at 23°C) Properties			
Hardness - @ 23°C - @ 80°C	D1 / D15 Shore	70 / 65 63 / -	
Abrasion loss	mm3	100	

Tensile strength	MPa	30
Elongation at break	%	160
Tear strength - Non cut specimen	kN/m	120
Impact strength (non cut specimen)	kJ/m2	> 80 Doesn't break
Glass temperature transition	°C	105
Thermal coefficient of expansion	10-6.K-1	175
Processing conditions		
Both parts (polyol and isocyanate) must be mixed at room temperature above 18°C according to the indicated ratio. UR 3569 should be degased after mixing in order to obtain a bubble-free product. The operation should not last more than 8 minutes to avoid gel in the vacuum machine. Before casting ensure parts or molds are free of any moisture trace. For additional information refer to www.axson.com for UR 3569 datasheet.		

Table A1.5: Power meter electronic device details

Type:	ECS LAB NO IOIR
Instrument number:	8354615
Date:	26-06-02

A1 Astech 8 Channel Analogue Recording Devise (ARM) Operating Instructions Manual

Contents Page

Operating Instructions Manual 112

1 GENERAL DESCRIPTION....113

2 INPUT CONNECTIONS & RANGE SETTING 114

3 ARM WINDOWS SOFTWARE....114
3.1 OVERVIEW....114
3.1.1 Hardware....114
3.1.2 Choose the Log Parameters and start the ARM Logging....114
3.1.3 Download the logged data....114
3.1.4 Save the Logged Data....115
3.1.5 View the logged data....115
3.1.6 Print or Export the logged data....115
3.2 PRE-OPERATING SET-UP 115
3.2.1 Connection To Laptop or PC....115
3.2.2 Power Supply 115
3.2.3 Running Control & Display Software 115
3.2.4 Configure Serial Port 116
3.3 SET OPERATING MODES 116
3.3.1 Select Active Channels & Scan Intervals 117
3.3.2 Set Logging Modes....118
3.3.3 Remote Start 119
3.3.4 ARM Set-up Control Buttons 119
3.3.5 Setting Triggered Start 119
3.3.6 Setting Delayed Start....120
3.3.7 Setting Channel Options....121
3.4 STARTING & STOPPING LOGGING AND DOWNLOADING THE DATA 124
3.4.1 Start Logging 124
3.4.2 Stop Logging 125
3.4.3 Retrieval of the Logged Data....125
3.5 GRAPHICAL DISPLAY OF MEASUREMENT DATA....126
3.5.1 Graph Key Window....126
3.5.2 Graph Panning and Zooming 126
3.6 SAVING, LOADING AND PRINTING DATA 128
3.6.1 New Data File....128
3.6.2 Open an Existing Data File....128
3.6.3 Save the Logged Data File....128
3.6.4 Save the Logged Data File for Export to Another Program 128
3.6.5 Printing 128

1 GENERAL DESCRIPTION

The Astech ARM is a compact, self-contained solid-state recording module which logs or records single or multiple channels of analogue measurement data into an internal memory. Memory size is 262,000 x 12 bit measurements. It can be used with many types of transducer/sensor and also voltage or current signals. The original analogue input circuit board is removable and can be replaced with a different version to suit new measurement tasks.

Several choices of start mode are available including time delayed start, start on preset input threshold crossover at one or more channels and rolling/pretrigger mode. Mixable sample rates may be set, ranging from 10,000 per second to one every 33 minutes. Configuration of these options is carried out via a graphical user interface running on a laptop or PC, ensuring that setup of the ARM is both simple and straightforward. All communication with the ARM - configuration commands, manual recording start and downloading of stored measurement data, is carried out using an infra-red communications link to a small handheld interface unit which connects to the laptop/PC serial port. The 1-2 metre range of this interface eliminates cable connections and simplifies operation when the ARM is installed in an inaccessible measurement location.

Two versions of the unit are available, one in a lightweight ABS housing for general purpose application and one in a diecast 1P67 sealing enclosure for use in very hostile environments. The infra-red link is made with a second, hand held module which plugs into the serial port of a laptop or PC, or (using the DOS software) via the IrDA port built into many laptop or notebook PCs. In addition to the setup program, the supplied software includes a graph generation facility.

Note: The supplied DOS software will run on any MS-DOS based PC having an 80286 or better processor. However, as the ARM memory contents can be 262,000 measurements, a 486 is recommended for good graph drawing performance. EGA or VGA screens may be used, the latter providing better graph detail.
Most software functions may be controlled via the keyboard, although a mouse is required for the ‘Window Zoom’ facility. The supplied Windows software should work on any PC running Windows 95 or later. The Windows software will load data and INI (channel scalings, names, etc.) files generated by the DOS software. The DOS software cannot load files created by the Windows software.

2 INPUT CONNECTIONS & RANGE SETTING

In the case of the ABS housing, these are made to a separable miniature screwblock connector and for the diecast enclosure version, to an 1P67 sealing version of a 15 way “D” connector. In either version the transducer or signal leadwires are prewired to a connector rather than hardwired to the ARM module, simplifying installation. In the case of the diecast enclosure version, direct connection analogue input boards can also be supplied. These reduce the overall module dimensions and improve reference junction compensation, but require the signal leads to be brought in through holes drilled in the enclosure lid. Two pre-set input ranges are available at each input channel for the thermocouple version, whilst for the strain gauge type each input channel range is set by an individual resistor soldered across terminal posts. Other versions are set up similarly. Final trimming of each channel scaling may be carried out in software
- see Sections 3.3.7 and 4.5.2.

3 ARM WINDOWS SOFTWARE

3.1 OVERVIEW

The general method of using the ARM is as follows;

3.1.1 Hardware

Connect the external sensors, RS232 cable to handheld unit and connect batteries in ARM unit and handheld unit. Install the ARM software. Set the Serial Port to the correct corn port

3.1.2 Choose the Log Parameters and start the ARM Logging

Click ‘Arm Setup’ in the ‘Logging’ menu. Set the channels to be logged and logging rates — Optionally set channel names and scaling. Click ‘Ok’ to send the settings to the ARM and start the log. A communication status window will be show, while the settings and start command are sent to the ARM. The ARM will then start logging.

3.1.3 Download the logged data

Click ‘Get Data’ in the ‘Logging’ menu. ‘Stop Log and Get Data?’ will be displayed. Click ‘Yes’. A communication status window will be shown, while the settings and data are fetched the ARM. This may take a couple of minutes, depending on the amount of logged

data — the percentage bar shows how far it has to go. Once all data is downloaded, a message will be displayed — 'Data Downloaded'. Click 'Ok' and the logged data will be displayed on the graph display.

3.1.4 Save the Logged Data

Click 'Save As' or 'Save' in the 'File' menu. In the filename selection window, two file types can be selected.

3.1.5 View the logged data

Logged data is displayed graphically; use the mouse to zoom and pan the graph.

3.1.6 Print or Export the logged data

Click 'Print' in the 'File' menu to display the print preview. Click 'Export' in the 'File' menu to display the export .CSV form.

3.2 PRE-OPERATING SET-UP

Steps 3.1 to 3.4. must all be carried out before the ARM can be used.

3.2.1 Connection To Laptop or PC

Connection of the handheld unit to the serial port of the laptop or PC is made via the supplied DB9 terminated cable.

3.2.2 Power Supply

PP3 size alkaline or (high current version) lithium batteries must be installed into both the ARM and the handheld unit. When the battery connections are made the processors in each unit should be initialised. This is verified by the indicator LEDs on each unit responding as follows: ARM Module - LED should flash 5 times for 262K memory version, 2 times for 65k version. HANDHELD Unit - LED should flash 3 times. If not press either button or remove and reconnect battery. The ARM indicator LED should flash once every 5 seconds (idle mode) after the battery has been fitted.

3.2.3 Running Control & Display Software

After installation of the batteries and connection of the handheld unit to the serial port, the computer may be powered up and the files copied from the supplied floppy disc to a

suitable directory location, for example, C:/Program Files/Astech. Double click on the ArmWin icon to start the software. Note that the software will not run from a floppy disk (1 .44Mb capacity disks are not big enough for the software and logged data files). Files required to run the software, including help files are ArmWin.exe (the main program file), Arm.hlp (the help file), and Arm.cnt (the help contents file).

3.2.4 Configure Serial Port

Although the serial port communication protocol is set when the ARM control software is loaded, it is necessary to manually set the number (e.g. 'Com 1' or 'Com 2') of the serial port which is to be used for the ARM interface.

To do this:

• Click on the main screen menu bar item View, a pull down menu will appear

• Click on Options on the pull down menu, a dialogue box will appear - see Figure 1.

• Click on the Communications button and select the required Serial Port

• Click on the OK button

Note that when the software is run for the first time this window is displayed automatically. The ARM Version should be set to 'ARM with HHU V3'.

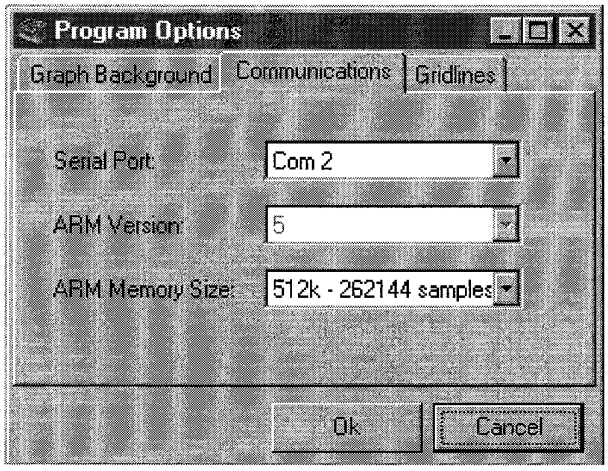


Figure A1.1 ARM Corn Port Selection

3.3 SET OPERATING MODES

The required ARM operating mode - the setup data, is entered via the control program and then downloaded from the laptop/PC to the ARM using the RS232 link. Measurement data is then logged/recorded and finally the stOred data is retrieved from the ARM, and put into a file in the laptop/PC. In practice these operations can be separated by weeks or even months if necessary. This section describes how to program the setup data into the control

program and download it to the ARM and commence the log. After setting the operating modes for the first time, it is possible to save them in a file as default settings - see section 3.3.4.1. The operating modes can then be set from a file instead of having to be entered manually. When no data file is open, the 'Logging' menu is available, and all settings can be edited to set the ARM up for a new log. If a data file is open, then the 'Logging' menu is disabled, and the 'Data' menu is available instead. Settings for names, colours, and scaling of channels can be edited, but the settings for channel speeds, logging rates, and logging mode (triggered, delayed, etc.) are fixed. To set up the ARM for a log, select 'ARM Set-up' in the 'Logging' menu. This displays the set-up window...

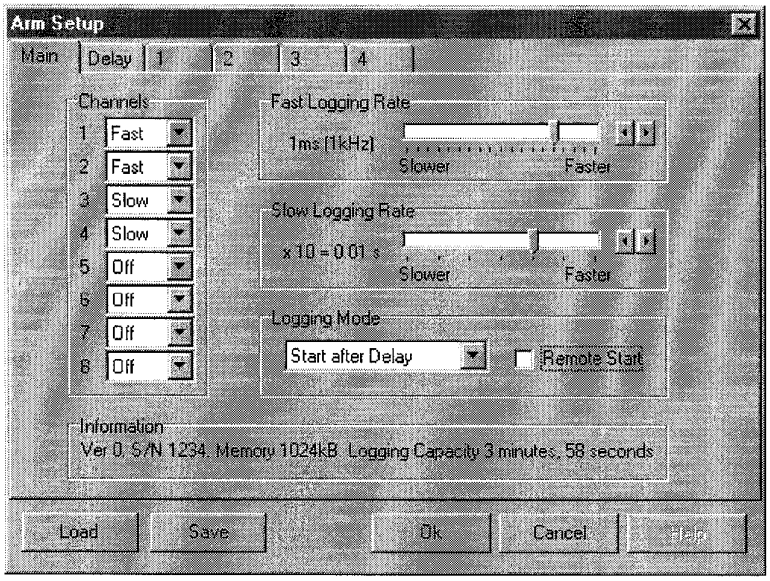


Figure A1.2 ARM Set-up Window

3.3.1 Select Active Channels & Scan Intervals

3.3.1.1 Select Active Channels

Each input channel can be set to one of two possible sample rates, FAST or SLOW or turned OFF, in which case the channel becomes inactive.

To do this:

• Pull down the selection box by the required channel number.

• Select the setting from choice of FAST, SLOW or OFF.

When a channel is selected as 'Fast' or 'Slow', a tab will appear (along the top of the set-up window) to set display settings for that channel.

3.3.1.2 Set Scan Interval

The fast scan interval is the time delay between each successive fast scan of all the active channels and may be set to any one of 15 time periods from a minimum of 100 micro

seconds to a maximum of 10 seconds. However, the sample rate, - the time taken to carry out one measurement, is also 100 microseconds and there are therefore certain scan interval settings which will be invalid. For example, trying to fast scan 3 channels would take 300 micro seconds and so setting a fast scan interval of 200 microseconds for 3 active channels would be impossible. For the same reason, the minimum scan interval of 100 microseconds can only be used with a single active channel Attempts to set impossible settings will not be accepted and a message 'Too Many Channels for this Logging Rate', will appear in the information box. In addition to fast scan, channels measuring slowly changing data - temperature for example, may be sampled at a slow scan interval. Available slow scan intervals are x2, x5, xlO, x20, x50, lxOO or x200 times the fast scan interval. This provides a slowest scan interval of 33 minutes (the slowest fast scan interval of 10 seconds multiplied by the largest multiplier of x200).

To set the scan interval: Click the left or right arrows on the Fast Logging Rate or the Slow Logging Rate areas to increment or decrement the available settings. The pointer may also be dragged to the required setting.

3.3.2 Set Logging Modes

This controls the way the ARM will start and finish a log. The ARM offers a total of five alternative modes. To select a mode click on the Logging Mode pull down arrow to display the available options. These are:

3.3.2.1 Log Until Memory Full

The log starts immediately after the start command, and will continue logging until the ARM log memory is full. When this occurs the ARM retUrns to low power mode signified by a 5 second LED flash rate.

3.3.2.2 Log Until Stopped

The log starts immediately after the start command, and will continue logging until the stop command. If the log goes on longer than the ARM can store, then the oldest data will be overwritten and the newest data is always available for download.

3.3.2.3 Start On Trigger

After the start command is received, the ARM will watch its inputs until the trigger conditions are satisfied, at which point the log will start. Logging continues until memory is full. Trigger conditions are set in the 'Triggers' tab, which is available only when this mode is selected. See section 3.3.2.3.

3.3.2.4 Start After Delay

Logging starts a set time after the start command, and continues until memory is full. The start delay is set in the 'Delay' tab, which is available only when this mode is selected. See section 3.3.2.4.

3.3.3 Remote Start

When the 'Remote Start' tick box is ticked, the PC will not start the ARM log. The settings are sent to the ARM, so the log can be started using the switch start input on the ARM. If the ARM is set to a delay or trigger mode, then the switch start will begin the delay, or start checking for trigger conditions.

3.3.4 ARM Set-up Control Buttons

3.3.4.1 Save

The 'Save' button saves the current set-up information (Log settings and Channel Settings) to a .INI file. This also contains all of the calibration information the particular ARM being used along with the graph colours, channels set to log etc. If a file called 'default.ini' is saved in the same directory as the program it will be automatically loaded when the program is next started.

3.3.4.2 Load

The 'Load' bufton reloads the .INI set-up information. This file contains all of the informatipn about the channel set-up, scaling, graph colours etc. and is specific to each ARM unit.

3.3.4.3 Cancel

The 'Cancel' button discards all changes and closes the settings window 33440k. The 'Ok' button saves all changes, closes the settings window, and asks 'Send Settings to ARM and Start Log now?'. This button is used to start a log after all the required setting have been made.

3.3.5 Setting Triggered Start

The triggered start window is shown below.

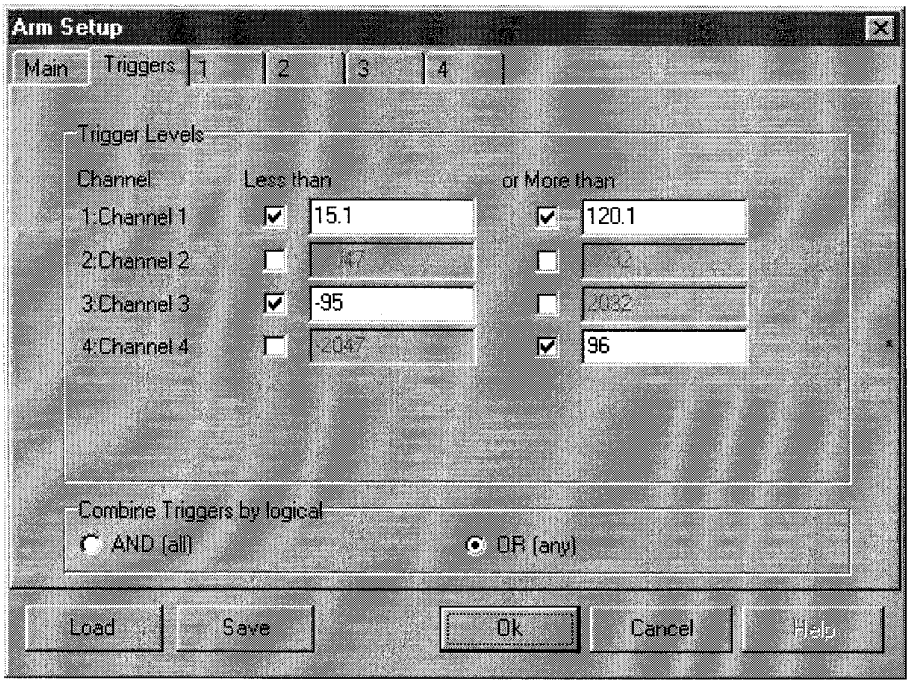


Figure A1.3 Triggered Start Setup Window

In the trigger start mode, the log will start only when the trigger conditions are satisfied. Each logged channel can have two trigger conditions — if the input to that channel is less than a specified level, or if the input is greater than a specified level. Triggering for each channel is enabled with the relevant tick box, and levels are entered into the edit boxes. The trigger levels may not stay exactly as entered — they will change to the nearest possible trigger level (the ARM stores trigger levels internally as 8 bit values, for 255 possible trigger levels). If 'Combine Triggers by logical' is set to 'AND' then logging will start when all the channels satisfy their trigger conditions together. If 'Combine Triggers by logical' is set to 'OR' then only one channel needs to — trigger to start the log.

3.3.6 Setting Delayed Start

When Delay Start has been selected a Delay Tab will appear. To set up the Delayed start time click on this tab. There are two modes of operation. Either a specific date and time may be set for the log to start or a specific time delay may be set.

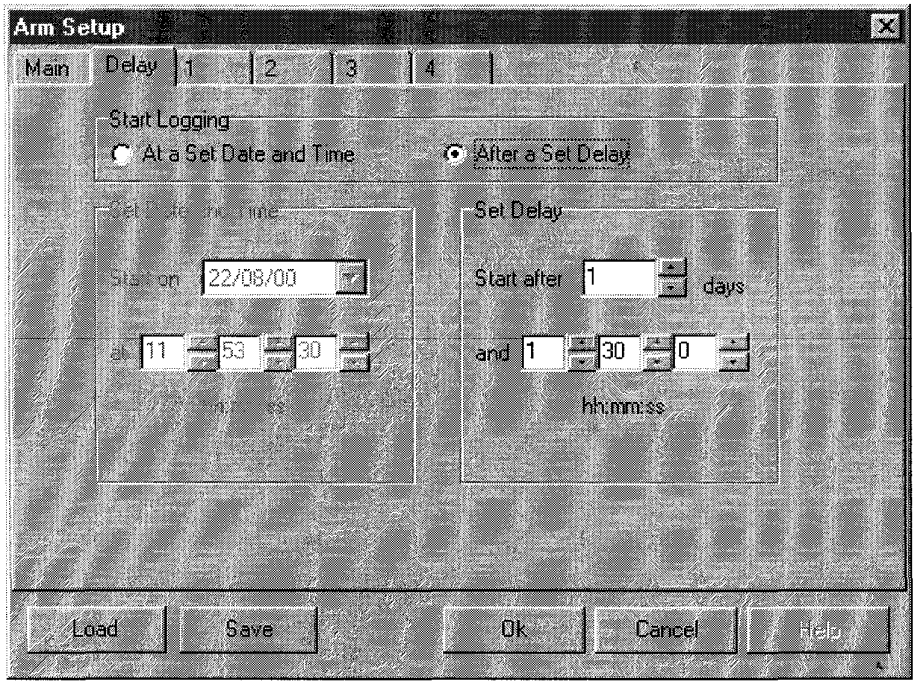


Figure A1.4: Delayed Start Setup Window

The delay time is set in days, hours, minutes, and seconds. Logging will start after the selected delay. If a 'At a Set Date and Time' is selected, then the delay sent to the ARM will be calculated from the PC's clock when the set-up is sent to the ARM. Note that as the ARM does not contain a real time clock, a 'Set Date and Time' log cannot use the 'Remote Start' option.

3.3.7 Setting Channel Options

Each channel has several options that are set in the channel menu, see Figure 5 below.
To display the settings for a particular channel when no graph data is loaded, select 'ARM Setup' in the 'Logging' menu and select the required channel tab. To display the settings for a particular channel when a graph is displayed, select 'ARM Setup' in the 'Data' menu and select the required channel tab, or right click a channel in the Key window and select 'Edit Channel'.

3.3.7. 1 Channel Name

To set name for the channel, edit the text in the relevant box. This name is used to identify the channel in the graph key window and is also used when data is exported.

3.3.7.2 Input Type

For use in future software versions - not yet implemented.

3.3.7.3 Channel Units

To set units for the channel, edit the text in the relevant box. To use one of the predefined symbols click on the appropriate box. The units are used to identify the channel in the graph key window.

3.3.7.4 Channel Line Colour

To set the colour for a channel (used on the main graph display) click on the 'Set' button in the 'Line Colour' box If the required colour is not available a custom colour may be defined

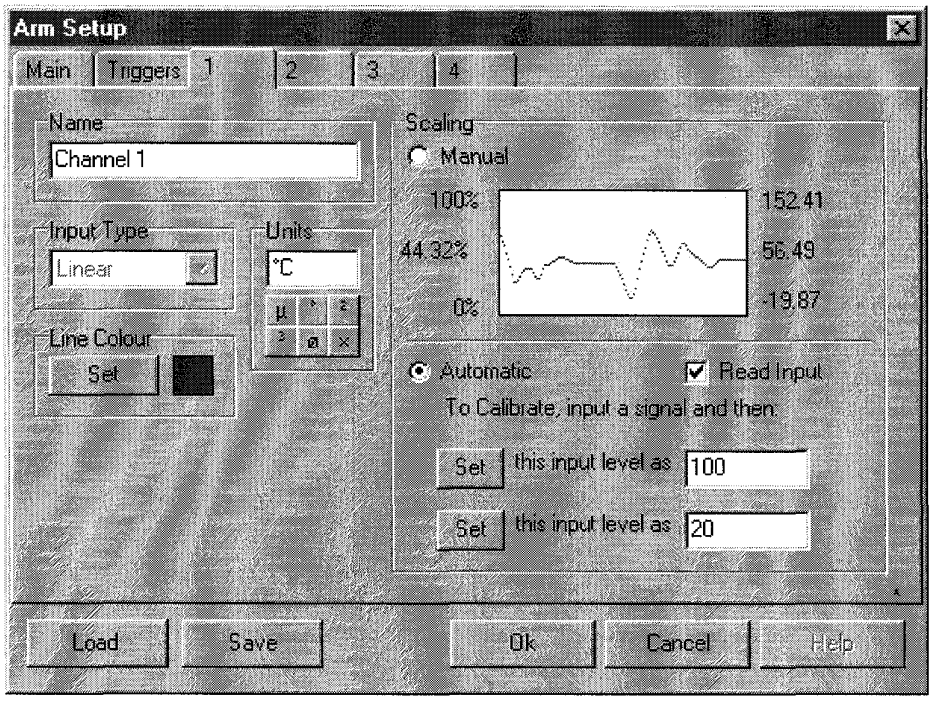


Figure A1.5: Channel Options Setup Window

3.3.7.5 Scaling

The ARM takes its measurements using a 12-bit ND converter. This provides 4096 bit levels, which are be converted to real world values using the numbers in the 'Scaling' box.

3.3.7.6 Manual Scaling

In the 'Manual' scaling mode, the maximum possible real world value (equating to 4095 bits) and the minimum possible real value (equating to 0 bits) are entered in the edit boxes next to the small graph. To check the scaling is correct, tick the 'Read Input' tickbox. This will read the selected channel from the ARM and display it as a percentage of full scale, and as a real world value scaled using the entered values.

3.3.7.7 Automatic Scafing

The ‘Automatic’ scaling mode calculates the minimum and maximum possible input values from two known input values. Input a known signal level into the ARM, enter the real value into the top ‘Set this input level as’ edit box, and click the ‘Set’ buffon. This will read the signal level from the ARM. Repeat this for a second known signal level, using the lower ‘Set this input level as’ edit box and ‘Set’ button. This should have correctly set the scaling. To check the scaling is correct, tick the ‘Read Input’ tickbox. This will read the selected channel from the ARM and display it as a percentage of full scale, and as a real world value scaled using the calculated values. Note that if the input reading was outside the input range of the ARM, the scaling will be incorrect. The ‘Read Input’ tickbox is useful to check that the input signal is within range. If the ‘Read Input’ tickbox will not stay ticked, then there is a communications problem with the ARM. Ensure that the ARM is connected and that the software is set to use the correct serial port.

3.3.7.8 Example: Scallng an Accelerometer

As an example of automatic scaling, channel 4 - in this case a ±50 accelerometer - is shown below. Display the channel 4 set-up window by clicking on the Channel 4 tab in the ARM set-up window. The window is shown below.

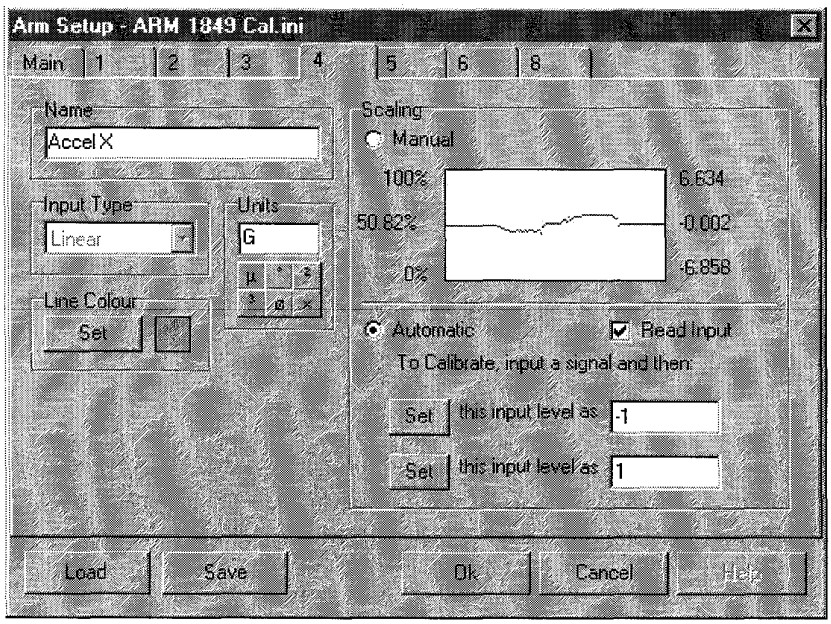


Figure A1.6: Channel 4 Set-up Window

Click on the Read Input check box. This turns on the accelerometer channel and displays the output on the graph in the manual scaling area. The graph in the example above shows a reading of 00 followed by ± This was achieved by placing the accelerometer on

each edge. Set the scaling to ‘automatic’ by clicking on the ‘Automatic’ bullet switch. Enter the desired scaling levels in the “set this input level as” boxes. Note that the order of these has no effect on the scaling. To scale the accelerometer, enter—i and +1 as shown above. Place the accelerometer on edge to input + 0. Click on the Set input level as 1 button. Then place the accelerometer on the opposite edge to input -i 0. Click on the Set input level as -i buffon. The input is now scaled. If the accelerometer is tilted the affect can be seen in the graphical window. Note that the Read Input option does not have to be turned on but is useful to see the effect of the calibration. The calibration data can now be saved to a ‘.INI’ file by clicking the ‘Save’ button.

3.4 STARTING & STOPPING LOGGING AND DOWNLOADING THE DATA

3.4.1 Start Logging

The log may be started by the PC, or by the Run/Hold pins on the ARM board. After the set-up has been completed clicking OK on the ARM set-up will bring up the Start ARM Logging menu. Clicking on OK will start the ARM logging and will destroy any previously logged data. It is therefore vital to ensure that any previously logged data has been downloaded before commencing a new log. Ensure that the correct logging mode has been selected and that Remote Start is ticked if a switch controlled log is required

3.4.1.1 Immediate Start Logging

To do this:

• Connect the RS232 Cable between the PC and handheld unit, and point the handheld unit IR window towards the IR lenses on the ARM.

• From the ARM Set-up window set the desired log parameters j

• Click on OK.

Whilst the ARM is logging its indicator LED will flash once per second for scan intervals of 20 milliseconds or less, once every 2 seconds for scan intervals of 50 milliseconds or longer.

3.4.1.2 Delayed Switch Start Log using the RUN/HOLD switch

To do this:

• Connect the RS232 Cable between the PC and handheld unit, and point the handheld unit IR window towards the IR lenses on the ARM.

• From the ARM Set-up window set the desired log parameters and set Remote Start.

• Click on OK and send the set-up data to the ARM

• To start the log use a switch to connect the Run/Hold pin (Pin 50) to Ground (Pin 8) Whilst the ARM is logging its indicator LED will flash once per second for scan intervals of 20 milliseconds or less, once every 2 seconds for scan intervals of 50 milliseconds or longer.

3.4.1.3 Conserving ARM Battery in Threshold Crossing Mode by Delay Enable

In the threshold crossing triggered mode strain gauge or transducer conditioning power supplies are turned on immediately the “enable” start command is received. To reduce battery drain therefore, if possible the ARM should not be enabled until shortly before logging/recording is to take place.

3.4.2 Stop Logging

Other than in the Log Until Stopped mode, the ARM will continue to record data until its memory is fu a stop command is received. If a switch start log is in progress, opening the switch will stop the log.

To stop logging:

• Select Logging I Stop Log from the main window. This will stop the ;log without downloading the data. The ARM LED should illuminate solidly for 10 seconds - this indicates that the ARM has stopped logging. If the comms fails a message will be displayed on the laptop/PC screen.

• Select Logging / Get Set-up from the main window. This will get the set-up data and stop the log.

• Select Logging / Get Data from the main window. This will get the set-up data, the logged and stop the log.

• If a switch start log is in progress, opening the switch will stop the log.

3.4.3 Retrieval of the Logged Data

Measurement data stored in the ARM is retrieved via the serial port. Control program software then stores it into a file, from which it may be displayed in graphical form or exported to another application.

To retrieve ARM stored data:

• Select Logging / Get Data from the main window. This will get the setup data, the logged and stop the log. A window will open showing the progress of the data download. This may take up to 2 minutes for a full-length log. When this has finished click on OK and a graph of the data will be displayed. Note that when the data is downloaded from an ARM unit, if the current .INI file loaded does not match the serial number of the ARM being

downloaded the load .INI file window is displayed automatically. At this point load the correct file to ensure that the correct calibration data is used.

3.5 GRAPHICAL DISPLAY OF MEASUREMENT DATA

After opening a file or downloading data from the ARM, the data is shown graphically in the main program window. Initially all logged channels are displayed.

3.5.1 Graph Key Window

'Graph Key' in the 'View' menu displays a key for the displayed data, along with information about the log. It may be necessary to resize the graph key window (by clicking and dragging on its edges or corners), and change the column widths (click and drag the column heading dividers) to see all the information together without scroll bars.

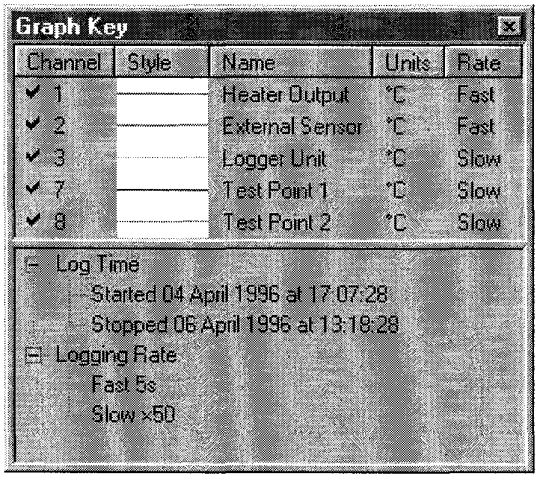


Figure A1.7: Graph Key Window

Double clicking a channel in the graph key (or right clicking and selecting Show/Hide on the popup menu) sets or clears the tick on the left of the channel number. Only channels that are ticked are plotted on the graph. The same 'ticks' are also available in the 'Channels' sub-menu in the 'View' menu. Right clicking a channel in the key window and selecting 'Edit Channel' brings up the Channel Settings window where channel name, colour, and scaling can be edited.

3.5.2 Graph Panning and Zooming

To get a closer view of a section of the data, use the left mouse button to click and drag a selection rectangle around the area of interest. Release the mouse button, then click

inside the selection rectangle to zoom in so that the selected area fills the window. Selecting an area the clicking inside it with the right mouse button will zoom out so that the whole window area is fitted inside the selected area, so showing more of the graph. Scro show which part of the data is currently displayed, by the position and size of their thumb tabs. To pan around the data, either use the scrol or click and drag with the right mouse button. Clicking the right mouse button (outside of the selection box) pops up a menu...

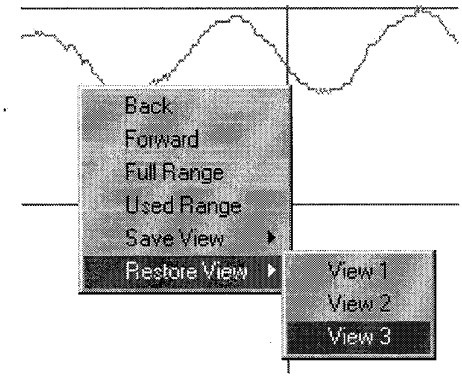


Figure A1.8: Graph right click menu

'Back' will go back to the previous graph view (before the last pan, zoom, etc.).
'Forward' will go forward again (if back was clicked too many timesl).
'Full Range' will zoom out to show alt the logged time, and the maximum possible value-axis range. 'Used Range' shows all the logged time, and sets the value axis to show all the used values. 'Save View' allows up to 3 favourite views to be saved, and
'Restore View' zooms/pans the graph back to a previously saved view.
Several different kinds of time axis grids are available —
• Real Time show the time and date the log was taken,
• Log Time shows hours, minutes and seconds since the start of the log,
• Seconds shows number of seconds since the start of the log,
• Samples shows the sample scan number with zero at the start of the tog.
Any combination of time axis grids can be selected, with the 'Grids' sub-menu in the 'View' menu.
'Options' in the 'View' menu displays the Program Options window.
The 'Graph Background' tab allows a background image and the graph background colour to be selected. A sample of the colour (and the bitmap) is show in the box on the left. Note that large bitmap images can take a while to load and display. The 'Communications' tab allows the ARM's serial port to be selected. The ARM should be set to 'ARM with HHU V3'. The 'Gridlines' tab allows each kind gridline to be a set colour. Choose the gridline to

change from the drop-down list, then select its colour with the ‘Change Colour’ button. A sample of the selected gridline and colour is shown in the box on the right.

3.6 SAVING, LOADING AND PRINTING DATA

These operations are available from the File pull down in the main window.

3.6.1 New Data File

When data is being displayed to perform a new log a new file must be opened first. Click on File — New to open a new window and make the Logging pull down menu active.

3.6.2 Open an Existing Data File

To open a previously saved data file click on File — Open to bring up the windows file open menu. Selected the required file in the usual way.

3.6.3 Save the Logged Data File

To save the Logged Data click ‘Save As’ or ‘Save’ in the ‘File’ menu. In the filename selection window, select ‘ARM data file’. This is the program’s native format, and saves all the data, along with channel names, scaling, etc.

3.6.4 Save the Logged Data File for Export to Another Program

To save the Logged Data for export to another program click ‘Export’ in the ‘File’ menu. In the filename selection window, select ‘Save As Type’ to ‘Comma Separated Values’ or ‘CSV with 65000 line limit’. This is a text format, suitable for importing into other programs (such as Excel). Only the data currently shown (current time range and enabled channels) will be exported. Note that Excel cannot handle .CSV (or any other) files past 65535 lines so choose ‘65000 line limit’ to automatically split the data into several .csv files. This will create as many files as needed with filenames like ‘test [of 5].CSV’. Click ‘Ok’ to close the export window once it has finished (or ‘Abort’ to stop the export before it is finished).

3.6.5 Printing

To print the logged data click on ‘Print’ in the ‘File’ menu. Only the data currently shown (current time range and enabled channels) will be printed. The print preview will be displayed as shown below in Figure 9. Use the ‘Printer Setup’ button to select the printer

to use. The ‘Options’ button displays a form for setting title and axis text, fonts, margins, etc..

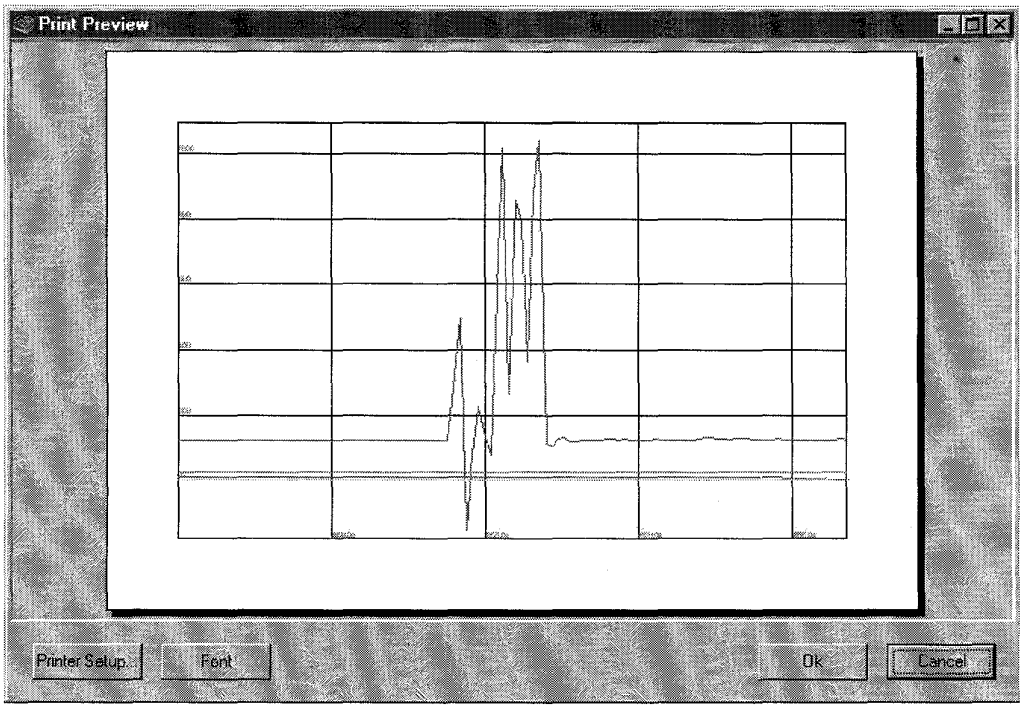
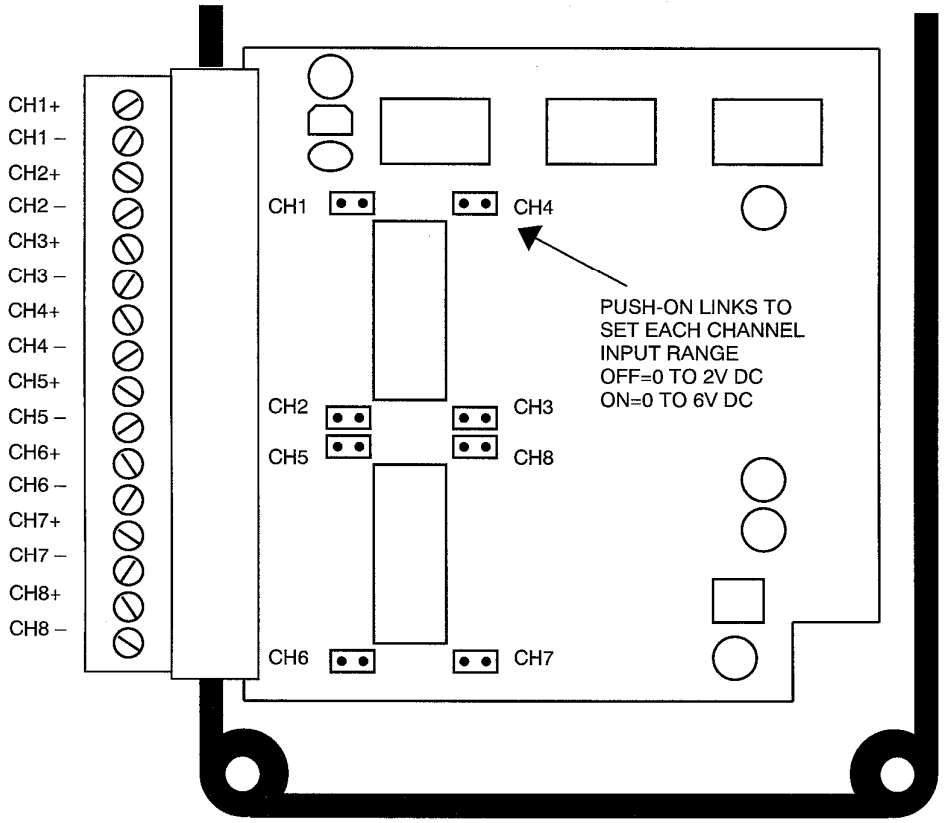


Figure A.19: Print Preview Window

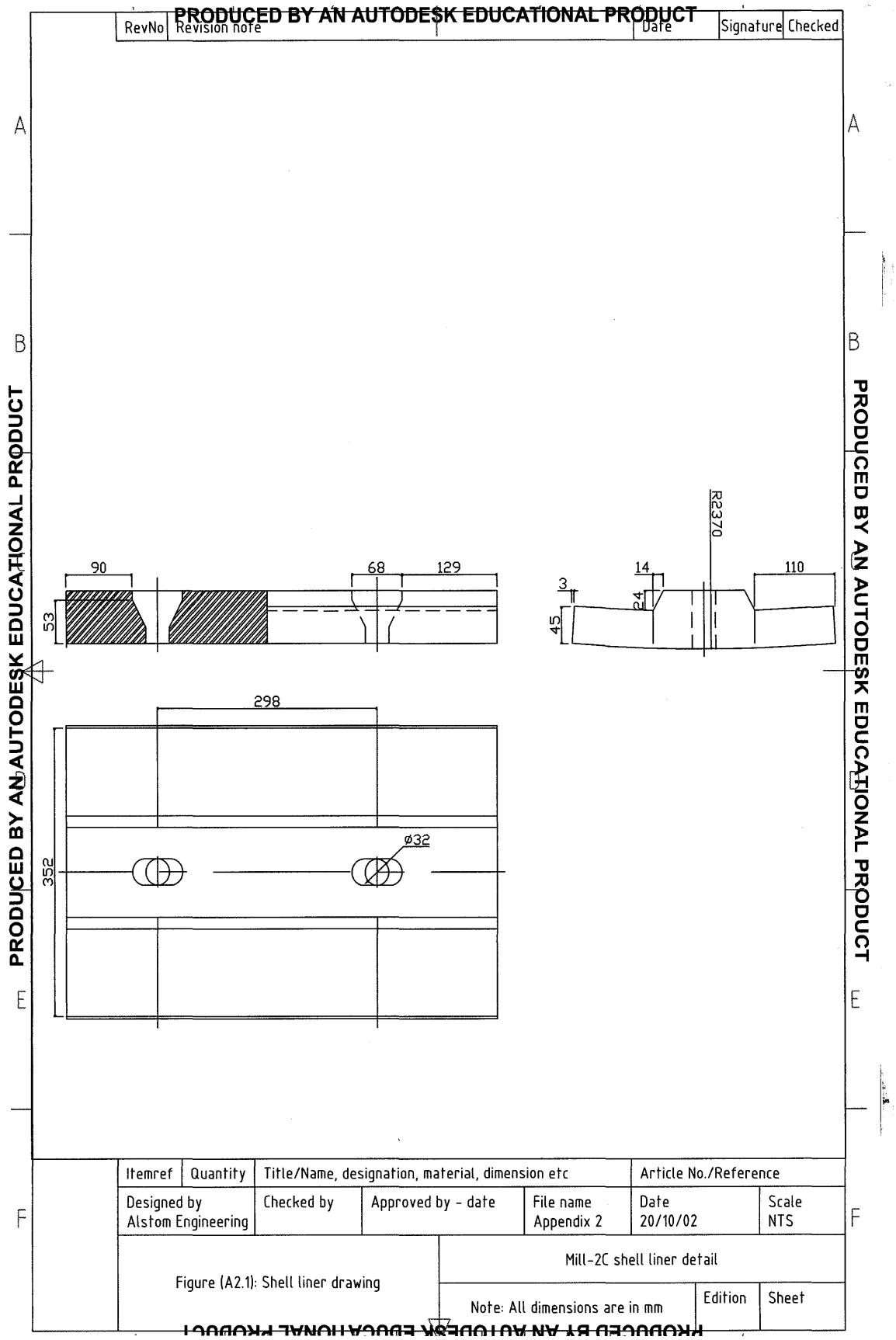
J817 - INPUT CONNECTIONS AND CONFIGURATION 8 CHANNEL ANALOGUE INPUT BOARD FOR UNIVERSITY OF WITWATERSRAND



This version of the ARM will accept up to 8 analogue inputs. Each channel may be set to an input range of 0 to +2V or 0 to +4V full scale by means of push-on links.

APPENDIX 2

PROBE MECHANICAL DESIGN DRAWINGS


PRODUCED BY AN AUTODESK EDUCATIONAL PRODUCT
RevNo
Revision note
Date
Signature
Checked
90
68
129
53
R2370
14
110
3
24
45
298
352
ø32
Itemref
Quantity
Title/Name, designation, material, dimension etc
Article No./Reference
Designed by
Alstom Engineering
Checked by
Approved by - date
File name
Appendix 2
Date
20/10/02
Scale
NTS
Figure (A2.1): Shell liner drawing
Mill-2C shell liner detail
Note: All dimensions are in mm
Edition
Sheet

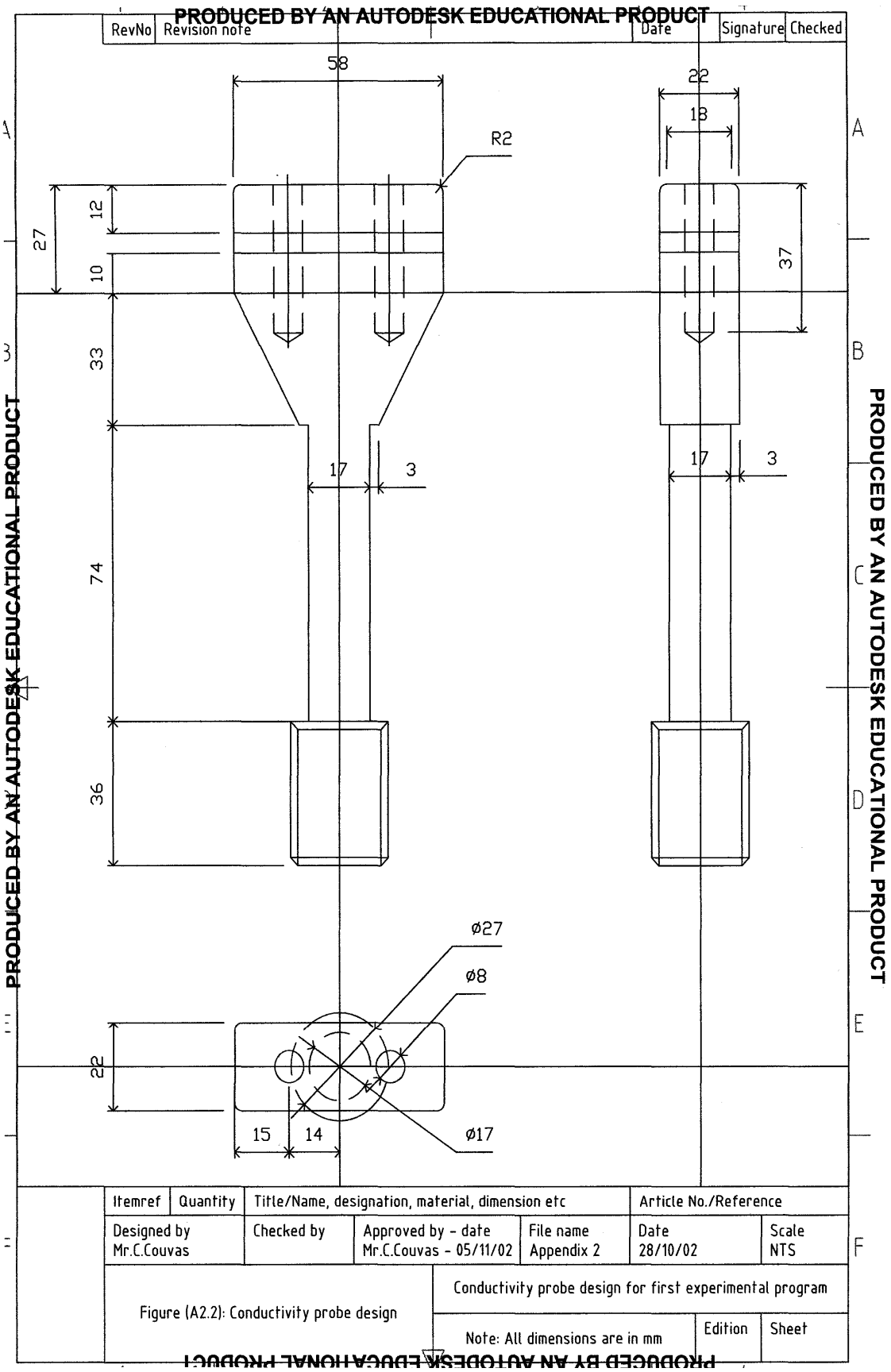
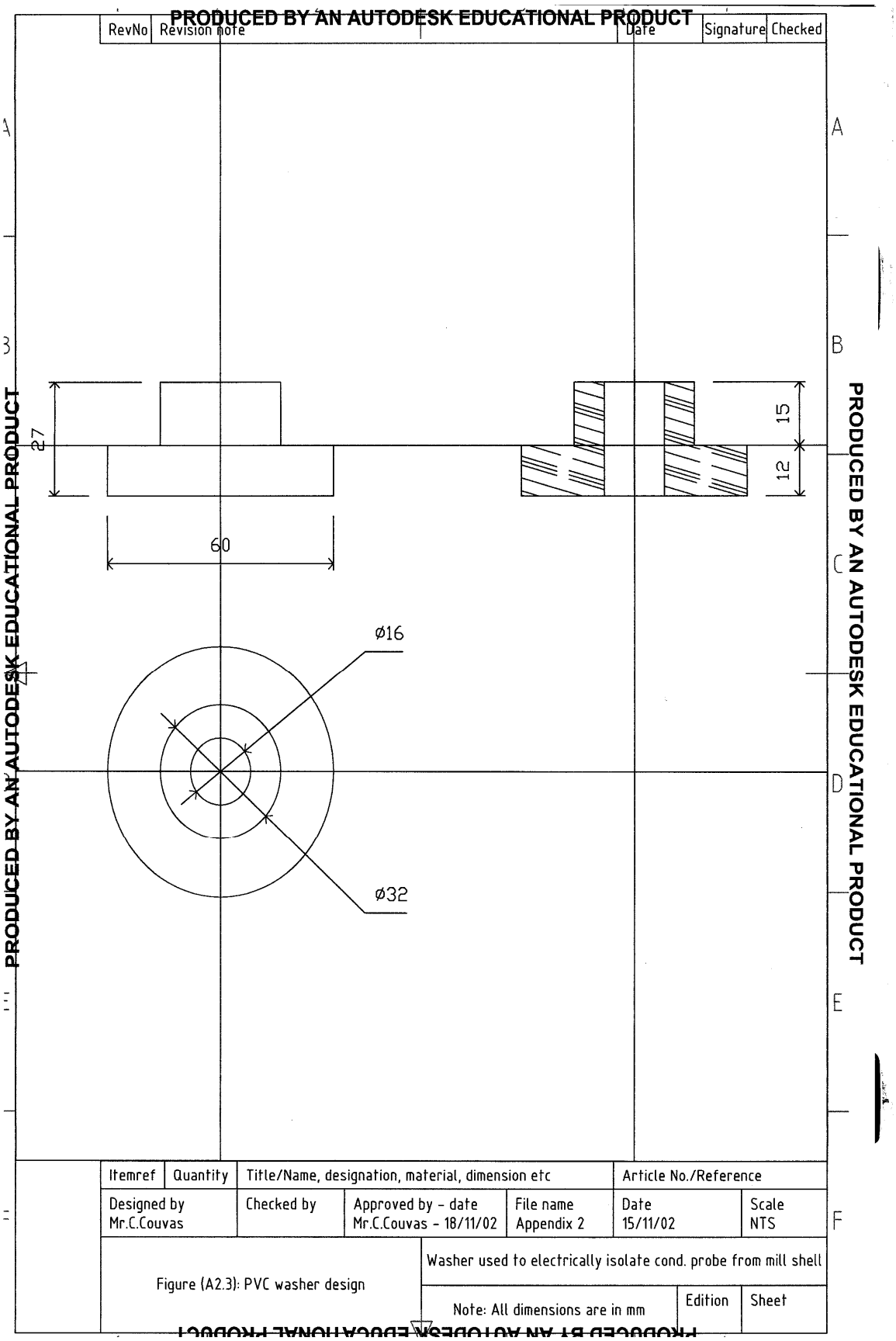
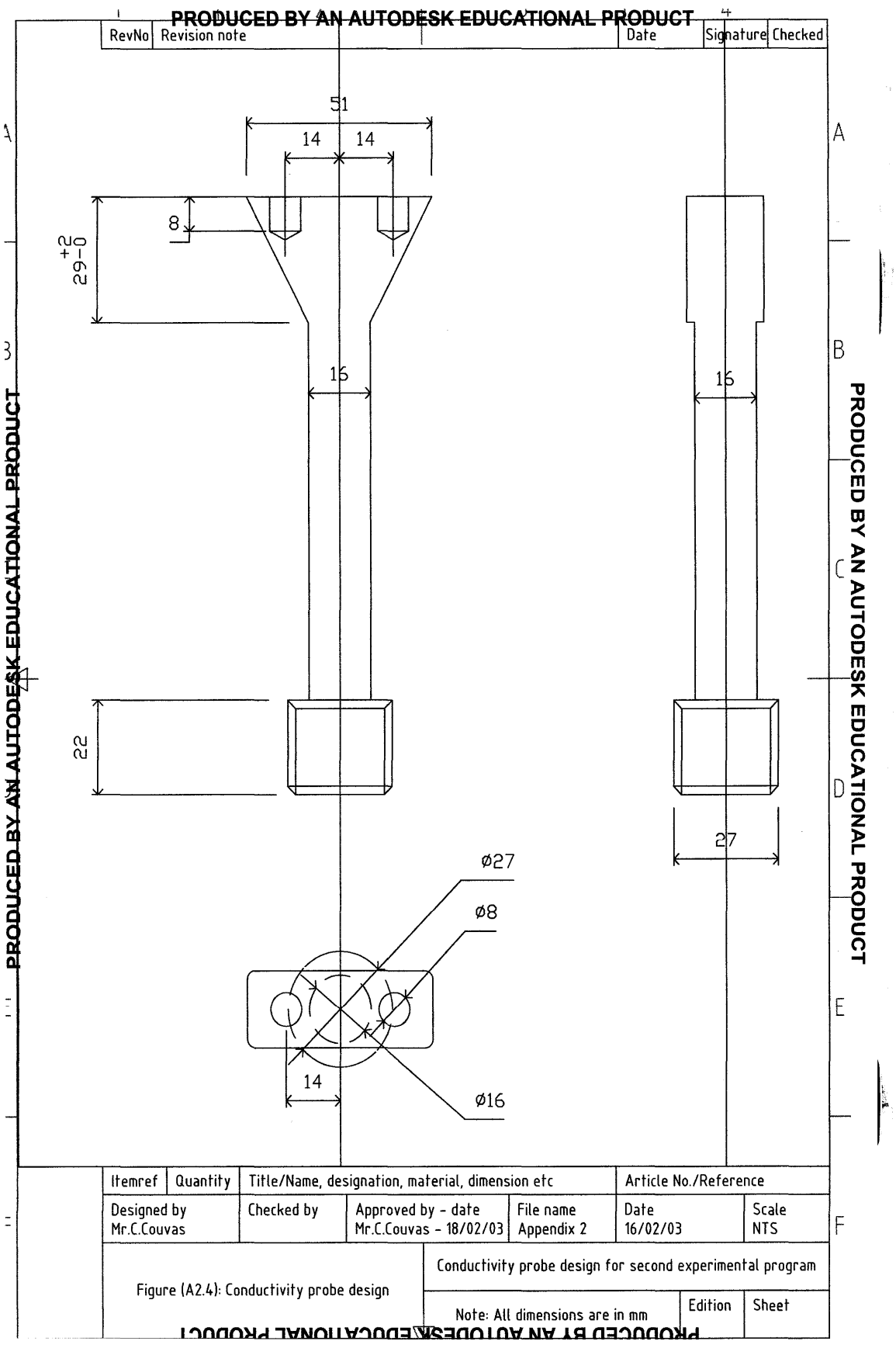


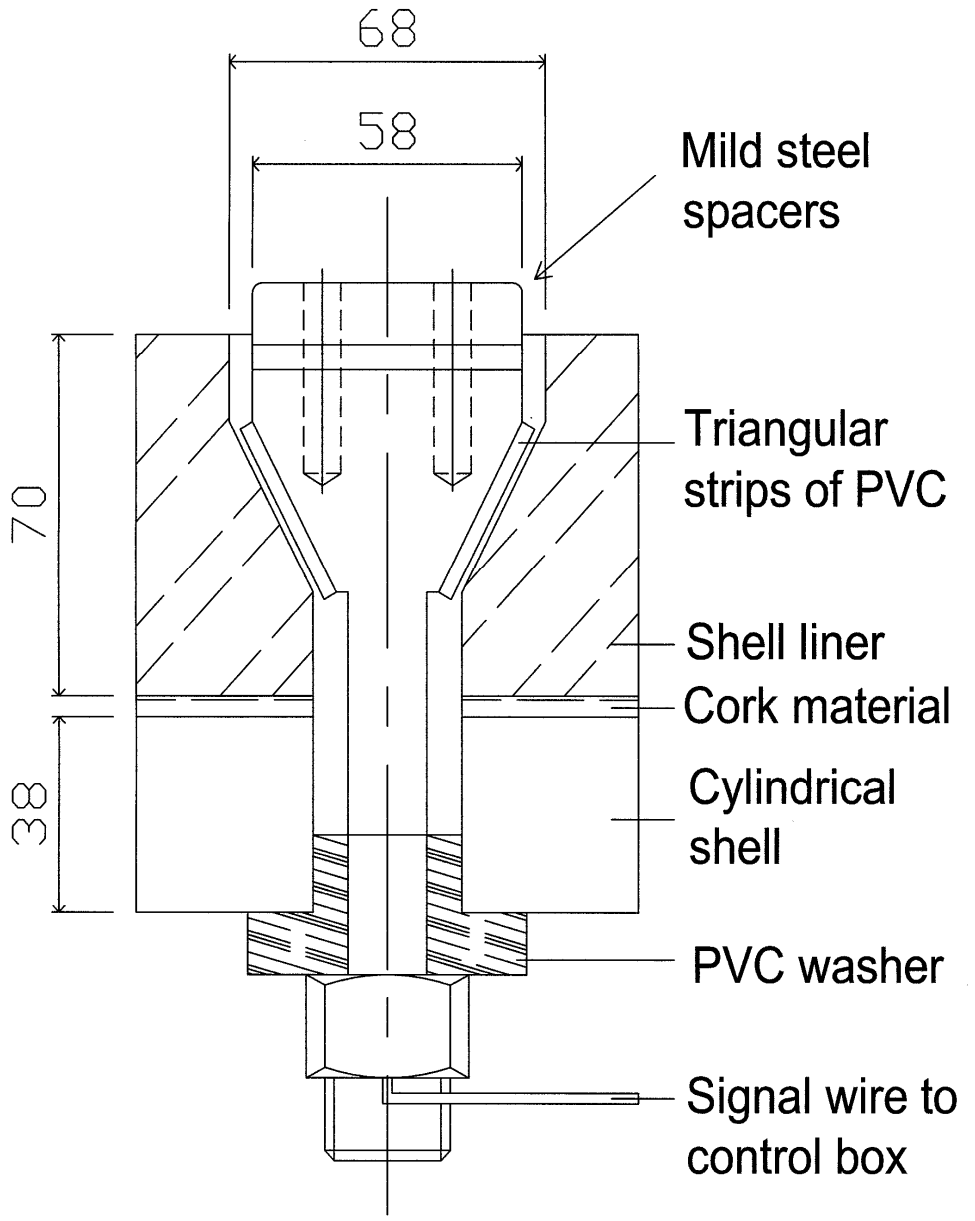
Figure (A2.2): Conductivity probe design


PRODUCED BY AN AUTODESK EDUCATIONAL PRODUCT
RevNo
Revision note
Date
Signature
Checked
27
15
12
60
ø16
ø32
PRODUCED BY AN AUTODESK EDUCATIONAL PRODUCT
PRODUCED BY AN AUTODESK EDUCATIONAL PRODUCT
Itemref
Quantity
Title/Name, designation, material, dimension etc
Article No./Reference
Designed by Mr.C.Couvas
Checked by
Approved by - date Mr.C.Couvas - 18/11/02
File name Appendix 2
Date 15/11/02
Scale NTS
Figure (A2.3): PVC washer design
Washer used to electrically isolate cond. probe from mill shell
Note: All dimensions are in mm
Edition
Sheet


PRODUCED BY AN AUTODESK EDUCATIONAL PRODUCT
RevNo
Revision note
Date
Signature
Checked
51
14
14
8
29-0 +2
16
16
22
27
ø27
ø8
14
ø16
PRODUCED BY AN AUTODESK EDUCATIONAL PRODUCT
PRODUCED BY AN AUTODESK EDUCATIONAL PRODUCT
Itemref
Quantity
Title/Name, designation, material, dimension etc
Article No./Reference
Designed by Mr.C.Couvas
Checked by
Approved by - date Mr.C.Couvas - 18/02/03
File name Appendix 2
Date 16/02/03
Scale NTS
Figure (A2.4): Conductivity probe design
Conductivity probe design for second experimental program
Note: All dimensions are in mm
Edition
Sheet

PRODUCED BY AN AUTODESK EDUCATIONAL PRODUCT

RevNo	Revision note	Date	Signature	Checked

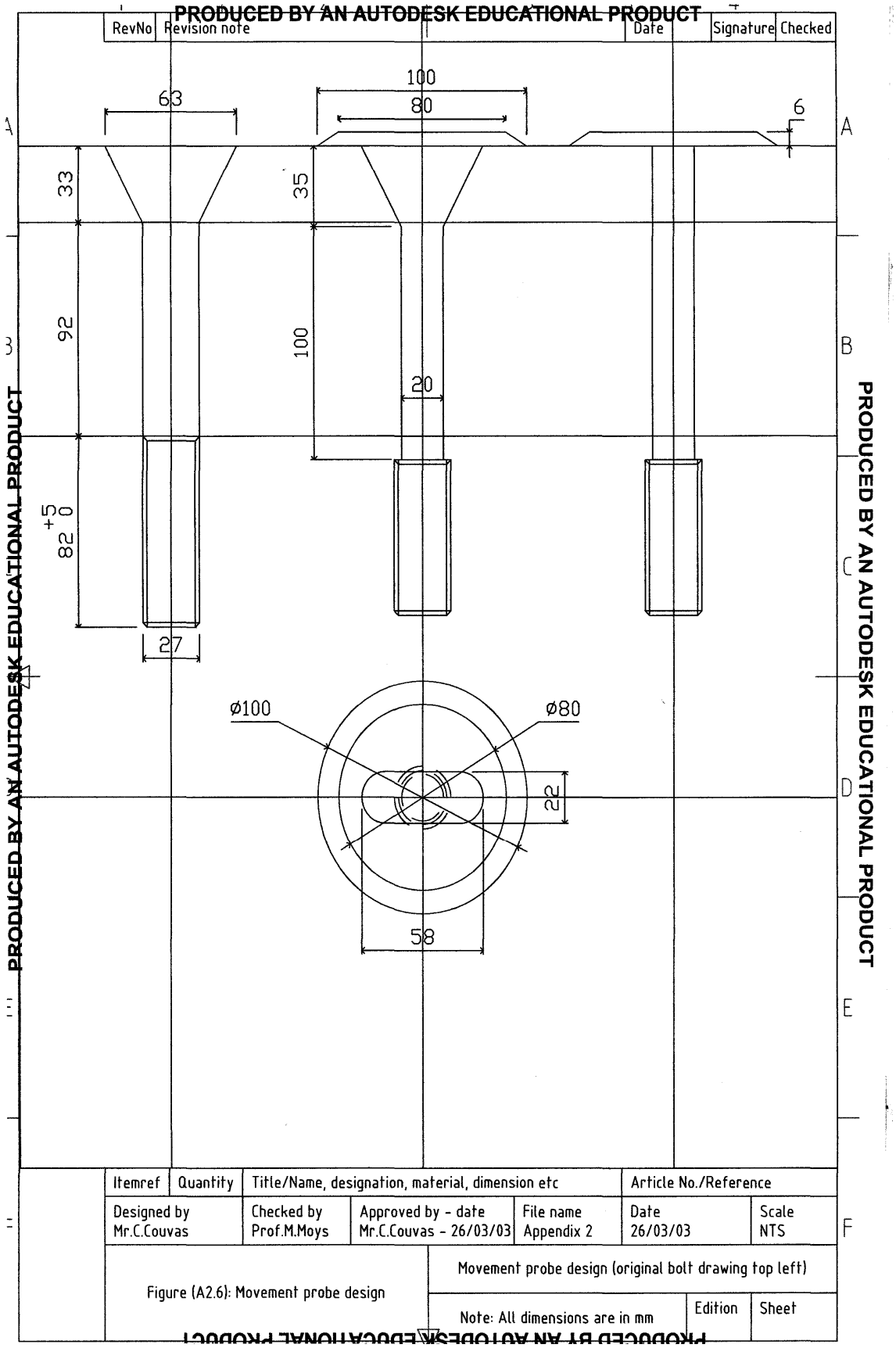


PRODUCED BY AN AUTODESK EDUCATIONAL PRODUCT

PRODUCED BY AN AUTODESK EDUCATIONAL PRODUCT

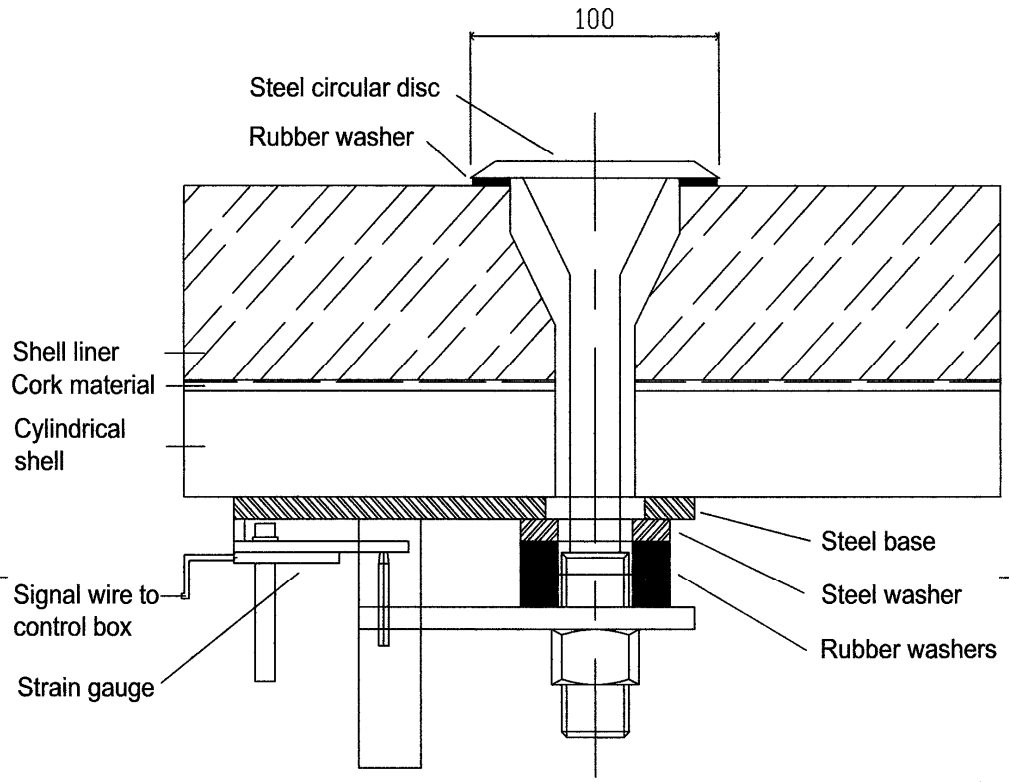
Itemref	Quantity	Title/Name, designation, material, dimension etc			Article No./Reference	
Designed by Mr.C.Couvas		Checked by	Approved by - date	File name Appendix 2	Date 13/11/02	Scale NTS
Figure (A2.5): Conductivity probe installation			Schematic of installed conductivity probe (First program)			
			Note: All dimensions are in mm		Edition	Sheet

PRODUCED BY AN AUTODESK EDUCATIONAL PRODUCT


PRODUCED BY AN AUTODESK EDUCATIONAL PRODUCT
RevNo
Revision note
Date
Signature
Checked
100
80
63
6
33
35
92
100
20
82 +5 0
27
ø100
ø80
22
58
PRODUCED BY AN AUTODESK EDUCATIONAL PRODUCT
PRODUCED BY AN AUTODESK EDUCATIONAL PRODUCT
Itemref
Quantity
Title/Name, designation, material, dimension etc
Article No./Reference
Designed by
Mr.C.Couvas
Checked by
Prof.M.Moys
Approved by - date
Mr.C.Couvas - 26/03/03
File name
Appendix 2
Date
26/03/03
Scale
NTS
Figure (A2.6): Movement probe design
Movement probe design (original bolt drawing top left)
Note: All dimensions are in mm
Edition
Sheet

PRODUCED BY AN AUTODESK EDUCATIONAL PRODUCT

RevNo	Revision note	Date	Signature	Checked

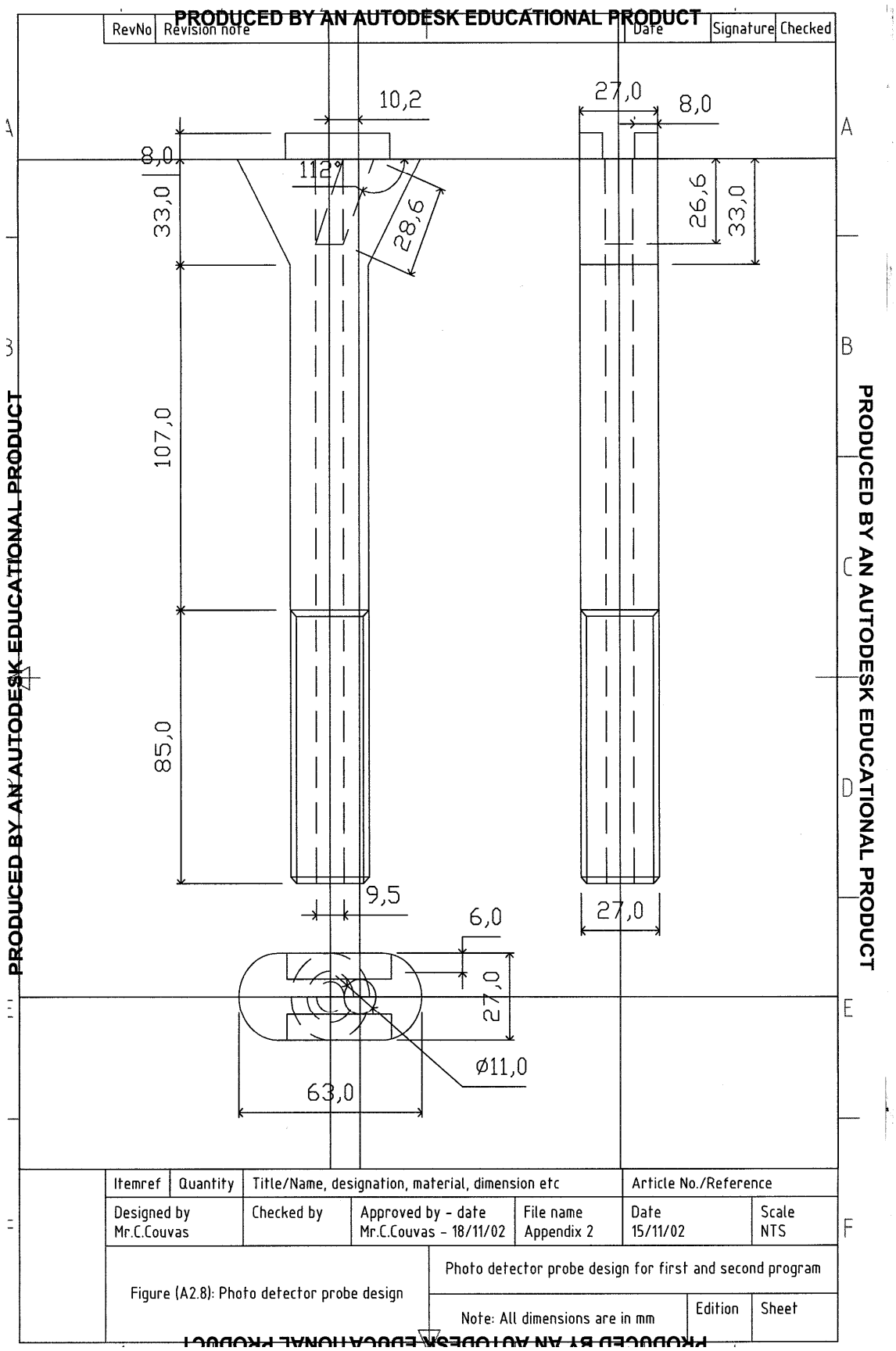


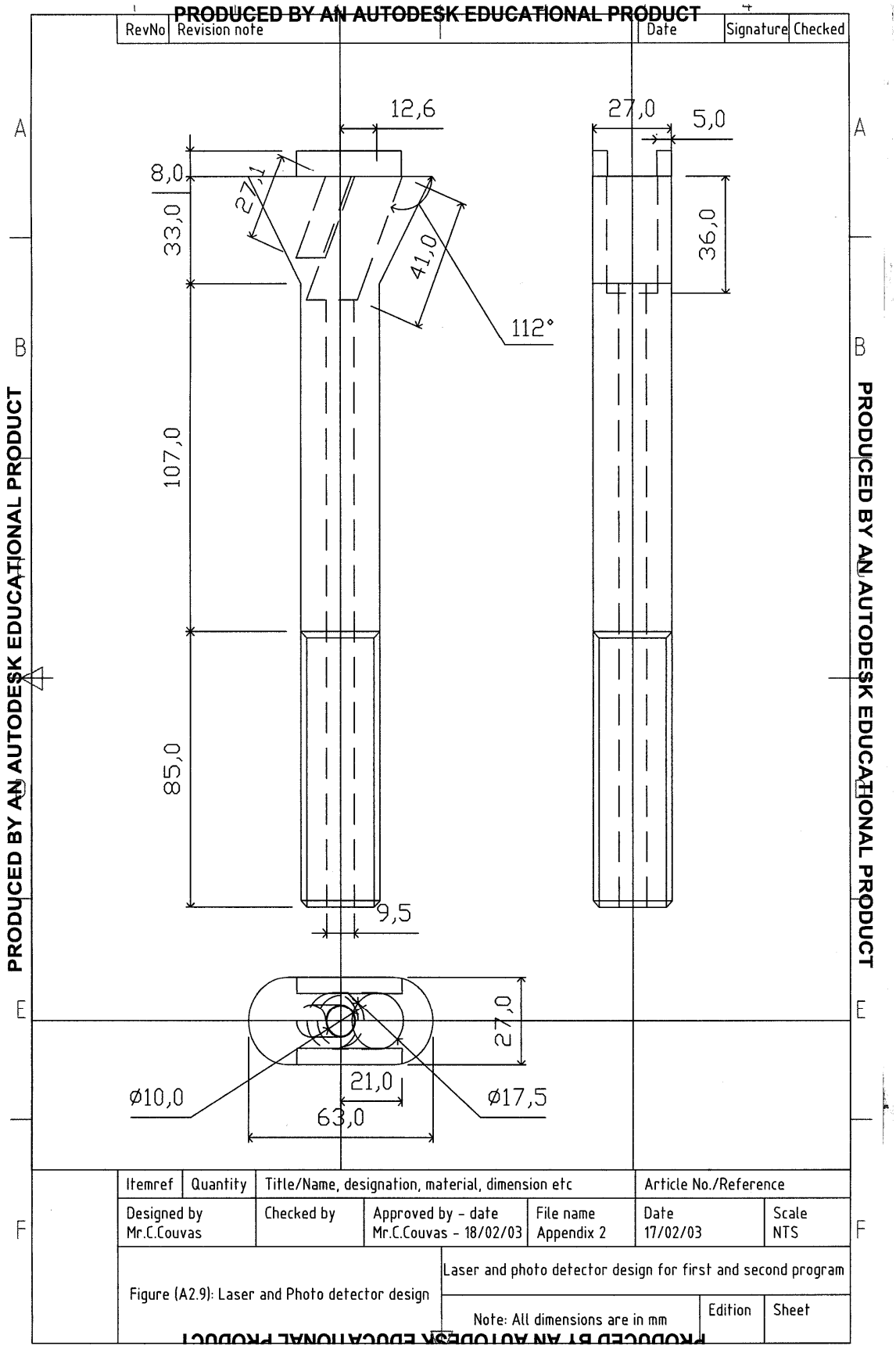
PRODUCED BY AN AUTODESK EDUCATIONAL PRODUCT

PRODUCED BY AN AUTODESK EDUCATIONAL PRODUCT

Itemref	Quantity	Title/Name, designation, material, dimension etc			Article No./Reference	
Designed by Mr.C.Couvas		Checked by	Approved by - date	File name Appendix 2	Date 20/04/03	Scale NTS
Figure (A2.7): Movement probe installation			Schematic of installed movement probe (Second program)		Edition	Sheet

PRODUCED BY AN AUTODESK EDUCATIONAL PRODUCT


PRODUCED BY AN AUTODESK EDUCATIONAL PRODUCT
RevNo
Revision note
Date
Signature
Checked
10,2
27,0
8,0
8,0
112°
33,0
28,6
26,6
33,0
107,0
85,0
9,5
6,0
27,0
27,0
Ø11,0
63,0
PRODUCED BY AN AUTODESK EDUCATIONAL PRODUCT
PRODUCED BY AN AUTODESK EDUCATIONAL PRODUCT
Itemref
Quantity
Title/Name, designation, material, dimension etc
Article No./Reference
Designed by
Mr.C.Couvas
Checked by
Approved by - date
Mr.C.Couvas - 18/11/02
File name
Appendix 2
Date
15/11/02
Scale
NTS
Figure (A2.8): Photo detector probe design
Photo detector probe design for first and second program
Note: All dimensions are in mm
Edition
Sheet


PRODUCED BY AN AUTODESK EDUCATIONAL PRODUCT
RevNo
Revision note
Date
Signature
Checked
12,6
27,0
5,0
8,0
27,1
33,0
41,0
36,0
112°
107,0
85,0
9,5
27,0
21,0
Ø10,0
Ø17,5
63,0
PRODUCED BY AN AUTODESK EDUCATIONAL PRODUCT
PRODUCED BY AN AUTODESK EDUCATIONAL PRODUCT
Itemref
Quantity
Title/Name, designation, material, dimension etc
Article No./Reference
Designed by
Mr.C.Couvas
Checked by
Approved by - date
Mr.C.Couvas - 18/02/03
File name
Appendix 2
Date
17/02/03
Scale
NTS
Figure (A2.9): Laser and Photo detector design
Laser and photo detector design for first and second program
Note: All dimensions are in mm
Edition
Sheet

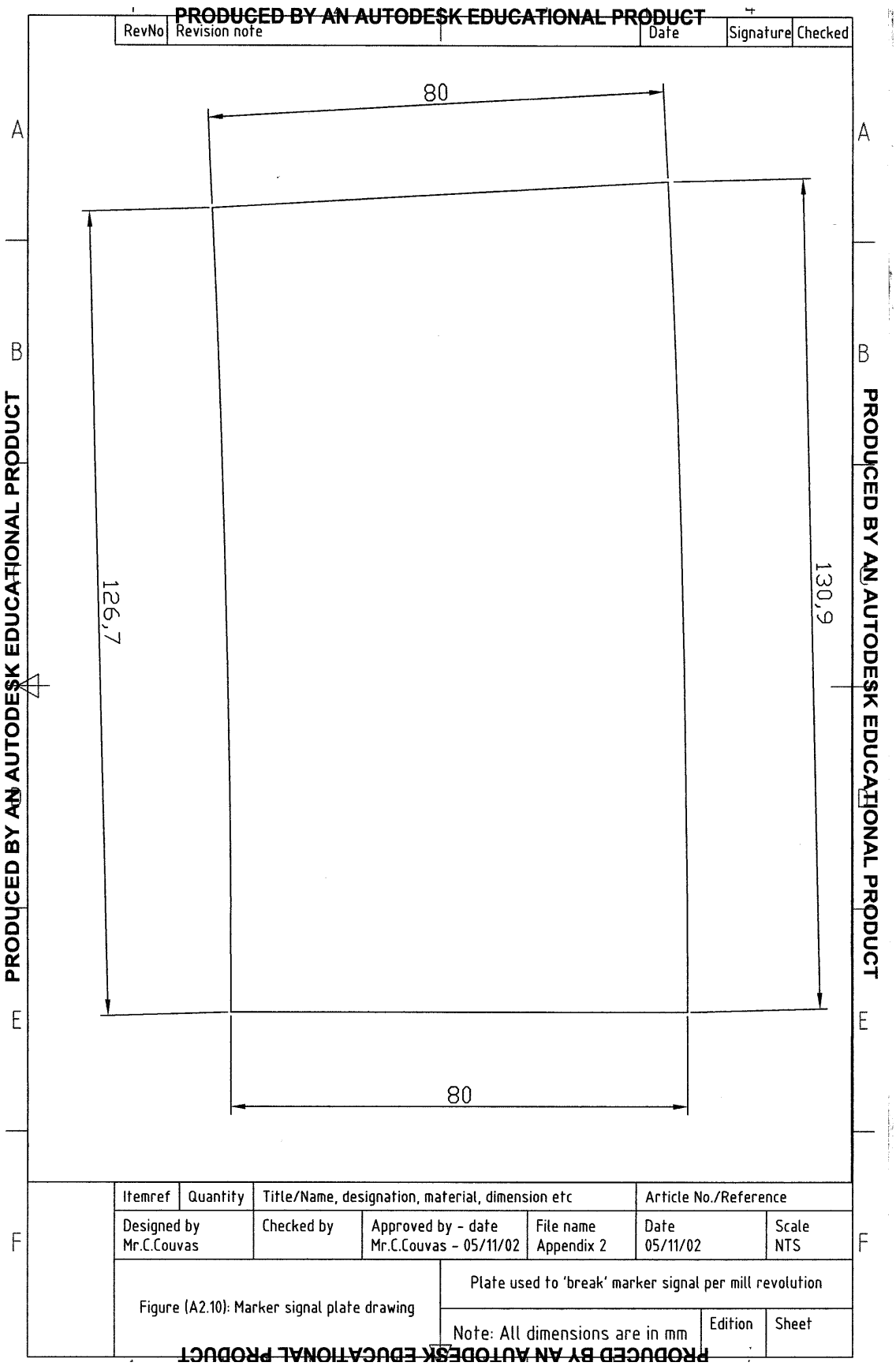
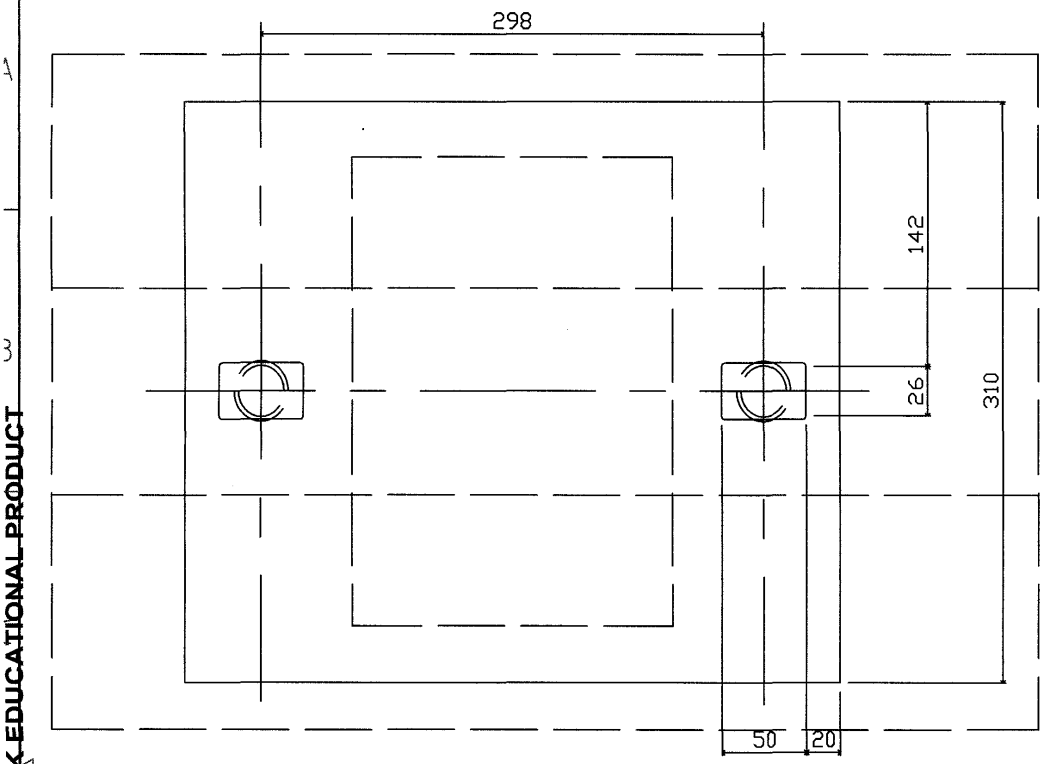


Figure (A2.10): Marker signal plate drawing

PRODUCED BY AN AUTODESK EDUCATIONAL PRODUCT

RevNo	Revision note	Date	Signature	Checked



PRODUCED BY AN AUTODESK EDUCATIONAL PRODUCT

PRODUCED BY AN AUTODESK EDUCATIONAL PRODUCT

Itemref	Quantity	Title/Name, designation, material, dimension etc			Article No./Reference	
Designed by Mr.C.Couvas		Checked by	Approved by - date Mr.C.Couvas - 05/11/02	File name Appendix 2	Date 05/11/02	Scale NTS
Figure (A2.11): Control box baseplate drawing			Electronics control box secured to baseplate			
			Note: All dimensions are in mm		Edition	Sheet

PRODUCED BY AN AUTODESK EDUCATIONAL PRODUCT

APPENDIX 3

FIRST AND SECOND PROGRAM PROBE INSTALLATION PICTURES

A3.1 First experimental program probe installation pictures

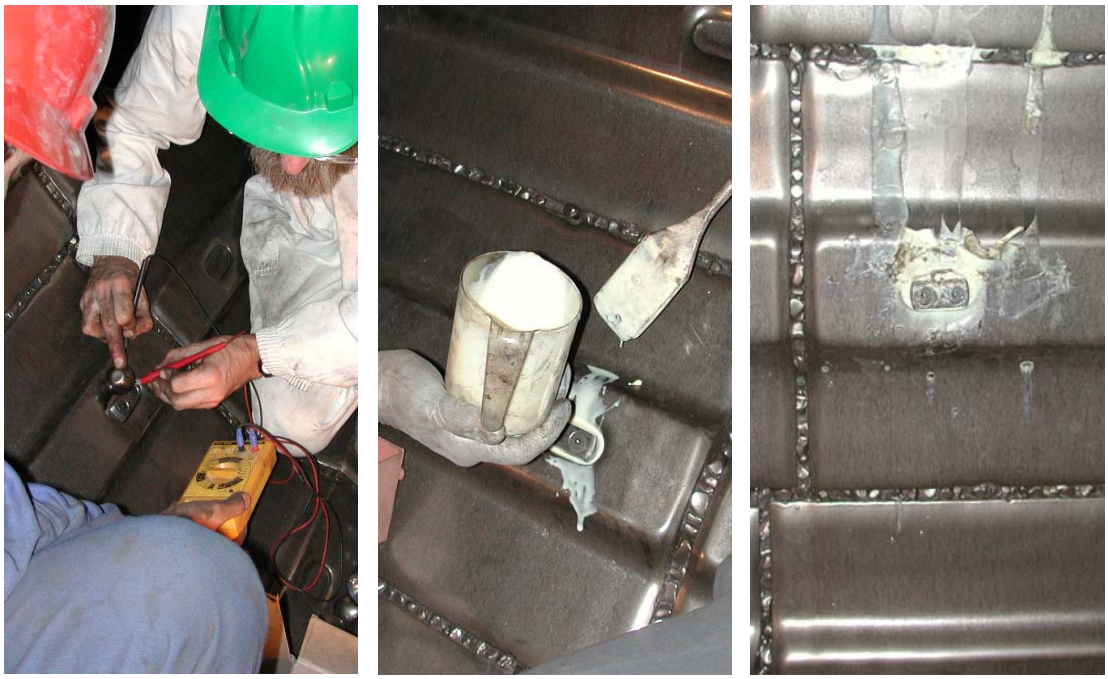


Figure A3.1.1: Conductivity probe installation process: Probe electrical isolation (left); Mixing and pouring of the resin between the bolt and liner (middle). Solidified resin, ready for surface grinding (right).



Figure A3.1.2: Conductivity probes CM1 and CM2, installed and connected to control box.

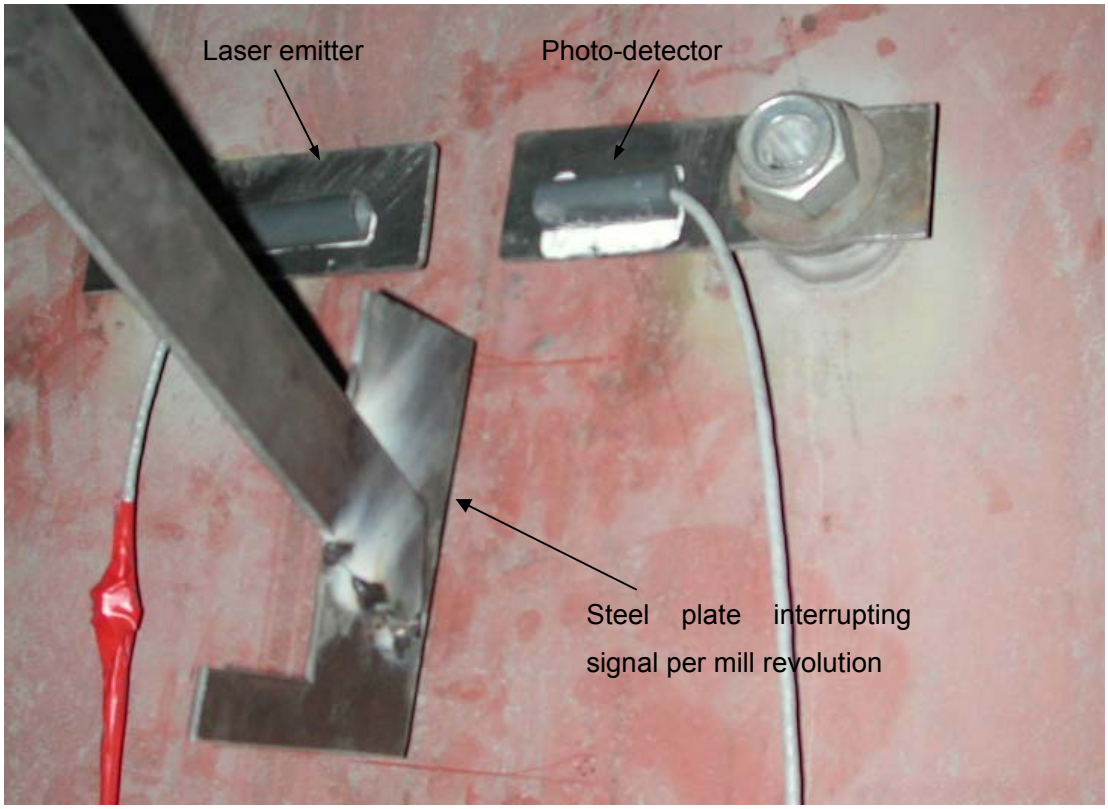


Figure A3.2.3: Picture illustrates marker signal setup; laser and photo-detector mounted on mill shell; steel plate positioned to interrupt laser signal per mil revolution.



Figure A3.2.4: Control box mounted to steel base plate and onto mill shell. Bubble wrap was used between the steel base plate and control box to absorb vibrations from the mill shell.

A3.2 Second experimental program pictures



Figure A3.2.1: Conductivity probes (bolts only) including pieces of PVC triangular strips already glued onto the probes. Matching PVC washers included per probe.



Figure A3.2.2: Installed conductivity probes CM1 (left) and OCM1 (right) as viewed from inside the mill. Pictures indicate the 3mm and 9mm height difference above the liner between CM1 and OCM1, respectively.



Figure A3.2.3: Pictures of Movement probe M1, taken from inside the mill. Pictures were taken before (left) and after (right) mill testing.



Figure A3.2.4: Movement probe M1 support base and strain gauge.



Figure A3.2.5: Laser and photo-detector reflector (PDCR) after installation (left) and after testing (right). PDCR operated for only two tests. Testing of detector after mill tests proved that the detector was faulty, indicating that harsh milling environment affected detector functionality.



Figure A3.2.6: Picture illustrates marker signal setup (left); and photo-detector (right) with its base supported by quickset Pratley putty.



Figure A3.2.7: CCD camera and spot-light (left); Video camera, flashlight and spot-light (right).

APPENDIX 4

FIRST AND SECOND PROGRAM PROJECT SCHEDULES

Table A4.1: First experimental program project schedule (Part 1 of 3)

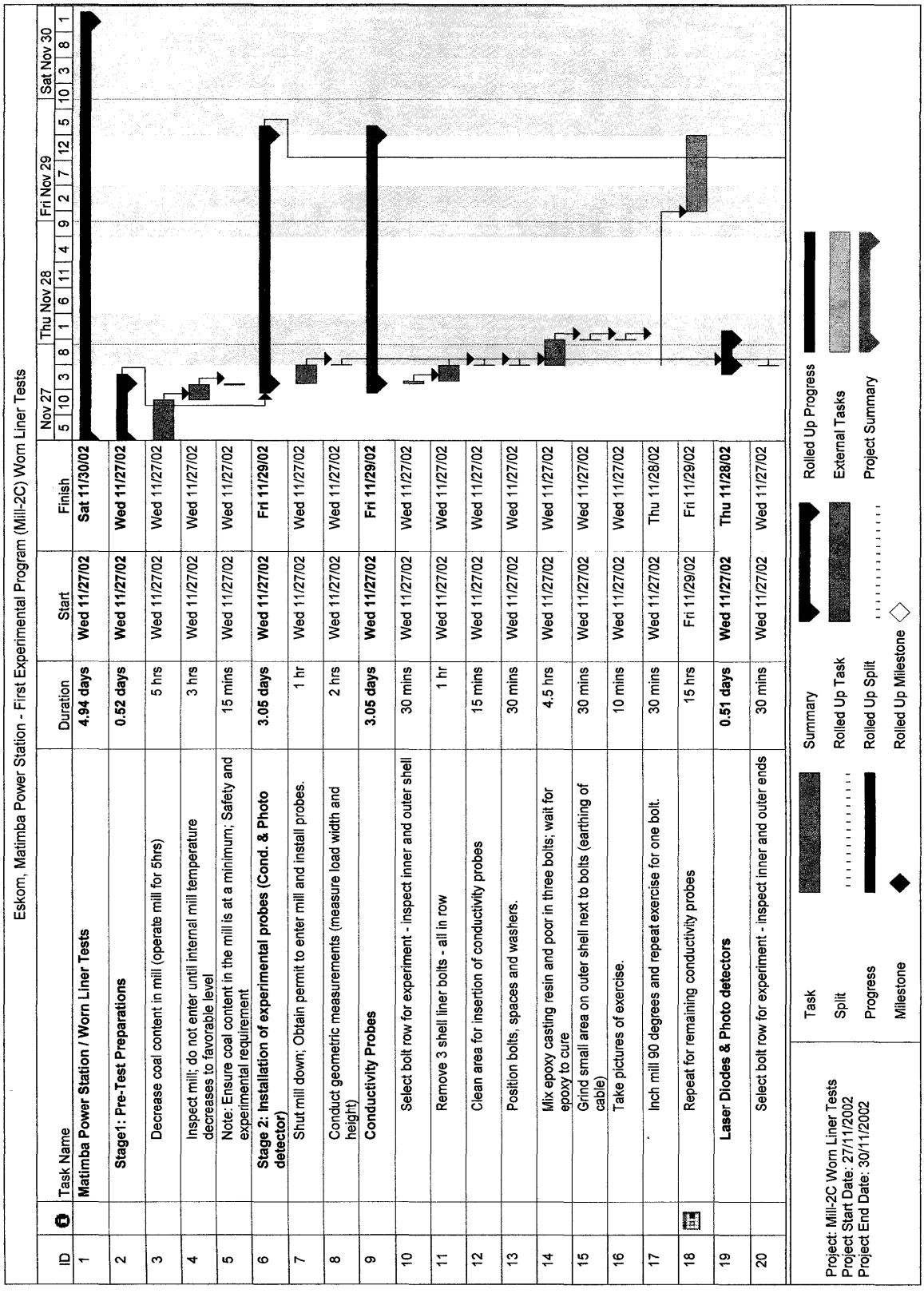
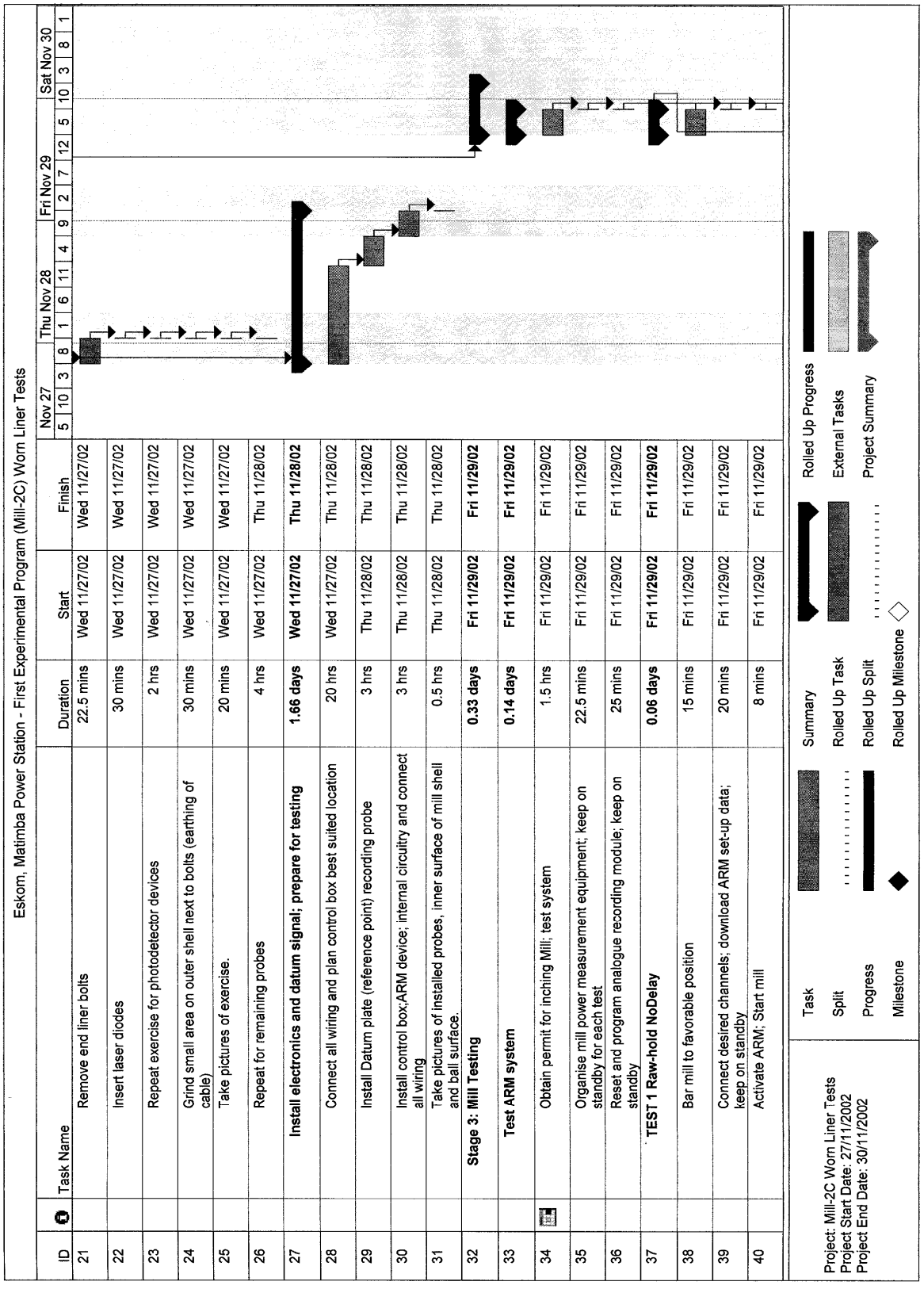


Table A4.2: First experimental program project schedule (Part 2 of 3)



ID	Task Name	Duration	Start	Finish
21	Remove end liner bolts	22.5 mins	Wed 11/27/02	Wed 11/27/02
22	Insert laser diodes	30 mins	Wed 11/27/02	Wed 11/27/02
23	Repeat exercise for photodetector devices	2 hrs	Wed 11/27/02	Wed 11/27/02
24	Grind small area on outer shell next to bolts (earthing of cable)	30 mins	Wed 11/27/02	Wed 11/27/02
25	Take pictures of exercise.	20 mins	Wed 11/27/02	Wed 11/27/02
26	Repeat for remaining probes	4 hrs	Wed 11/27/02	Thu 11/28/02
27	**Install electronics and datum signal; prepare for testing**	**1.66 days**	**Wed 11/27/02**	**Thu 11/28/02**
28	Connect all wiring and plan control box best suited location	20 hrs	Wed 11/27/02	Thu 11/28/02
29	Install Datum plate (reference point) recording probe	3 hrs	Thu 11/28/02	Thu 11/28/02
30	Install control box;ARM device; internal circuitry and connect all wiring	3 hrs	Thu 11/28/02	Thu 11/28/02
31	Take pictures of installed probes, inner surface of mill shell and ball surface.	0.5 hrs	Thu 11/28/02	Thu 11/28/02
32	**Stage 3: Mill Testing**	**0.33 days**	**Fri 11/29/02**	**Fri 11/29/02**
33	**Test ARM system**	**0.14 days**	**Fri 11/29/02**	**Fri 11/29/02**
34	Obtain permit for inching Mill; test system	1.5 hrs	Fri 11/29/02	Fri 11/29/02
35	Organise mill power measurement equipment; keep on standby for each test	22.5 mins	Fri 11/29/02	Fri 11/29/02
36	Reset and program analogue recording module; keep on standby	25 mins	Fri 11/29/02	Fri 11/29/02
37	**TEST 1 Raw-hold NoDelay**	**0.06 days**	**Fri 11/29/02**	**Fri 11/29/02**
38	Bar mill to favorable position	15 mins	Fri 11/29/02	Fri 11/29/02
39	Connect desired channels; download ARM set-up data; keep on standby	20 mins	Fri 11/29/02	Fri 11/29/02
40	Activate ARM; Start mill	8 mins	Fri 11/29/02	Fri 11/29/02

Table A4.3: First experimental program project schedule (Part 3 of 3)

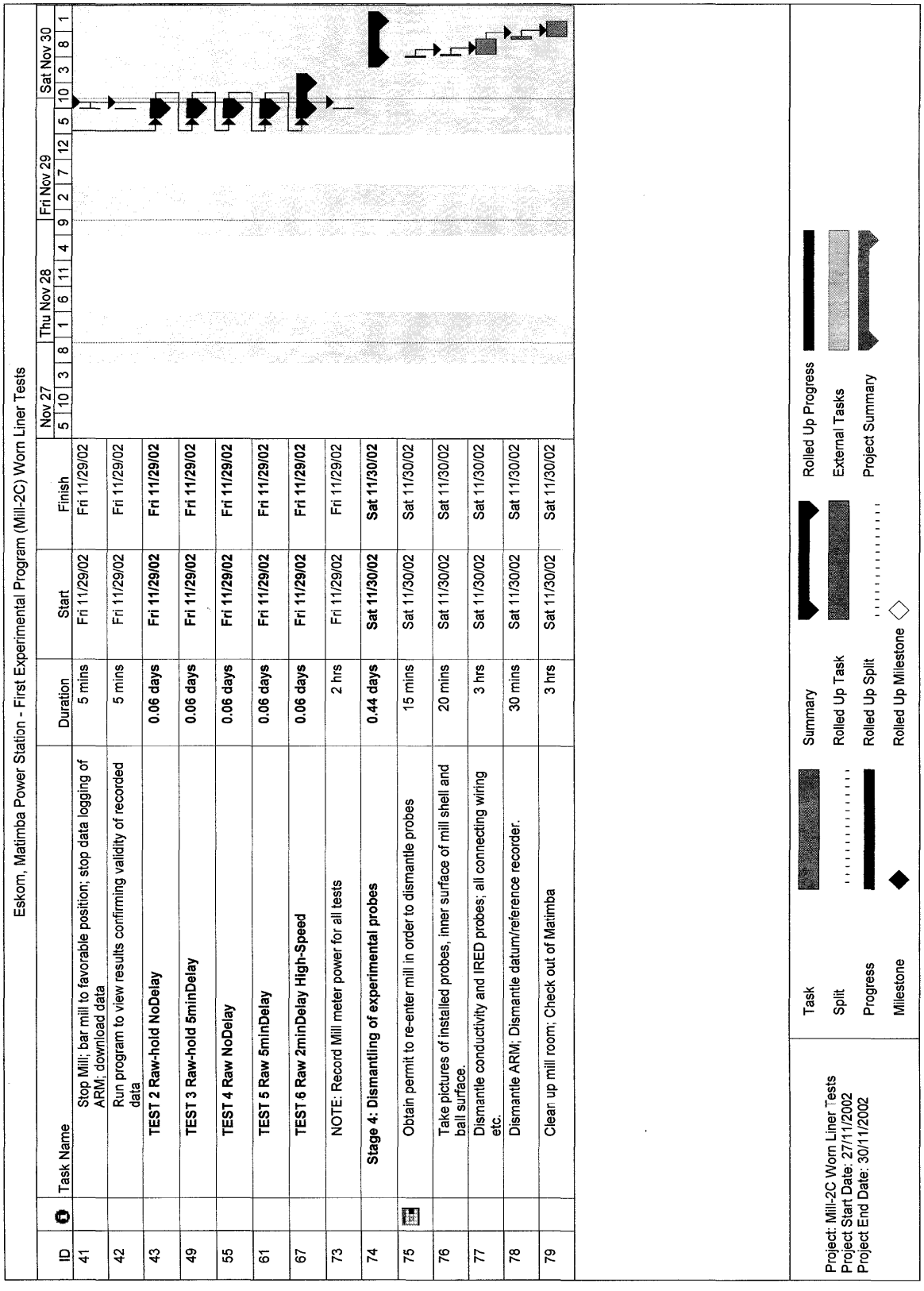


Table A4.4: Second experimental program project schedule (Part 1 of 2)

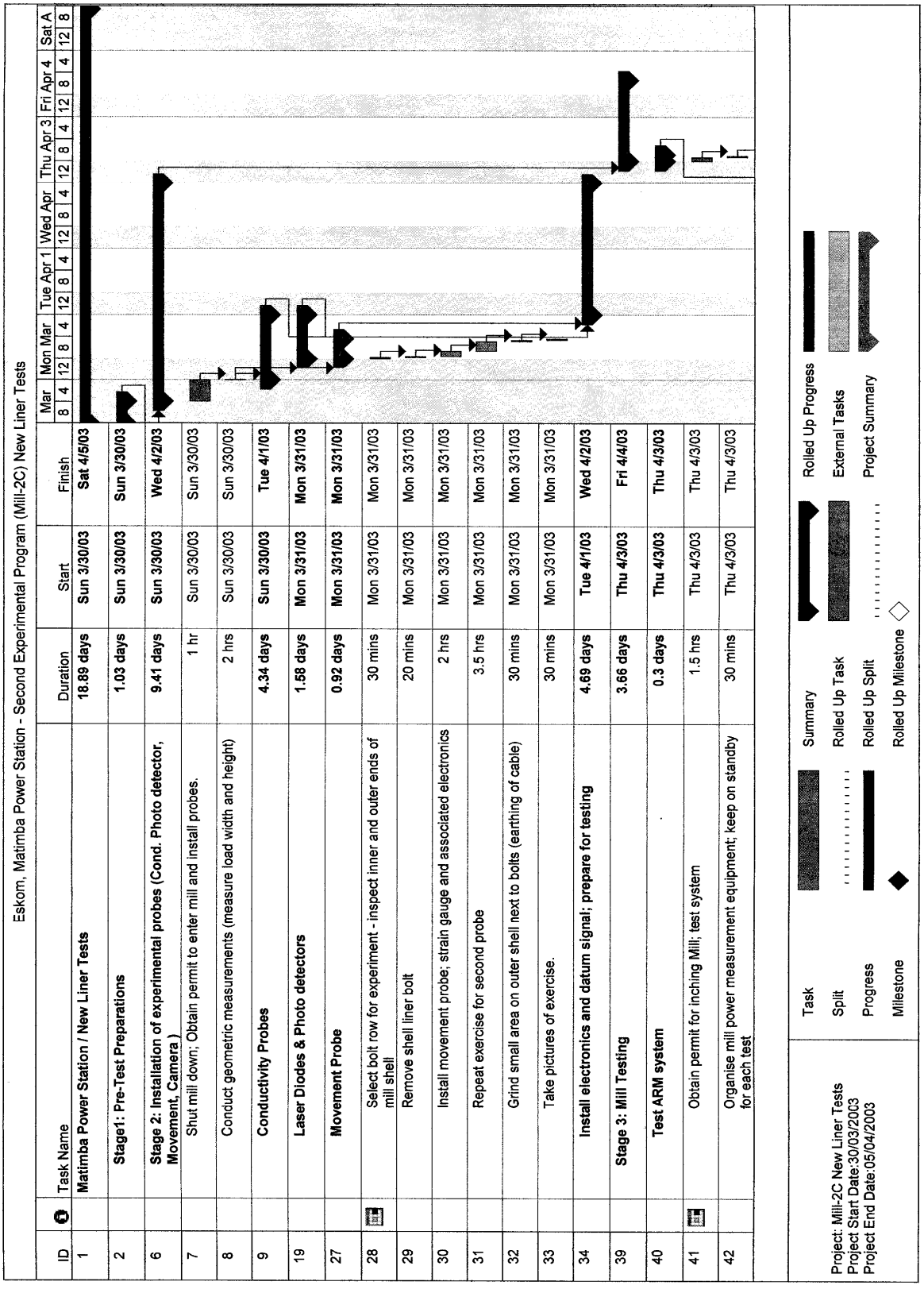
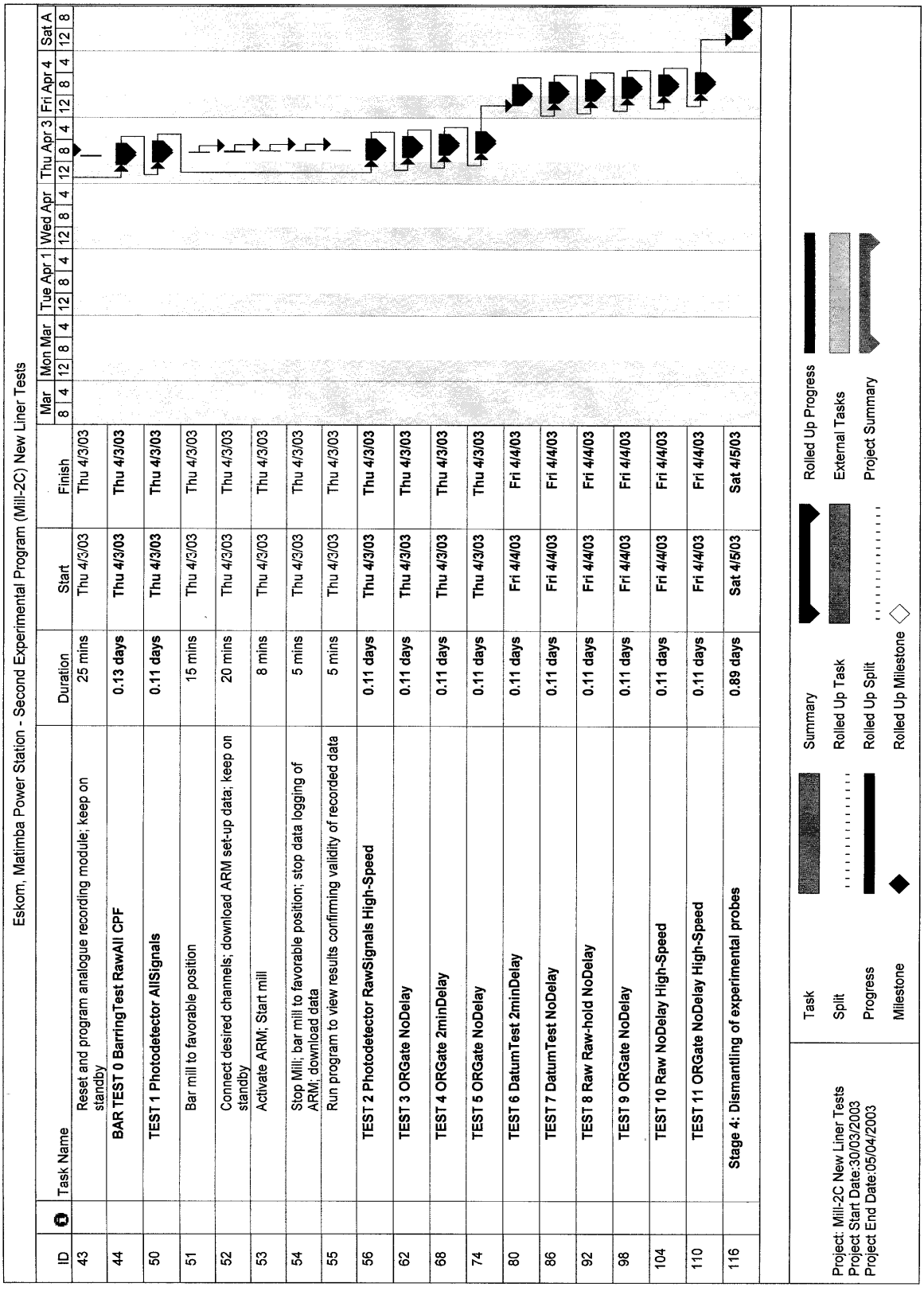


Table A4.5: Second experimental program project schedule (Part 2 of 2)



APPENDIX 5

EXPERIMENTAL TEST RESULTS

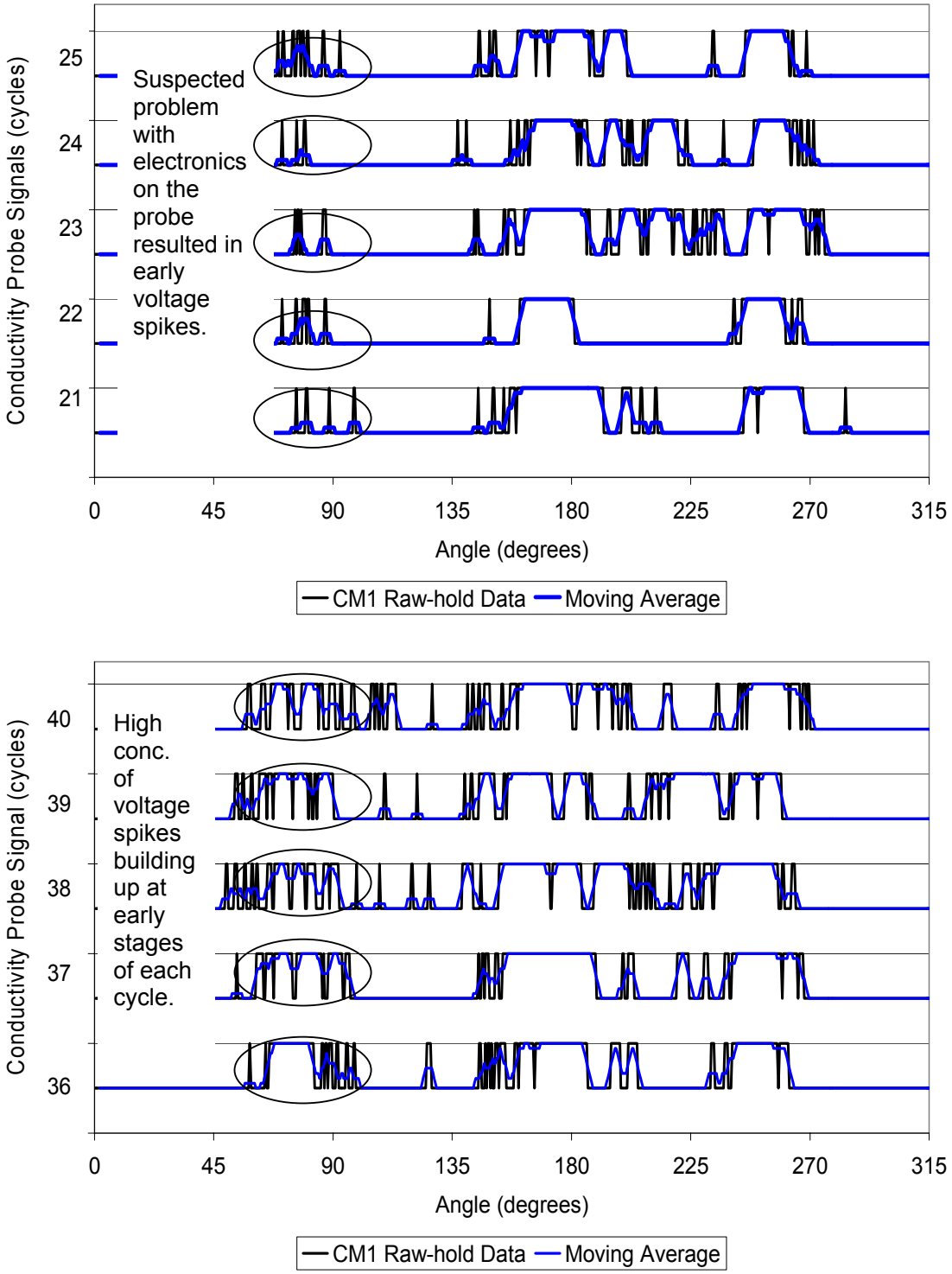


Figure A5.1: Conductivity probe CM1 data profiles from first experimental program: TOP: Test 2 (Raw-holdNoDelay), Cycles (21-25)); BOTTOM: Test 3 (Raw-hold 5minDelay), Cycles (36-40)). Conductivity cycles illustrate the increase in magnitude and duration of voltage spikes and their affect on the moving average trend line.

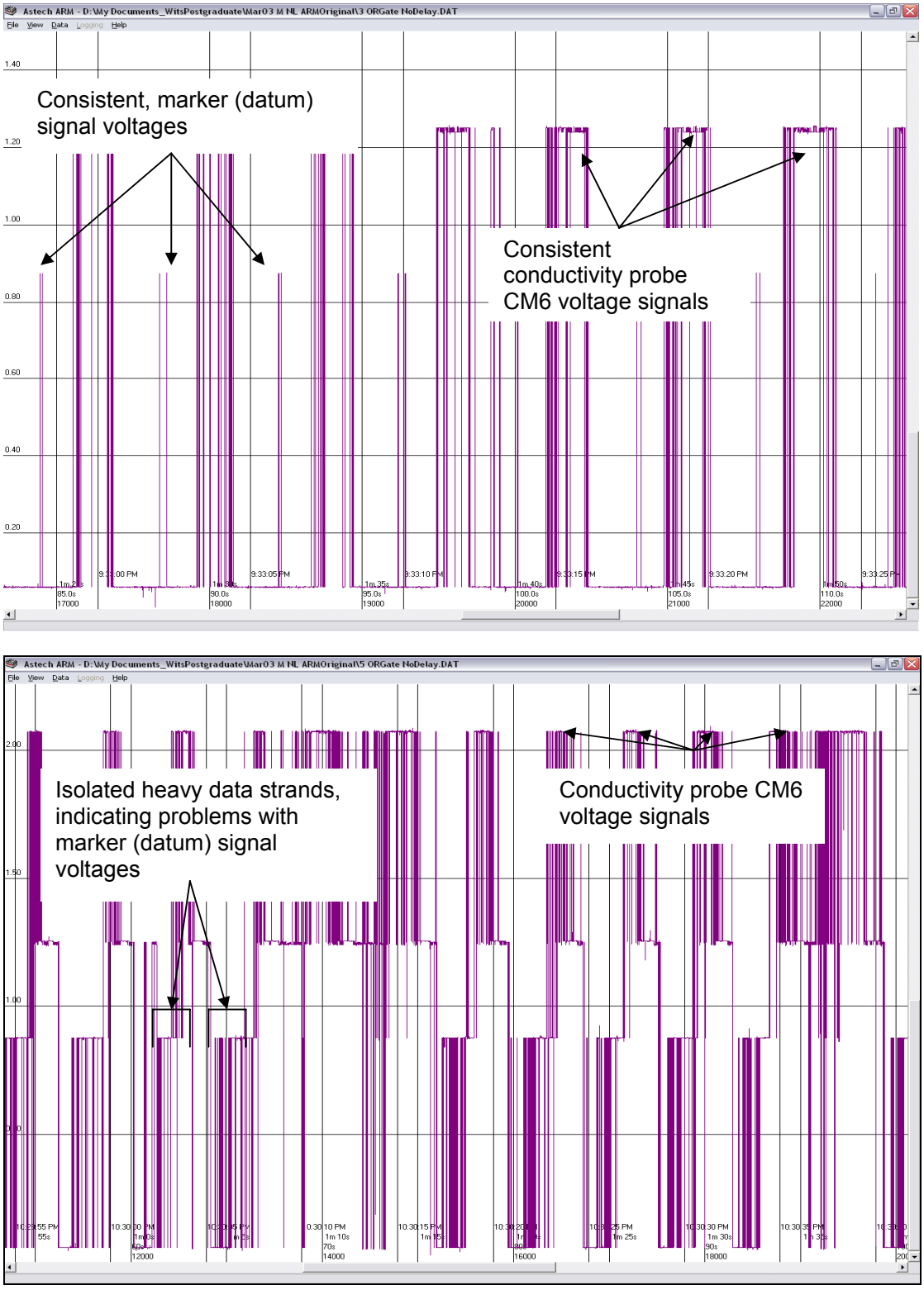


Figure A5.2: ARM graphical display of conductivity probe CM6 and marker signal data from second experimental program. X and Y scales represent time and voltage, respectively. TOP: Test 3 (ORGateNoDelay) Cycles (17-24), well defined marker and CM6 voltage signals; BOTTOM: Test 5 (ORGateNoDelay) Cycles (17-27)), poor data (less than 40% of useful data).

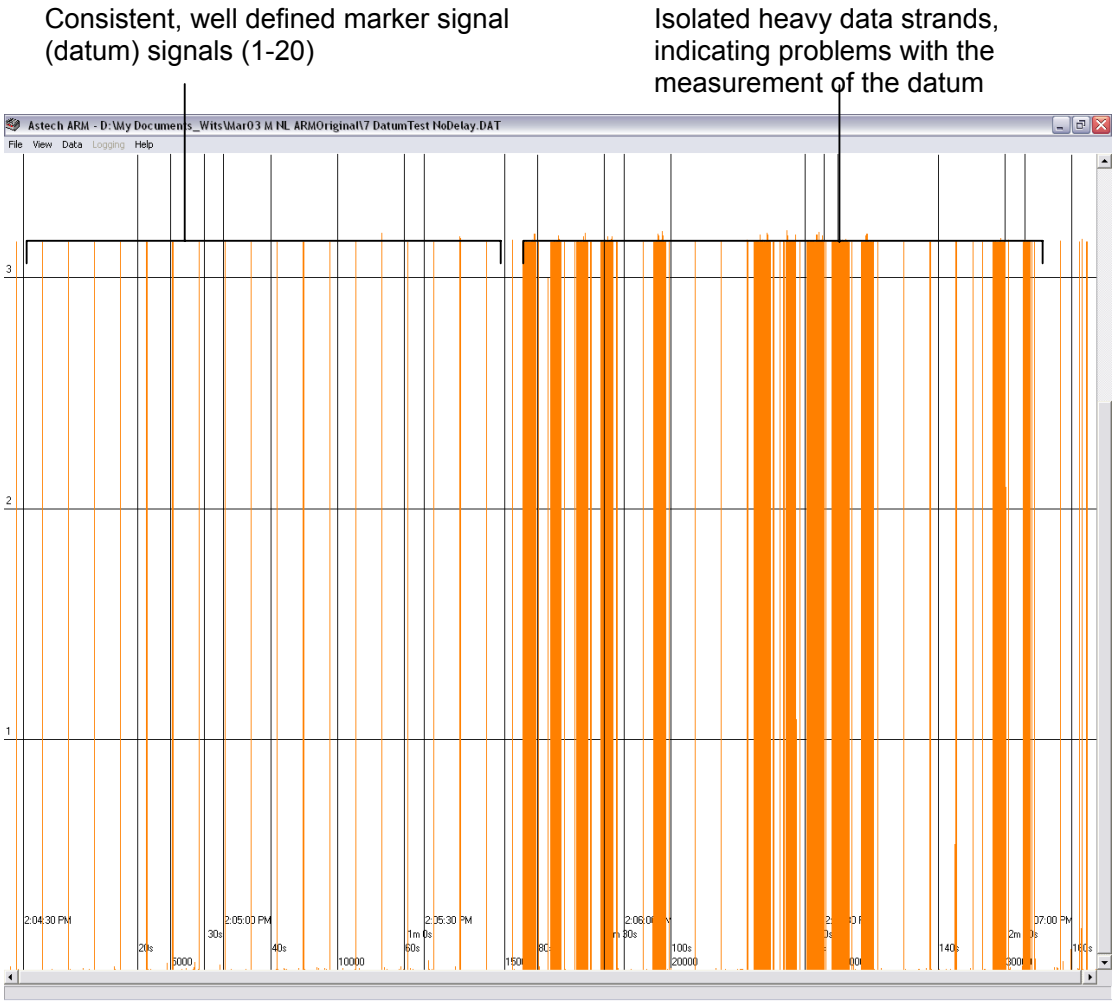


Figure A5.3: ARM graphical display of marker signal data, second experimental program. X and Y scales represent time and voltage, respectively. Test 7 (DatumTestNoDelay) Cycles (1-42). Well defined marker signal for first 21 cycles.

Figure A5.3 displays test 7's datum plot (test 7 was conducted once the datum recording method was repaired). It is clear that up to cycle 20, the datum signals appear clear, consistent and well defined. Contrary to the heavy data strands existing between cycles 20-24, 25-26, 29-34 and 38-40, the data processing program used the identical period measured in the early cycles (cycles 1-20) as a basis from which to reference movement probe data during the heavy data strands.

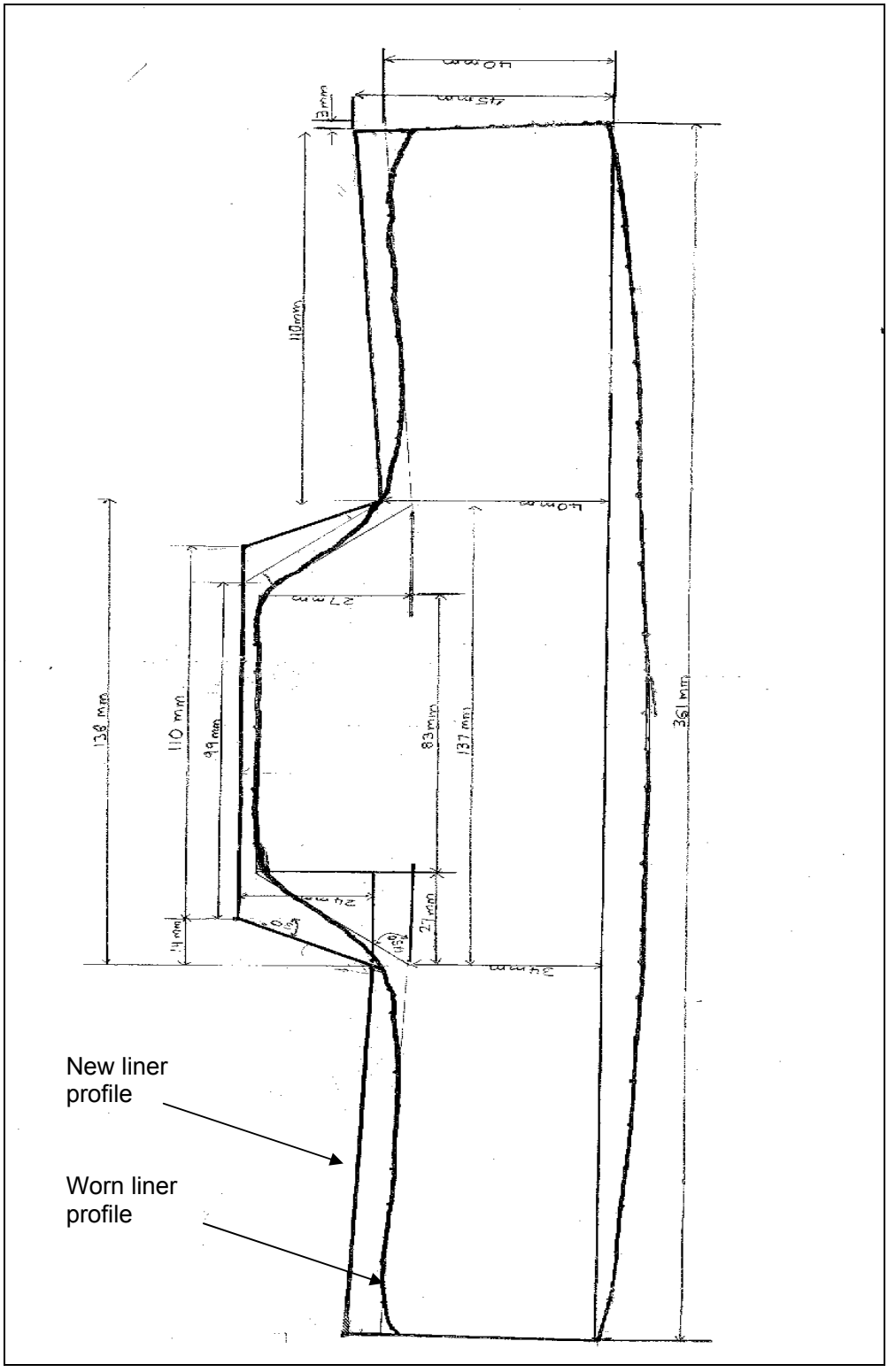


Figure A5.4: Cross-sectional dimensioned view comparing new and worn liner wear profile